Defense Nuclear Agency
Alexandria, VA 22310-3398

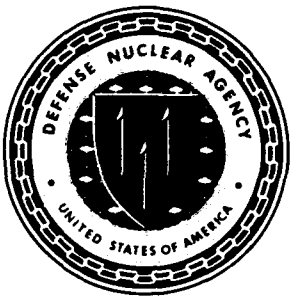

DNA-TR-87-244-V2

Underground Test Sensor Development

Volume II—Electric Field Sensor Development

John Bahns
Pacific-Sierra Research Corporation
12340 Santa Monica Boulevard
Los Angeles, CA 90025-2587

May 1990

Technical Report

CONTRACT No. DNA 001-86-C-0124

Destroy this report when it is no longer needed. Do not return to sender.

PLEASE NOTIFY THE DEFENSE NUCLEAR AGENCY, ATTN: CSTI, 6801 TELEGRAPH ROAD, ALEXANDRIA, VA 22310-3398, IF YOUR ADDRESS IS INCORRECT, IF YOU WISH IT DELETED FROM THE DISTRIBUTION LIST, OR IF THE ADDRESSEE IS NO LONGER EMPLOYED BY YOUR ORGANIZATION.

DISTRIBUTION LIST UPDATE

This mailer is provided to enable DNA to maintain current distribution lists for reports. We would appreciate your providing the requested information.

☐ Add the individual listed to your distribution list.

☐ Delete the cited organization/individual.

☐ Change of address.

NOTE:
Please return the mailing label from the document so that any additions, changes, corrections or deletions can be made more easily.

NAME: _____

ORGANIZATION: _____

OLD ADDRESS	**CURRENT ADDRESS**
_____	_____
_____	_____
_____	_____

TELEPHONE NUMBER: (___) _____

SUBJECT AREA(s) OF INTEREST:

_____	_____
_____	_____
_____	_____

DNA OR OTHER GOVERNMENT CONTRACT NUMBER: _____

CERTIFICATION OF NEED-TO-KNOW BY GOVERNMENT SPONSOR (if other than DNA):

SPONSORING ORGANIZATION: _____

CONTRACTING OFFICER OR REPRESENTATIVE: _____

SIGNATURE: _____

CUT HERE AND RETURN

Director
Defense Nuclear Agency
ATTN: TITL
Washington, DC 20305-1000

Director
Defense Nuclear Agency
ATTN: TITL
Washington, DC 20305-1000

REPORT DOCUMENTATION PAGE

Form Approved OMB No. 0704-0188

1. AGENCY USE ONLY *(Leave blank)*	2. REPORT DATE	3. REPORT TYPE AND DATES COVERED
	900501	Technical 860915 to 880315

4. TITLE AND SUBTITLE
Underground Test Sensor Development
Volume II—Electric Field Sensor Development

5. FUNDING NUMBERS
C - DNA 001-86-C-0124
PE - 62715H
PR - RV
TA - RX
WU - DH014810

6. AUTHOR(S)
John Bahns

7. PERFORMING ORGANIZATION NAME(S) AND ADDRESS(ES)
Pacific-Sierra Research Corporation
12340 Santa Monica Boulevard
Los Angeles, CA 90025-2587

8. PERFORMING ORGANIZATION REPORT NUMBER
PSR Report 1738

9. SPONSORING/MONITORING AGENCY NAME(S) AND ADDRESS(ES)
Defense Nuclear Agency
6801 Telegraph Road
Alexandria, VA 22310-3398
RAEE/Tousley

10. SPONSORING/MONITORING AGENCY REPORT NUMBER
DNA-TR-87-244-V2

11. SUPPLEMENTARY NOTES
This work was sponsored by the Defense Nuclear Agency under RDT&E RMC Code B4662D RV RX 00091 RAEE 3260A 25904D.

12a. DISTRIBUTION/AVAILABILITY STATEMENT
Approved for public release; distribution is unlimited.

12b. DISTRIBUTION CODE

13. ABSTRACT *(Maximum 200 words)*

A concept for the nonperturbative measurement of electric fields in a plasma is described. The concept is based on laser-induced fluorescence from Stark-mixed states. This work reviews the electric field measurement concept, the choices of an active medium, and the laser and detector characteristics. A proof-of-principle experiment was set up and executed. The experimental results which demonstrate the feasibility of this technique for source region electromagnetic pulse measurements are presented.

14. SUBJECT TERMS
SREMP
Plasma Diagnostics
Electric-Field Measurement
Laser-Induced Fluorescence
Stark Effect

15. NUMBER OF PAGES
124

16. PRICE CODE

17. SECURITY CLASSIFICATION OF REPORT	18. SECURITY CLASSIFICATION OF THIS PAGE	19. SECURITY CLASSIFICATION OF ABSTRACT	20. LIMITATION OF ABSTRACT
UNCLASSIFIED	UNCLASSIFIED	UNCLASSIFIED	SAR

PREFACE

A goal of the Defense Nuclear Agency (DNA) electromagnetic pulse (EMP) phenomenology program is the invention and development of new, improved methods to measure source region electromagnetic pulse (SREMP) environments. As part of the Pacific-Sierra Research Corporation (PSR) contribution to that effort, this report documents the concept development and proof-of-principle experiments for a new method to measure SREMP electric fields. The sensor principle of operation is outlined, the sensor design parameters are identified, and the results of a sensor proof-of-principle experiment are presented.

This report represents one area of the PSR research in SREMP underground test instrumentation development. This document was prepared as one volume of the multivolume final technical report for DNA under contract DNA 001-86-C-0124. The technical monitor was CPT Scott Tousley.

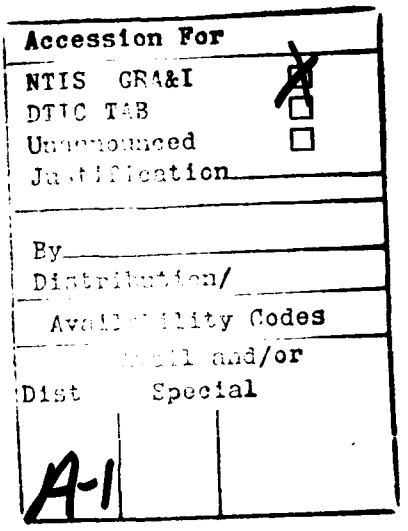

CONVERSION TABLE

Conversion factors for U.S. Customary to metric (SI) units of measurement

MULTIPLY → / ← TO GET	BY → / ← BY	TO GET → / ← DIVIDE
angstrom	1.000 000 X E -10	meters (m)
atmosphere (normal)	1 013 25 X E +2	kilo pascal (kPa)
bar	1.000 000 X E +2	kilo pascal (kPa)
barn	1.000 000 X E -28	meter^2 (m^2)
British thermal unit (thermochemical)	1.054 350 X E +3	joule (J)
calorie (thermochemical)	4.184 000	joule (J)
cal (thermochemical)/cm^2	4.184 000 X E -2	mega joule/m^2 (MJ/m^2)
curie	3 700 000 X E +1	*giga becquerel (GBq)
degree (angle)	1.745 329 X E -2	radian (rad)
degree Fahrenheit	t_K = (t°f + 459.67)/1.8	degree kelvin (K)
electron volt	1.602 19 X E -19	joule (J)
erg	1.000 000 X E -7	joule (J)
erg/second	1.000 000 X E -7	watt (W)
foot	3.048 000 X E -1	meter (m)
foot-pound-force	1.355 818	joule (J)
gallon (U.S. liquid)	3.785 412 X E -3	meter^3 (m^3)
inch	2.540 000 X E -2	meter (m)
jerk	1 000 000 X E +9	joule (J)
joule/kilogram (J/kg) (radiation dose absorbed)	1.000 000	Gray (Gy)
kilotons	4.183	terajoules
kip (1000 lbf)	4.448 222 X E +3	newton (N)
kip/inch^2 (ksi)	6 894 757 X E +3	kilo pascal (kPa)
ktap	1.000 000 X E +2	newton-second/m^2 ($N-s/m^2$)
micron	1 000 000 X E -6	meter (m)
mil	2.540 000 X E -5	meter (m)
mile (international)	1.609 344 X E +3	meter (m)
ounce	2.834 952 X E -2	kilogram (kg)
pound-force (lbs avoirdupois)	4.448 222	newton (N)
pound-force inch	1.129 848 X E -1	newton-meter (N·m)
pound-force/inch	1.751 268 X E +2	newton/meter (N/m)
pound-force/foot^2	4.788 026 X E -2	kilo pascal (kPa)
pound-force/inch^2 (psi)	6.894 757	kilo pascal (kPa)
pound-mass (lbm avoirdupois)	4.535 924 X E -1	kilogram (kg)
pound-mass-foot^2 (moment of inertia)	4.214 011 X E -2	kilogram-meter^2 ($kg \cdot m^2$)
pound-mass/foot^3	1.601 846 X E +1	kilogram/meter^3 (kg/m^3)
rad (radiation dose absorbed)	1.000 000 X E -2	**Gray (Gy)
roentgen	2.579 760 X E -4	coulomb/kilogram (C/kg)
shake	1 000 000 X E -8	second (s)
slug	1.459 390 X E +1	kilogram (kg)
torr (mm Hg, 0° C)	1.333 22 X E -1	kilo pascal (kPa)

*The becquerel (Bq) is the SI unit of radioactivity; 1 Bq = 1 event/s.
**The Gray (Gy) is the SI unit of absorbed radiation.

TABLE OF CONTENTS

TABLE OF CONTENTS (Continued)

LIST OF ILLUSTRATIONS

LIST OF ILLUSTRATIONS (Continued)

LIST OF TABLES

LIST OF TABLES (Continued)

SECTION 1
INTRODUCTION

The electric field E is a primary quantity in all electromagnetic pulse applications. For example, the electric field is the driver of source-region electromagnetic pulse (SREMP) and electromagnetic pulse (EMP) induced cable currents. It affects the SREMP air conductivity through electron equilibration and attachment rates, and determines high-power microwave (HPM) air breakdown. Understanding the spatial distribution of the electric field is the key to unraveling the complicated boundary layer effects of SREMP and system-generated electromagnetic pulse (SGEMP). Despite its importance to these phenomena, the electric field has not been reliably and successfully measured.

It is difficult to measure the electric field because standard sensors cause distortions so that the measured field is not related (in a simple calculable manner) to the field in the absence of the sensor. Pacific-Sierra Research Corporation (PSR) has been developing an electric field sensor that allows nonperturbative, sensitive, and independently calibrated measurements of electric fields. The sensor is intended to work in both benign and hostile underground test (UGT) environments encountered in Defense Nuclear Agency (DNA) testing programs.

The sensor concept is based on the quantum mechanical behavior of atoms or molecules in an electric field, which induces mixing of quantum mechanical energy levels of opposite parity. This effect, which is called Stark mixing, allows optical radiation that would be forbidden in the absence of the electric field. The intensity of the "forbidden radiation" can be detected and is proportional to the magnitude of the electric field. Because the radiation can be stimulated and detected by instruments outside the spatial region of interest, the technique can be nonperturbative. A laser is used to raise electrons of the molecule to an excited state. Line radiation is produced when the excited molecule returns to its ground state. Both

the exciting laser and the radiation detector can be outside the measurement region of interest. The concept is based on a discovery by Moore, Davis, and Gottscho [1984], at Bell Laboratories, Murray Hills, New Jersey, who demonstrated the technique by measuring the electric field in a parallel plate radio frequency discharge. In the basic concept, a laser illuminates the measurement region of interest (Fig. 1). A gas of specially prepared material (the active medium) is used to measure the electric field. The gas may be in a transparent vial or in the experimental atmosphere. The laser radiation may get in and out of the region of interest directly, as shown in Fig. 1, or by optical fibers. The fluorescent radiation induced by each laser pulse is detected in the spectrometer. A typical spectrum is shown in graph 1 in the bottom right corner of Fig. 1. The strength of the forbidden transition and, hence, the intensity of the fluorescent radiation, is related to the electric field. The spectra shown in graphs 2 and 3 indicate the effect of increasing the electric field. Measuring the height of the forbidden Stark-mixed transition determines the electric field strength.

This sensor concept is unique and represents significant advancement in the ability to measure electric fields for EMP applications. However, the basic concept must be turned into a workable laboratory instrument. This report documents the progress made in the first two years of the three year program. In this time, PSR has compiled and developed the basic theory, evaluated and identified the appropriate active media, identified the necessary laser and instrumentation characteristics, built a laboratory facility for performing LIF experiments, demonstrated the basic principles of sensor operation by making electric field measurements using sodium-potassium (NaK) as the active medium, and designed a sensor based on NaK as the active medium. These sensor concepts could make subnanosecond measurements in the radiation and background environment of a UGT.

The program not funded after the second year.

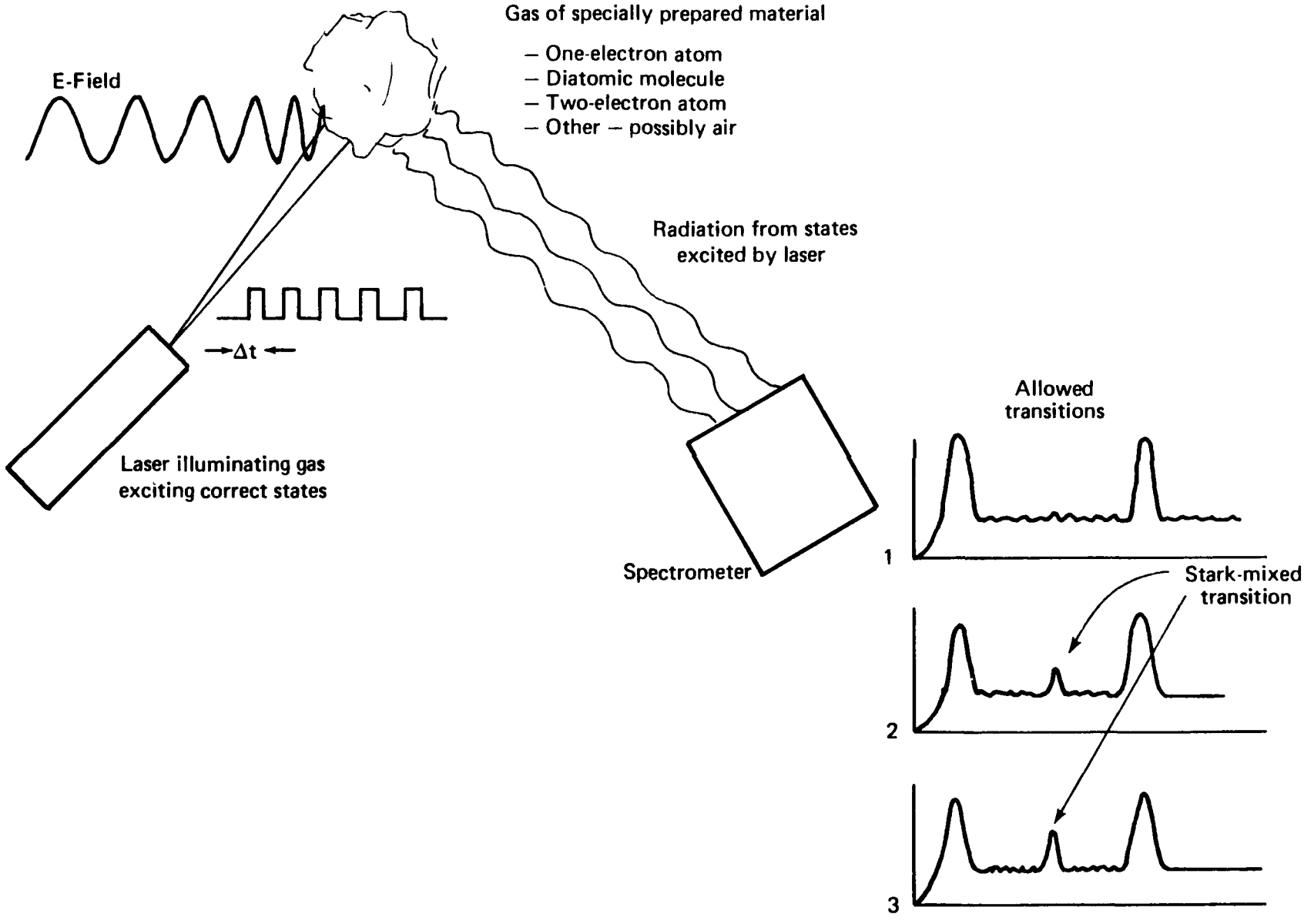

Figure 1. Schematic of electric field sensor.

SECTION 2
REVIEW OF ELECTRIC-FIELD MEASUREMENT CONCEPT

The PSR concept would produce a sensor that is nonintrusive, nonperturbative, and has temporal resolution in the nanosecond range and spatial resolution of a few microns. One version of the sensor uses a small quantity of the active gas in the plasma of interest. A laser is directed into the plasma from outside. The resulting laser-induced fluorescence is detectable from outside the plasma. This arrangement would allow electric-field measurements to be made in plasma sheaths, breakdown arcs, and many other places never before accessible. The following sections describe the discovery of the effect, its advantages, and the basic theory of the sensor operation.

2.1 DISCOVERY OF EFFECT.

Moore, Davis, and Gottscho [1984] discovered the use of the Stark-mixing technique to probe and measure the electric field in an electrical discharge. Their basic idea was to measure the amount of electric-field-induced coupling of two near-degenerate states of opposite parity. Such parity mixing in the presence of the electric field causes radiative transitions which are normally forbidden. By comparing the strength of the allowed transitions to the forbidden transitions, the electric-field magnitude can be determined.

Different forms of atomic and molecular species display state mixing phenomena and are useful for electric field measurement. Stark-mixing of the Rydberg states of Cs atoms was demonstrated to be a sensitive way to detect electric fields [Zimmermann et al., 1974; Herrmann et al., 1986]. In Herrmann et al., Stark-mixing effects in Rydberg atoms were applied to measure fields as small as 1 V/cm. Rydberg atoms possess an electron in a highly excited electronic orbit, such that states with different parity are nearby in energy. Thus, electric-field-induced crossing between the Rydberg state and the perturbing level could be observed in a very low electric field. However, a Rydberg atom may readily lose its electron by field

ionization to form an ion. Consequently, Rydberg atoms are easily destroyed in a high field or radiation environment and are probably not suitable for our purposes. Diatomic molecules appear more suitable as the active medium in the electric field sensor because they are less sensitive to the high field and radiation environment.

Moore, Davis, and Gottscho [1984] used the diatomic molecule BCl as the active medium and applied this technique to measure the electric field in a plasma. However, the BCl molecule is highly unstable, toxic, and highly reactive. Because of these properties, other molecular species may be more desirable.

2.2 ADVANTAGES.

The basic problem with most electric-field sensors is that they perturb the field to be measured. In a nuclear radiation environment, the presence of any sensor material changes the field distribution when electrons are knocked into or out of the sensor. Even out of a radiation environment, standard E sensors distort the field. Capacitive probes--the ones most commonly used for electric field measurements--must be carefully placed along expected equipotentials. If not, the sensor will change the field distribution. Also, capacitive sensors must be large enough to eliminate the effects of fringing fields. Consequently, their spatial and temporal resolution is poor. Langmuir probes have often been used to measure potentials in plasmas (SREMP/SGEMP). However, sheaths develop at the probe surface and the interpretation of the results is difficult and theory dependent. Stark-induced line broadening is a possible measurement technique, but it usually lacks sensitivity because of collision broadening and Doppler shifts. Stark-induced line broadening is more appropriate at extremely high fields, such as those used in laser fusion applications.

The PSR sensor concept had the potential to solve all these problems because the sensor could be made nonintrusive and nonperturbative. Because the sensor requires no equipment in the area of interest, the laser-induced fluorescence sensor would allow electric-field

measurements to be made in plasma sheaths, breakdown arcs, and many other places never before accessible.

2.3 SIMPLE DESCRIPTION OF ELECTRIC-FIELD SENSOR.

The basic operation of the sensor is simple. When an external electric field is applied to an atom or molecule, the energy levels are shifted. In addition, the unperturbed quantum mechanical states of the system are mixed together. In perturbation theory and for the dipole approximation, the change in the energy level is zero in the first order. However, the unperturbed states having energy close together and opposite parity are mixed in first order.

Mixing of states is a quantum mechanical concept. An unperturbed atom, for instance, is described quantum mechanically as a set of possible stationary states of the electrons. In the presence of a perturbation, a new set of stationary states exists. Each new set of states can be described as a linear combination of the original unperturbed states. Because each new state looks like a mixture of the original states, this is often called mixing. In first-order perturbation theory, the amount of mixing is directly proportional to the matrix element of the perturbing potential between the states and inversely proportional to the energy difference between the states. The matrix element of an operator describing the perturbation between two states is, in one representation, the integral of the perturbation multiplied by the wave functions describing each state. In this application, the matrix element is proportional to the dipole moment of the transition.

Because the mixing combines states of opposite parity, radiative transitions are allowed which would be forbidden (by the principle of parity conservation) if the electric field were zero. The frequency or energy of the radiative transition is barely changed by the field (for the fields of interest here the energy of the transition is not changed a measurable amount by the field) because the energy level shift is zero to the first order. The strength of the forbidden line radiation is directly related to the electric field. The sensor operates by measuring the intensity of the forbidden line radiation and, consequently, the electric field can be determined.

In practice, a laser is used to raise electrons of the active material to an excited state. The excited state and, hence, the laser frequency, are chosen so that the gas has radiative transitions to several lower states and so that it has several radiative transitions ordinarily forbidden by the parity selection rule. The forbidden line radiation is detected with a spectrometer and the applied electric field determines strength of the radiation.

Choosing the active material is quite complicated because there are several quantum mechanical selection rules that must be obeyed when an atom or molecule radiates. Two selection rules hold rigorously (for dipole radiation). First, the parity of the final and initial states of the radiating electron must be different. Second, the angular momentum J, of the final and initial electron states must differ by ±1 or 0 units of $\hbar$ (Planck's constant), but states of J = 0 cannot radiate to state of J = 0. These selection rules also must be obeyed to connect the states that are mixed by the electric field. The strength of the forbidden transition determines the sensitivity of the method. The transition rate is directly proportional to the dipole matrix element between the mixed states and inversely proportional to the energy difference between the mixed states. Consequently, the active material must be chosen carefully for states with the correct properties.

2.4 THEORY FOR ATOMIC TRANSITIONS.

The sensor operation is most clearly described for one-electron atoms such as sodium or potassium. However, these atoms are not appropriate for use as the active sensor element. Figure 2 shows the energy-level diagram of Na. (The other alkalies have similar spectra.) The states are labeled by principal quantum number n which has values of 3, 4, 5, ..., angular momentum ℓ (s = 0, p = 1, d = 2, f = 3, ...,), and parity = $(-1)^{\ell}$. Even-parity states s and d have no superscripts; odd-parity states p and f have a superscript 0. In this case, the operation of the electric-field sensor is very simple.

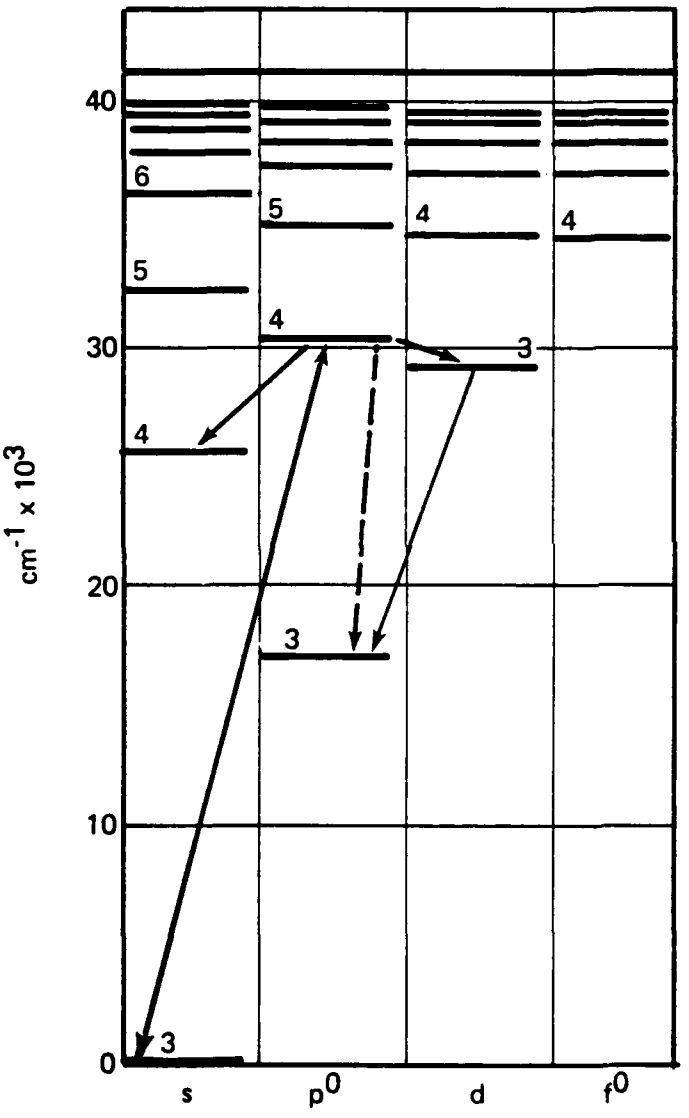

Simplified energy-level diagram of Na. The allowed transitions are shown as solid lines, the "forbidden" transitions as dotted lines.

Figure 2. Simplified energy-level diagram of Na.

Imagine a laser tuned to excite electrons from the ground state n = 3, s (ℓ = 0) to the n = 4, p(ℓ = 1) state (the energy difference between these states is about 3.74 eV.) These excited electrons can radiate back to the ground state or the n = 3, d(3d) state. The n = 3 d(3d) state may also radiate back to the n = 3, p(3p) state. All these transitions are denoted in Fig. 2 as solid lines. However, in the absence of a field, the 4p state cannot radiate to 3p because both states have the same parity. In the presence of an electric field, however, the 4p and 3d states are mixed and the dotted transition from 4p to 3p is consequently allowed. The energy of this transition would be 1.65 eV. (The 3p → 3s transitions are the sodium D lines with energies 2.1051 eV and 2.1029 eV.) The strength of the forbidden transition increases as the electric field increases. Consequently, measurement of the forbidden transition determines the electric field.

This discussion can be made quantitative using Dirac's bra and ket notation. In the presence of an electric field E, the quantum mechanical state $|4p\rangle$ becomes the following, in first-order perturbation theory

$$|4p\rangle = |4p^o\rangle + a(4p,\ 3d)\ |3d^o\rangle\ , \tag{1}$$

where (o) denotes the state in the absence of an electric field. The factor a(4p, 3d) is the Stark mixing coefficient and is given by

$$a(4p,\ 3d) = \frac{\langle 3d^o|\vec{ex}|4p^o\rangle \cdot E}{E_{4p} - E_{3d}}\ , \tag{2}$$

where $\langle 3d^o|\vec{ex}|4p^o$ denotes the dipole moment or matrix element of the position operator (times the electric charge e) between states $|4p^o\rangle$ and $|3d^o\rangle$, and E_{4p} and E_{3d} are the energies of the 4p and 3d states (without the field). The matrix element that describes the radiation (which was zero in the absence of a field) between the 4p and 3p states is given by

$$\langle 3p|R|4p\rangle = \langle 3p^o|R|4p^o\rangle + a(4p,\ 3d)\ \langle 3p^o|R|3d^o\rangle \quad , \tag{3}$$

where R is the radiation operator. The first term on the right vanishes because both states have the same parity giving the transition matrix element as

$$\langle 3p|R|4p\rangle = \frac{\langle 3d^o|e\vec{x}|4p^o\rangle \cdot E}{E_{4p} - E_{3d}} \langle 3p^o|R|3d^o\rangle \quad , \tag{4}$$

This states that the forbidden transition is proportional to the dipole moment (associated with the 3d and 4p states), the electric field, and the strength of the allowed (3p-3d) transition and inversely proportional to the separation between the $4p^o$ and $3d^o$ states. The matrix element for the allowed transition (3d-3p) in the presence of the field is*

$$\langle 3p^o|R|3d^o\rangle \quad . \tag{5}$$

The intensity of the radiation is given by the square of the matrix elements in Eqs. (4) and (5). In electric field measurements, one is interested in the ratio of the intensity I of the forbidden transition to the allowed transition which becomes [from Eqs. (4) and (5)]

$$\frac{I(3p - 4p)}{I(3p - 3d)} = \frac{|\langle 3d^o|e\vec{x}|4p^o\rangle|^2\ E^2}{(E_{4p} - E_{3d})^2} \quad . \tag{6}$$

Hence, we find that the ratio of the intensities varies as $\mu^2E^2/(E_{4p} - E_{3d})^2$ when μ is the dipole moment matrix element. These matrix elements can vary quite a bit but they typically have values of about 10^{-10} m (or 4.8 debye). Consequently, to have the forbidden transition comparable in intensity to the allowed transition for an

*The term involving the Stark mixing coefficient vanishes in this case due to the factor $\langle 3p^o|R|4p^o\rangle = 0$.

electric field of 10^4 V/m, the energy difference between the mixed states must be ~ 10^{-6} eV. Such small energy differences between states are found only in very large principal quantum number (n) states of atoms or molecules (so called Rydberg states). As mentioned previously, the Rydberg states of atoms are sensitive to field ionization, making them inappropriate for our purposes. Thus, the search for an appropriate medium leads to the study of diatomic molecules.

2.5 THEORY FOR DIATOMIC MOLECULES.

Moore, Davis, and Gottscho [1984] used a diatomic molecule in their successful experiment. They took advantage of the fact that the rotational states in degenerate electronic states of diatomic molecules (e.g., Π, Δ, etc.) have opposite parity states that are quite close in energy [using states close in energy produces high sensitivity because the energy difference appears in the denominator of the expression for the ratio allowed to forbidden intensity--Eq. (6)].

The rotational states of a diatomic molecule are labeled by J, the angular momentum (rotation) quantum number; Λ, the projection of the electronic angular momentum on the axis connecting the two atoms; and parity (as well as other quantum numbers not of interest here). In a nonrotating molecule, the states with projection $+|\Lambda|$ and $-|\Lambda|$ have the same energy. The states with $\Lambda = 0$ are called Σ and those with $\Lambda = 1$ are called Π. In a rotating molecule, Π states $\Lambda = +1$ and $\Lambda = -1$ are split by interaction with the molecular rotation into states of opposite parity and very similar energies.

The two Π energy states are called e and f states. The e, f splitting is known as Λ-type splitting and the energy difference between the states is given approximately by the expression:

$$\Delta E = qJ(J + 1) \ , \qquad (7)$$

where q is the Λ-type doubling coefficient which is typically 10^{-3} to 10^{-5} cm^{-1} (where 1 cm^{-1} corresponds to 1.2415×10^{-4} eV)) and J is the total angular momentum quantum number.

According to the transition dipole selection rule, a state of positive parity can only be radiatively excited or decay to a state of negative parity. The selection rule also requires 0 or ±1 change in rotational quantum number J. The transitions with $\Delta J = -1$ ($\Delta J = J' - J''$ where J' is in the excited electronic state and J" is the ground electronic state) are called P emission lines, those with $\Delta J = +1$ are called R lines and those with $\Delta J = 0$ are called Q lines. Thus, in an allowed transition, an excitation involving $\Delta J = \pm 1$ gives a series of P and R emission lines corresponding to different vibrational levels and an excitation of $\Delta J = 0$ gives a progression series of Q lines. The parity selection rule prohibits the simultaneous appearance of P, R, and Q lines. In an electric field, the e and f levels of the Π state are mixed. The extent of the mixing is proportional to the electric field. Consequently, the forbidden Q line is present in a P, R excitation when there is an electric field. This Q line intensity is proportional to the magnitude of the field and can be used to measure the electric field. Mathematically, the e/f mixing line intensity ratio given by Moore, Davis, and Gottscho [1984] may be approximated as:

$$\frac{\text{Forbidden line intensity}}{\text{Allowed line intensity}} \approx \left[\frac{V(J, m)}{\Delta E}\right]^2 \approx \frac{\mu^2 E^2 m^4}{q^2 J^4 (J + 1)^4} , \qquad (8)$$

where J and m are the total angular momentum quantum number and its projection on the electric-field direction, respectively, μ is the molecular dipole moment in the excited electronic state, and E is the electric field.

This expression has all of the features previously discussed in Eq. (6). The intensity is directly proportional to the square of the electric field times the square of the dipole moment μ in the excited state, and inversely proportional to the square of energy difference $[q^2J^2(J + 1)^2]$ between the mixed states. An additional factor, $m^2/J^2(J + 1)^2$, is needed for molecules and represents the projection of J onto the electric field. This factor is less than one and typically on the order of one-half. The sensitivity of the method is

determined primarily by the size dipole moment and energy difference between the mixed states.

This discussion can be clarified by considering an energy level diagram of a diatomic molecule. Three states of angular momentum (J, J + 1, J + 2) of the diatomic molecule are shown in Fig. 3. The parity of these states is indicated in the figure by a plus or minus sign. Assume that a laser, tuned to the correct frequency, excites electrons from the Σ, J state with parity +, to the Π state of J + 1, parity -. This state is labeled as -e. In Fig. 3, the transition is denoted as a solid line and is labeled R(J). Very close in energy to the -e state, lies a state of angular momentum J + 1, parity +. This state is labeled +f. In the absence of an electric field, the state -e can radiate back to Σ states J or J + 2, parity +. The latter transition--P(J + 2)--is also denoted with a solid line in Fig. 3. However, the Π state -e, J + 1 cannot, in the absence of an electric field, radiate to the state Σ, J + 1, parity -, because that transition, denoted with a dotted line, and labeled Q(J + 1), violates parity conservation.

When the electric field is nonzero, however, the states -e and +f are mixed by the field. A transition from the state -e, J + 1, to Σ, J + 1 (i.e., Q(J + 1) is now allowed; the strength of the transition is proportional to the electric field.

Since only molecules with a permanent electric dipole moment μ will exhibit Stark-mixing effects, homonuclear molecules such as O_2 and N_2, which are abundant in the atmosphere, are not useful. In addition, the extent of the e, f coupling depends inversely on the energy separation of the degenerate levels. The intensity ratio of the forbidden Q transition to the allowed P transition is given in Eq. (8).

Depending on the sensitivity requirements, one might select a J level best suited for the magnitude of the electric-field strength. As noted in Eq. (7), the energy separation increases quadratically with J, implying that only low J states will have high sensitivity to electric fields. But low J states have two disadvantages which must be dealt with. First, they are not the most highly populated

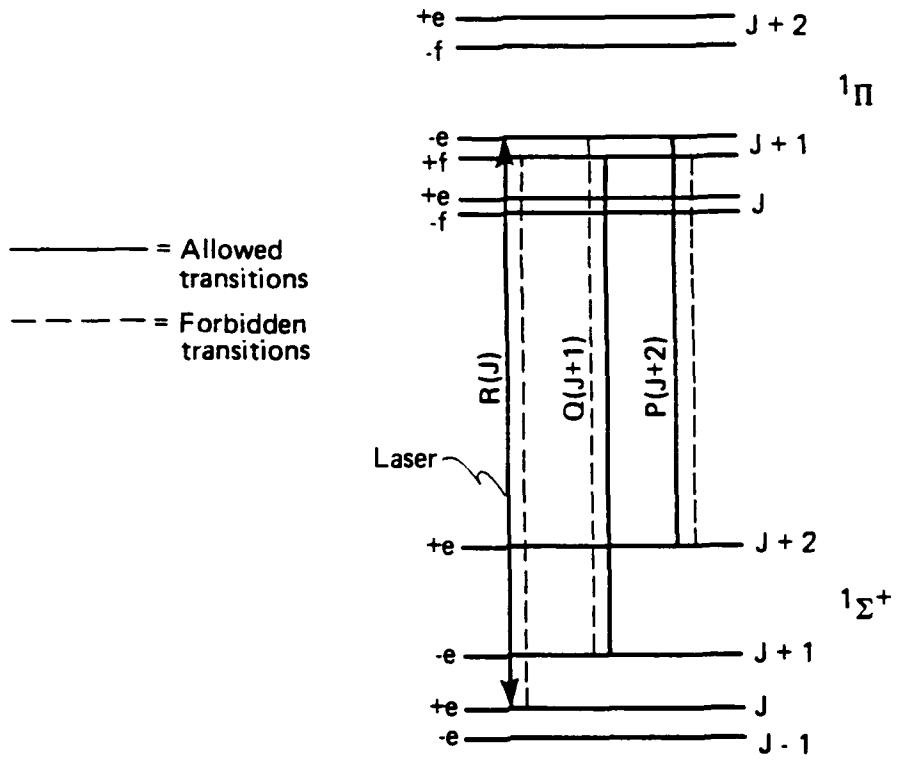

Source: Moore, Davis, and Gottscho [1984].

Figure 3. Schematic energy-level diagram for $^1\Pi$-$^1\Sigma^+$ transitions.

(thermally). The most desirable J in this regard is given by

$$J_{max} = 0.5896 \left[\frac{T}{B}\right]^{1/2} - \frac{1}{2} \quad , \tag{9}$$

where T is the temperature (Kelvin) and B is the rotational constant in the ground state (wavenumbers). Second, the RP transitions in fluorescence must be spectrally resolved. The spacing between RP doublets is given by

$$\Delta_2 F(J) = 4B_v\left(J + \frac{1}{2}\right) , \qquad (10)$$

where B is the ground state rotational constant in a given vibrational level. The larger this spacing the better, since this reduces resolution requirements, allowing one to reject less light and hence achieve larger signal noise ratios. Many electronic states of diatomic molecules are perturbed by neighboring states causing the e-f (lambda doublet) spacing to deviate dramatically from the unperturbed case represented by Eq. (7). Hence, the main strategy has been to satisfy both of these constraints by searching for perturbed states with J's close to the thermal maximum.

Molecules consisting of more than two atoms can also be used in the Stark-mixing experiment. The linear polyatomic molecules exhibit Λ-type splitting and have nearly degenerate states of opposite parity. The spectrum of such polyatomic molecules could be very complicated because of additional vibrational and rotational degrees of freedom. Very often, even the very *simple* polyatomics do not exhibit clean spectral structures. In order to resolve the spectral structures, complicated experimental setups such as supersonic molecular beam expansion may be necessary. Thus, we began our investigation with diatomic molecules.

SECTION 3
CHOICE OF ACTIVE MEDIUM

In the initial stage of the experiment, only diatomic molecules were considered. The following requirements had to be met.

1. The molecule must possess a permanent dipole moment*. As predicted by Eqs. (1) or (4), the extent of e, f mixing depends linearly on the dipole moment of the molecule, such that a strong dipole would exhibit large e, f mixing effects. A collection of dipole moments of some selected diatomic molecules are listed in Table 1.

Table 1. Ground state dipole moments of selected diatomic molecules.

Molecule or Radical	Ground State Dipole Moment μ (debye)
AgCl	6.1
BF	0.5
BCl	$\approx$ 1.0
CO	0.11
CsCl	10.387
HBr	0.827
HCl	1.108
NaCl	9.001
NaK	2.67
SO	1.55
ICl[b]	0.60

NOTE: 1 debye = 3.3×10^{-32} cm-C.
[a]Derived from Radzig and Smirnov [1985].
[b]From Moody and Thomas [1971].

*The dipole moment in the excited state is the important quantity in the selection process. However, because this quantity is not known for most molecules we chose instead to select on the basis of ground state dipole moments, which are well tabulated, and which should be similar to that in the excited state.

2. The molecule must have the correct electronic states, with Σ and Π as the ground and the excited state, respectively. The two electronic states must be of the correct spin and symmetry so they can be connected by radiative transitions which are allowed by the selection rules. The energy separation of the two states should be in the region of 200 to 800 nm so that the Π state can be excited by commonly available lasers.
3. The transitions should be strong and the radiative lifetime of the upper state should be short, so that effects of collisional quenching are reduced.
4. The collisional lifetime in the Π state should be long--equivalent to a small collisional quenching rate. A large quenching rate rapidly depletes the excited molecule by allowing it to relax into various decay channels. This reduces the fluorescence signal.
5. The molecule would preferably be a constituent of air, such that the atmospheric environment is unperturbed. If an air molecule cannot be used, the active material should be produced easily and should require no extra containers, heaters, etc. The produced materials should be chemically and physically stable over the detection duration ($\approx$ 1 μs or so).

To evaluate appropriate molecules, we searched the available literature, identified possible molecules, and characterized their ground states, transition energy and lifetimes, and stable forms. A representative sample of this search is given in Table 2.

According to Huber and Herzberg [1979], only a few diatomic molecules have the desired characteristics. They are divided into the following four groups:

1. **Mixed alkali diatomics.** These consist of the heteronuclear diatomic molecules of the elements in the first column of the periodic table; examples are LiNa, LiK, and NaK. In particular, Derouard and Sadeghi [1986] have conducted an exten-

Table 2. Representative list of possible molecular species with correct states.

Molecule	Transition	ΔE	τ(ns)	Stable Form
AgAℓ	$X^1\Sigma^+ - C^1\Pi$	31744	--	--
AgH	$X^1\Sigma^+ - C^1\Pi$	41261	--	--
AℓBr	$X^1\Sigma^+ - A^1\Pi$	35879	--	AℓBr, 97.5 mp, 264 bp
AℓCl	$X^1\Sigma^+ - A^1\Pi$	38254	--	$A\ell Cl_3$, 177 sublimation temperature
AℓF	$X^1\Sigma^+ - A^1\Pi$	43949	--	$A\ell F_3$, 1291 sublimation temperature
AℓH	$X^1\Sigma^+ - A^1\Pi$	23470	--	--
$A\ell H^+$	$X^2\Sigma^+ - A^2\Pi$	27667	--	--
AℓO	$X^3\Sigma^+ - C^2\Pi_r$	33153	--	$A\ell 2O_3$, 2015 mp, 2980 bp
AsF	$X^2\Sigma^+ - A^3\Pi_r$	25719	--	ASF_3, gas
AsH	$X^3\Sigma^- - A^3\Pi_i$	29822	--	AsH_3, gas
AsN	$X^1\Sigma^+ - A^1\Pi$	35999	--	--
AsO^+	$X^1\Sigma^+ - A^1\Pi$	42594	--	AS_2O_3, 312 mp
AsP	$X^1\Sigma^+ - A^1\Pi$	32417	--	AsP, sublimation temperature
AsS^+	$X^1\Sigma^+ - A^1\Pi$	37359	--	AS S , 360 mp, 707 bp
AuBe	$X^2\Sigma^+ - B^2\Pi$	18946	--	--
AuMg	$X^2\Sigma^+ - B^2\Pi$	31058	--	--
BaBr	$X^2\Sigma^+ - C^2\Pi$	19192	17	$BaBr_2$, col, 847 mp, bp
BaCl	$X^2\Sigma^+ - C^2\Pi$	19450	17	$BaCl_2$, col, 963 mp, 1560 bp
CS	$X^1\Sigma^+ - A^1\Pi$	38904	176	CS_2
CuBr	$X^1\Sigma^+ - A^1\Pi$	20498	--	CuBr, white, 492 mp, 1345 bp
CuCl	$X^1\Sigma^+ - A^1\Pi$	19001	--	CuCl, white, 430 mp, 1490 bp
GeO	$X^1\Sigma^+ - A^1\Pi$	37767	--	GeO, sublimation temperature 710
GeS	$X^1\Sigma^+ - A^1\Pi$	32889	--	GeS, yellow-red, sublimation temperature 430
InCl	$X^1\Sigma^+ - C^1\Pi$	37484	--	InCl, white, 225 mp, 608 bp $InCl_3$, vol. 600
NaK	$X^1\Sigma^+ - C^1\Pi$	16994	--	--
CO	$X^1\Sigma^+ - A^1\Pi$	65076	10	CO, gas
O_2	$X^3\Sigma_g^- - C^3\Pi_g$	65530	Metastable	O_2, gas
SO	$X^3\Sigma^- - A^3\Pi$	38622	16 μs	SO_2, gas
ICl	$X^1\Sigma^+ - A^3\Pi_1$	13745	100 μs	ICl, gas

sive study on the Stark-mixing of the NaK molecules. Molecules in this group are characterized by their high chemical reactivity and low vapor pressure. To produce sufficient diatomic molecules for detection, external heating is often necessary.

2. **Diatomics of the group IVA and VIA.** Examples are CO and CS, which consist of elements from each of the IVA and VIA group. In particular, CO exists in gaseous state at standard temperature and pressure, which makes storage and handling of the chemical easy. The energy separation between the upper and the ground electronic state for these molecules is, however, very large. Excitation of the A-X transition of CO requires a two-photon transition process. In addition, the upper Π states of both of the molecules are known to be strongly perturbed.
3. **Diatomics of the group IIIA and VIIA.** Examples of this group are BCl, BBr, BF, and AlF. Diatomics in this group are highly unstable. The chemical lifetime of such molecules could be as short as 10^{-6} s. They do not exist in nature as a stable molecule, and must be produced from fragmentation from their parent molecules by laser photo fragmentation or by microwave discharge methods. The extreme reactivity of such molecules makes handling the chemicals difficult.
4. **Mixed halogen diatomics (interhalogens) of group VII.** Examples are ICl, IBr, IF, and BrCl. Diatomics in this group are volatile, stable, and exist primarily as a gas. They have long radiative lifetimes (~100 μs) due to the fact that the excited Π state is a triplet (rather than singlet) state. They are corrosive and require special handling techniques.

Our evaluation of the molecules indicated that CO is the most attractive candidate. It has the correct ground and excited states and has a strong transition with a radiative lifetime of 10 ns. Also CO is a constituent of air and is easily produced and handled. There

is much information about CO and a great deal of spectroscopic data are available. Many experiments have been done on this molecule. The disadvantage of CO is that the transition we must use is in the ultraviolet (UV). The smallest wavelength we can achieve with commercially available lasers is about 280 nm. Thus, CO requires two-photon excitation which, in turn, requires high laser power and small bandwidth. Also, the radiation is in the UV which makes it difficult to detect. Furthermore, CO has a large quenching cross section. Thus, the excited states rapidly quench and the experiment may require even higher excitation energy.

The backup or secondary molecule we identified is NaK or the other mixed alkali dimers. These molecules offer many advantages. With these molecules the technique could be very sensitive, only one-photon excitation is required and the transition is in the visible part of the spectrum. Thus, an inexpensive laser and detection system is adequate. The spectroscopic data are available for these molecules and even some Stark-mixing experiments have been done (NaK) [Derouard, 1987; Derouard and Sadeghi, 1986]. However, for these molecules, the experiments must be done in a closed cell which may distort the field. Furthermore, the molecules are difficult to make and handle.

Based on these considerations, we decided to design a system that could evaluate both the CO and NaK molecules for this application.

SECTION 4
LASER AND DETECTOR CHARACTERISTICS

Designing a laboratory to develop the Stark-mixing technique into a standard tool requires estimates of the laser and detector requirements. In this section, we outline the preliminary estimates for these requirements and the choices of lasers and detectors that follow from them. We also discuss some details of the laboratory setup.

4.1 REQUIREMENTS.

The laser characteristics include frequency, power per pulse, energy per pulse, bandwidth, and pulse temporal behavior. Because we plan to evaluate several molecules for the active substance in our sensor, the laser we use must have a wide range of frequencies and ample power. Tuning the laser to the number of frequencies required to excite particular rotational-vibrational lines of different molecules calls for tunable dye lasers. These are typically driven by lower frequency, high-power lasers (e.g., glass).

The detection requirements dictate the detailed laser characteristics. To detect LIF in our setup we can estimate (see Sec. 4.2) that the laser must generate 10^8 LIF photons per pulse. The number of LIF photons generated per incident photon depends on the number of molecules per unit volume times the length of the excitation region and the cross section for excitation. For single-photon excitation, this translates into laser energy through the formula

$$N = 10^8 \text{ photons} = \frac{E_{laser}}{h\nu} \cdot n\sigma L \ , \qquad (11)$$

where n is the number of molecules per unit volume, $h\nu$ is the energy of the laser photons, σ is the absorption cross section, and L is the length of the excited region. The single-photon excitation cross sections are typically about 10^{-16} to 10^{-18} cm^2/molecule. Since we

plan to work at pressures from atmospheric to 10^{-3} torr, n varies from 10^{19} to 10^{13} molecules/cm^3. Thus, the laser energy must be about 10^{-5} J. Since this is not a large energy requirement, it does not put a severe constraint on the laser energy required.

Two-photon excitation, however, is required for CO experiments. The estimates for such excitation are less certain. Simple arguments, however, lead to the expression

$$N = 10^8 \text{ photon} = \left(\frac{E_{laser}}{h\nu}\right)^2 \cdot \frac{\delta h L}{\left(2 \times 10^{-3}\right)^2 \Delta t} \approx \frac{E^2 n}{10^{10} \Delta t} , \qquad (12)$$

where Δt is the pulse width and δ is the two-photon excitation cross section. Typically $\delta \sim 3 \times 10^{-53}$ cm^4-s/photon molecule and we have assumed that we can focus the laser to 20-μm spot size. For a 6-ns pulse and n of 10^{13} this becomes E ~ 30 mJ at the lowest pressure. This is a much more stringent energy requirement than for single-photon excitation.

The laser requirements are thus:

- tunable dye laser,
- 10-ns-type pulse width,
- usable bandwidth (about 15 cm^{-1}),
- En = 10^8 for single-photon excitation,
- $E^2n/\Delta t = 10^{18}$ for two-photon excitation,
- adjustable to multipulse use.

The available choices and the advantages and disadvantages of each are shown in Table 3. We believe that the best compromise is the Quantel YG581C-10 with a TDL-50 YAG pumped dye laser. That laser should be capable of driving the experiments we envision and flexible enough to be useful in future concept evaluation experiments.

Table 3. Laser candidates.

- PRA LN105 (nitrogen pumped dye laser)
  - 15 ps, bandwidth 300 cm^{-1}
  - 4.5 μJ per pulse
  - 400 to 900 nm tunability
  - Inexpensive ($27,000) but low power--only useful for single-photon excitation--single pulse
- PRA LN107 (nitrogen pumped dye laser)
  - 500 ps, bandwidth 4 cm^{-1}
  - 100 μJ per pulse
  - 220 to 900 nm tunability
  - Inexpensive ($25,000) but moderate power--not useful for two-photon experiment
- Quantel--YC581C-10 plus TDL-50 YAG pumped dye laser
  - 6 ns pulse width, bandwidth 0.8 to 0.08 cm^{-1}
  - 50 mJ (at 300 nm)
  - 240 to 800 nm
  - Sufficient energy for two-photon experiments and all single-photon experiments but long pulse and expensive ($110,000)
- Quantel YG500--mode locked Q-switched YAG pumped laser dye
  - 15 ps pulse width, bandwidth 30 cm^{-1}
  - 300 μJ per pulse
  - 9 pulses in 90 ns
  - May do multipulse, two-photon (CO) measurements
  - Expensive ($117,000), detection and operation are difficult
- Coherent--mode locked continuous wave YAG pumped dye laser
  - 5 ps pulse width bandwidth
  - 3 nJ pulse in UV
  - Tunable 275 to 900
  - 76 mHZ, 13 ns pulse separation
  - Multipulse picosecond operation but marginal for single photon, impossible for two-photon experiment

4.2 DETECTOR REQUIREMENTS.

The detector requirements were estimated by determining the fraction of LIF-produced photons from a particular transition that get to a detector located some distance (we took a representative distance of 20 cm) from the region of excitation. We next folded in the detection efficiency of the photomultiplier (PMT) which does the actual detection.

For a typical PMT it takes about 4 photons to generate an electron and about 100 electrons are necessary to detect a signal. Thus the PMT must intercept about 400 LIF photons for detection. Because the LIF is isotropic and the source region is about 1 cm in size, a detector located at 20 cm from the source region receives only $(1/20)^2$ of the emitted photons because of the solid angle factor. The monochromator reduces the intensity by about a factor of 10. The intensity is further reduced by a factor of 10 because the excited state can radiate to many other states--it typically radiates into the chosen state one-tenth of the time. Multiplying these factors implies that the LIF must produce about 10^8 photons per pulse for a detectable signal.

The monochromator characteristics follow from the requirement that it must be able to resolve the P, Q, and R lines of the transitions in question. The sensitivity of the monochromator is determined by its length and the quality of the grating. The monochromator we purchased could resolve most of the lines of CO and NaK.

SECTION 5
DESCRIPTION OF EXPERIMENTS

5.1 SETUP.

A pulsed Nd:YAG pumped dye laser system was used as the excitation source in the Stark-mixed laser-induced fluorescence experiments. This laser (model YG581C-10), purchased from Quantel International, Santa Clara, California, was able to deliver up to 1 J/pulse of energy in the fundamental (1064 nm) of the infrared (IR) laser. For pumping the dye laser (TDL-50), the second harmonic of the IR laser (produced by passing the 1064 nm laser radiation through a nonlinear crystal) was used. Different dyes were used depending on the spectral region desired. The average power of the dye laser was about 100 mJ/pulse over the spectral range of 550 to 650 nm. The CO experiments required doubling the fundamental radiation of the dye laser into the UV. This was achieved using a nonlinear crystal and an automated phase correcting system. With that laser system we were able to tune the laser continuously from UV to IR, which provided a flexible excitation source for spectroscopic studies.

A 0.75 m monochromator (a Spex Industries, Edison, New Jersey, model 1702) was used to resolve the collected LIF radiation. The monochromator is equipped with a 2400 groove per millimeter grating which is blazed at 240 nm. The diffraction efficiency of the grating is 70 percent at 240 nm, dropping steadily to 30 percent at 700 nm. In the carbon monoxide experiment, the grating was chosen primarily for its high diffraction efficiency at short wavelength. The useful spectral range of the monochromator system is from 190 nm to 700 nm. The upper limit is restricted by the blazing angle of the grating. Resolution of the system is 0.5 nm/mm of the slit width.

For photoelectric detection, a PMT was used. A bi-alkali PMT (Thorn EMI 9813QB) with spectral sensitivity maximum in the UV region, was used to monitor the CO and NaK emission. The output of the PMT was terminated into a 1 kΩ resistor. The voltage across the load resistor corresponds to the fluorescence signal detected by the PMT.

This voltage was amplified and integrated by a boxcar averager (Stanford Research Systems, Palo Alto, California, model SRS 250). The gate width, or integration time, of the boxcar was typically selected as 100 ns, which is longer than the lifetime of the excited state of the molecules. The analog signals were digitized by an analog-to-digital (A/D) converter (SRS 245), and collected by an IBM-AT personal computer through a general purpose interface bus (GPIB).

The equipment was controlled through the personal computer; a specially written program operated the data acquisition devices. With the program, data were collected and displayed on the video screen; the data could be stored, recalled, and plotted later. Data analysis such as peak position searching could be done easily with a simple command. Related devices included a Sigma 400 (Sigma Instruments, Braintree, Massachusetts) color graphic board and a halo-graphic routine for graphic display. An optical diode detecting the dye laser signal was used to trigger the data acquisition system; therefore, the data acquisition normally operated at the laser firing rate of 10 Hz.

A gas handling station, which consists of a vacuum pump, pressure measuring gauges, and buffer gas supply, was also set up in the laboratory. A vacuum pump was supplied by Sargent-Welch Scientific Company, Skokie, Illinois (model 1402), with free-air displacement of 160 l/min. Baratron pressure gauges were used in the experiments. These pressure sensors are capacitance-type manometers; they detect pressure changes by the deflection of the diaphragm in the sensor heads. This system provides accurate gas pressure readings from 1000 torr to 1 mtorr. The vacuum and gas handling system was connected to a gas supply, which could be either the sample gas source or the buffer gas source. With such a pumping station, the lowest pressure achieved was about 5 mtorr.

5.2 PROCEDURES.

Before Stark-mixing experiments can be performed, the detailed spectrum of the molecule must be determined. The spectrum is first calculated theoretically from the known and published molecular constants. The theoretical calculation provides a good starting place

for determining the spectrum, but it is usually not accurate enough for this application. The general experimental procedures followed for all molecules are summarized as follows.

5.2.1 Spectrum Identification.

The fluorescence or absorption lines (or at least the molecular constants) of many diatomic molecules have been reported in the literature. We can use the molecular constants of the excited and ground states to compute the approximate spectrum of the relevant electronic states of the molecule. The spectrum is experimentally determined by examining the total emission of the molecule. We start by setting the grating of the monochromator at the position of the expected fluorescence. With the exit slit of the monochromator opened to 2 mm, the monochromator system acts like a band-pass filter with a bandwidth of 1 nm. Therefore, emissions of less than ±0.5 nm from the monochromator wavelength setting will reach the PMT and be detected. Scanning the laser across the expected region of the electronic transition gives a resolved excitation spectrum of the molecule over a 1-nm range.

Since the line width of the fundamental radiation of the dye laser is 0.08 cm^{-1} (about 10^{-5} eV), we can resolve most of the rotational-vibrational structures of the electronic excitation spectrum. We can definitely assign the transitions of the different emission radiations by comparing the observed and calculated spectra. Even though the absolute positions of the observed and calculated lines are different because of the uncertainties of the molecular constants and the laser wavelengths, the differences between the various absorption lines are accurate enough to make the spectral assignments possible.

5.2.2 Stark-Mixing Experiments.

After the spectrum is assigned, such that each spectral peak has vibrational and rotational quantum numbers, we tune the laser to a particular absorption line position and examine the Stark-mixing effects.

For Stark-mixing experiments, both the entrance and the exit slits of the monochromator are closed to about 0.1 mm, giving resolution on the order of 0.05 nm. The slit width may have to be closed even more when higher resolution is required depending on the congestion of the spectrum and the separation of the P and R emission lines. With the dye laser fixed on an absorption line of the diatomic molecule, the grating of the monochromator is scanned slowly across the region of the expected P and R emissions. In this way, a pair of fluorescence P and R lines can be detected. After assignments of emission lines are confirmed, we can turn on the electric field and rescan the spectral region to examine the Stark-mixing effects. If the conditions are right, a forbidden Q line will appear between the P and R lines.

SECTION 6
NaK EXPERIMENTS

NaK vapor was investigated to determine its usefulness as a dynamic electric field sensor. This section presents a detailed account of the experiments and findings.

6.1 INTRODUCTION.

One group of gas phase molecules well suited for electric field measurements is the interalkalis (group 1A, excluding hydrogen). The interalkali molecules are useful because they have large dipole moments (NaK = 2.67 Debye) and appropriate states (NaK has $X^1\Sigma^+$ ground states and a $B^1\Pi$ excited state that are optically accessible). Figure 4 shows the potential curves [Stevens, Konowalow, and Ratcliff, 1984] for NaK. Our work concentrates on transitions between the $^1\Sigma^+$ and $B^1\Pi$ states which are in an optically convenient region which can be excited by radiation generated in a standard Rhodamine 6G dye. All of the interalkali molecules are difficult to work with in the laboratory because they ignite spontaneously on contact with air and they must be heated to form a sufficiently dense vapor. NaK was chosen because it is the most studied and has been used as a sensitive electric field sensor in pyrex cells using low power continuous wave lasers in work by Derouard and Sadeghi [1986a,b, 1988]. The work presented here uses a pulsed laser and heat pipe, thus demonstrating dynamic electric field measurements at much higher laser powers and molecular densities. Such demonstration is a necessary step in the development of a dynamic electric field sensor to be used in open air.

6.2 EXPERIMENTAL STRATEGY.

In order to obtain the highest sensitivity and signal to noise, one must correctly choose the right vibration rotation state in the $B^1\Pi$ state of NaK. This is done on the basis of the state having a small lambda doublet splitting, good Franck-Condon Factors (FCFs), low V" (vibrational quantum number), and J (rotational quantum number)

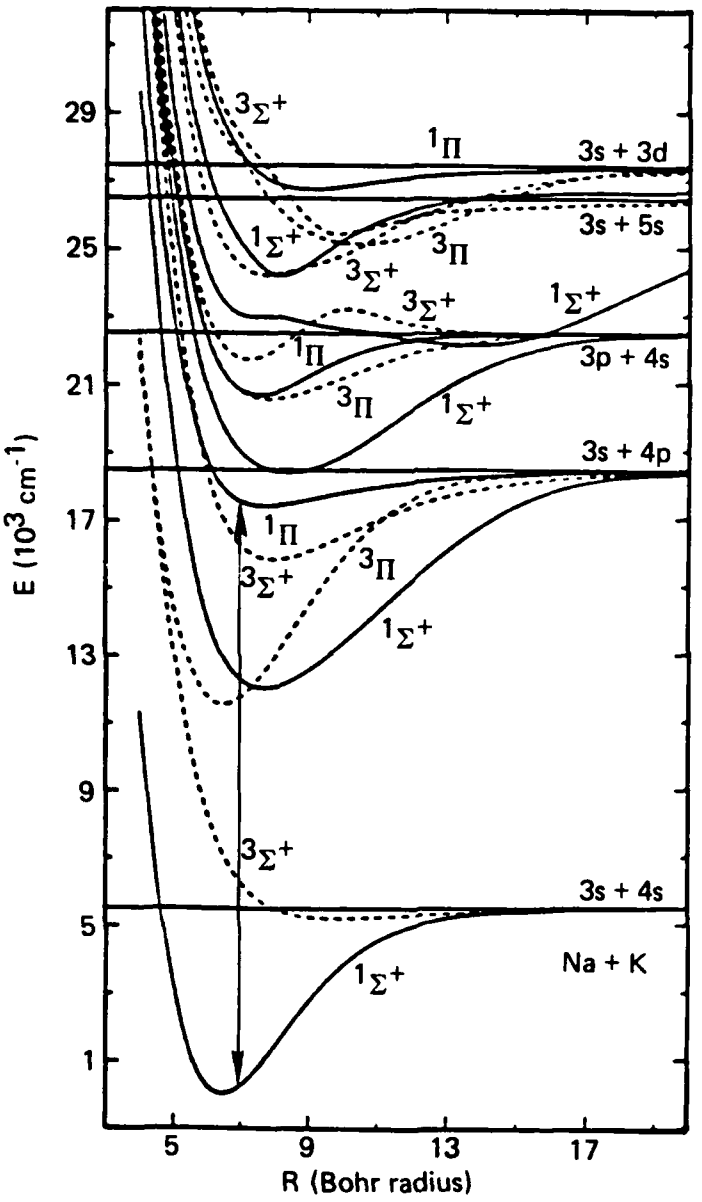

Note: Bohr radius = 5.2918 x 10^{-11} m.

Source: Stevens, Konowalow, and Ratcliff [1984].

Figure 4. Potential energy curves of lowest electronic state of NaK.

that is close to the maximum of the thermal population at the temperature of the vapor [$J_{max}(T = 663\ K) = 48$]. From the lists of perturbed levels supplied by Derouard [private communication, 1987], candidate levels were selected, they are listed in Table 4. Other relevant information for these studies are presented in Table 5. It was determined that V' = 2, J' = 40 level of the $B^1\Pi$ state was the overall best candidate. Although electric field measurements on other levels listed in Table 4 were performed, all of the studies in this report deal with exciting the (X → B) transition V" = 2, J" = 41 → V' = 2, J' = 40 and observing fluorescence resulting from the transitions (B → X) V' = 2, J' = 40 → V" = 13, J' = 39, 40, and 41. This is shown schematically in Fig. 5.

Spectroscopic constants for the two states are given in Tables 6 and 7. The FCFs were supplied by Derouard [1987] and are given in Table 8. The electronic transition moment function for these two states was obtained from Ratcliff, Konowalow, and Stevens [1985].

6.3 EXPERIMENTAL.

NaK was contained in a heat pipe oven shown in Fig. 6. This was preferred over glass cells for two reasons. First, heat pipes can be operated indefinitely (without darkening of windows) because the metal vapor is kept away from them by a buffer gas (Argon). Second, heat pipes allow one to perform studies over a much broader range of temperatures and pressures. A eutectic mixture of NaK (78 percent K) was used. This resulted in an alloy that was liquid at room temperature (see phase diagram in Fig. 7). The vapor pressure above this mixture is shown in Fig. 8 [Mausteller, Tepper, and Rodgers, 1967]. The equation for the curve is given by $Log_{10}[P(ATM)] = 4.1414$ to $4374.30/T(Kelvin)$. Argon buffer gas pressure was measured with a capacitance manometer (MKS Baratron Type 220).

The generation of a stable, well defined electric field in a metal heat pipe required a specially designed cathode. The cathode used is shown in Fig. 9. The cathode was made of 7052 borosilicate glass and was supported from the vertical flange of the heat pipe. The bottom of the borosilicate cathode was filled with graphite. The

Table 4. Perturbed levels in the $B^1\Pi$ state of NaK that should be useful as electric field sensors. (Also given are the excitation vibration and rotation quantum numbers, wavelengths, and Franck Condon factors.)

V'	J'	V"	J"	λ	FcF
2	40	0	39	5857.547	7(2)
		0	41	5862.792	
		1	39	5899.832	8(3)
		1	41	5905.127	
		2	39	5942.376	4(4)
		2	41	5947.722	
		5	39	6071.522	8(5)
		5	41	6077.016	
2	28	0	27	5850.966	7(2)
		0	29	5854.662	
		1	27	5893.284	8(3)
		1	29	5897.015	
		2	27	5935.864	4(4)
		2	29	5939.631	
		5	27	6065.143	8(5)
		5	29	6069.017	
8	42	0	41	5745.743	1(6)
		0	43	5751.034	
		1	41	5786.398	2(6)
		1	43	5791.739	
		2	41	5827.291	2(6)
		2	43	5832.681	
			Others		
2	30				
	32				
	34				
	35				
8	32				
	36				
	38				
	40				
	41				
	42				

Table 5. Relevant data in the NaK studies.

NaK $B^1\Pi$
$\mu\tau$ = 36 ± 1.8 Debye ns
$q(V' = 5) = 1.55 \times 10^{-6}$ cm^{-1}
e-f = 100 to 300 MHz
$\Delta\nu_{nat}$ = 33 MHz
$\Delta\nu_{doppler}$ = 650 MHz
$A = 5 \times 10^{7}$ s^{-1}
$\tau_{rad} \simeq$ 50 ns

Source: Derouard and Sadeghi, 1986a.

Collisional Quenching Crosssections (V' = 17, J' = 94)
He 138 ± 4 Å^2
Ne 213 ± 5
Ar 219 ± 6
Kr 257 ± 6
Xe 312 ± 8

Source: Auzin'sh, Ferbert, Harya, and Pirags, 1986.

NaK $X^1\Sigma^+$
$\Delta_2F(J) = 6.5 \cdot J$ GHz
J_{max} = 48

TDL 50 Dye Laser (Rhodamine 6G)
$\Delta\nu$ = 1.2 GHz
τ_{laser} = 7 ns

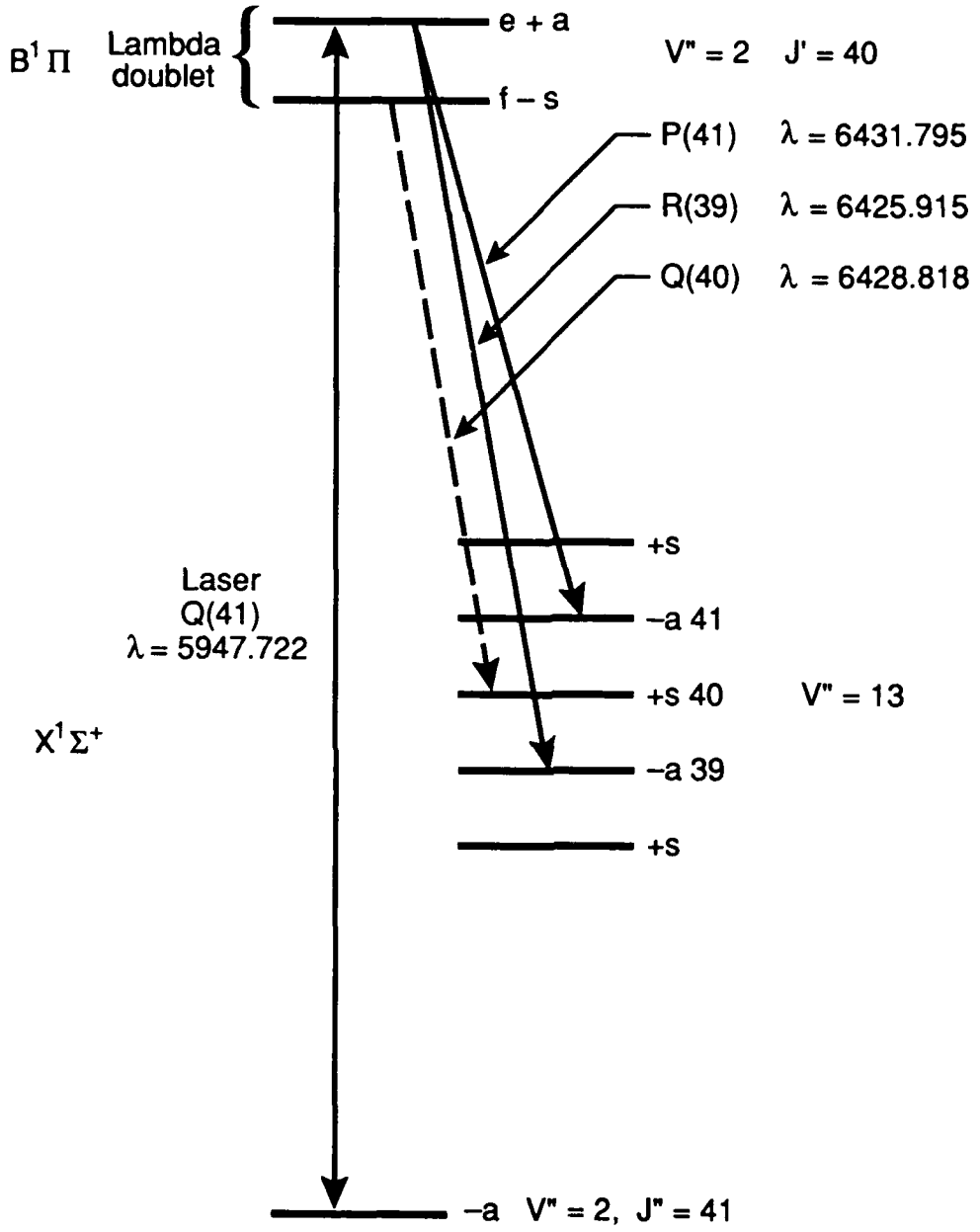

Note: Double arrow is the laser, solid lines are allowed transitions, and dashed line is the forbidden transition used to measure electric fields.

Figure 5. Schematic of the excitation of the perturbed level V' = 2, J' = 40 of the $B^1\Pi$ state of NaK.

Table 6. Molecular constants of ground state $X^1\Sigma^+$ of NaK (in wavenumbers).

$Y_{10} = 0.12402918 \times 10^{3}$	$Y_{51} = -0.33326919 \times 10^{-10}$
$Y_{20} = -0.49628545$	$Y_{02} = -0.22057475 \times 10^{-6}$
$Y_{30} = -0.66092780 \times 10^{-3}$	$Y_{12} = -0.17942494 \times 10^{-8}$
$Y_{40} = -0.25767638 \times 10^{-4}$	$Y_{22} = -0.12731163 \times 10^{-10}$
$Y_{50} = 0.30465660 \times 10^{-7}$	$Y_{32} = 0.12552724 \times 10^{-11}$
$Y_{60} = 0.17743135 \times 10^{-11}$	$Y_{42} = -0.51791743 \times 10^{-13}$
$Y_{70} = -0.30650023 \times 10^{-10}$	$Y_{03} = 0.35280369 \times 10^{-12}$
$Y_{01} = 0.95199891 \times 10^{-1}$	$Y_{13} = 0.13035033 \times 10^{-13}$
$Y_{11} = -0.44965613 \times 10^{-3}$	$Y_{23} = -0.10662389 \times 10^{-14}$
$Y_{21} = -0.18241614 \times 10^{-5}$	$Y_{04} = -0.62850566 \times 10^{-18}$
$Y_{31} = -0.10299474 \times 10^{-6}$	$Y_{14} = 0.65940467 \times 10^{-19}$
$Y_{41} = 0.20602544 \times 10^{-8}$	

Table 7. Molecular constants of state $B^1\Pi$ of NaK (in wavenumbers).

$T_e = 16992.305^a$	$Y_{11} = -0.1012 \times 1^{-2}$
$Y_{10} = 71.756$	$Y_{21} = -0.4358 \times 10^{-4}$
$Y_{20} = -1.2533$	$Y_{31} = 0.1354 \times 10^{-5}$
$Y_{30} = 0.4388 \times 10^{-2}$	$Y_{02} = -0.2288 \times 10^{-6}$
$Y_{40} = 0.7806 \times 10^{-4}$	$Y_{12} = -0.4435 \times 10^{-7}$
$Y_{01} = 0.7210 \times 10^{-1}$	$Y_{22} = 0.3548 \times 10^{-8}$

[a] T_e is the energy difference between minima of the $X^1\Sigma^+$ and $B^1\Pi$ states.

Table 8. Franck-Condon factors for the $X^1\Sigma^+$-$B^1\Pi$ band system of NaK.

V' / V''	0	1	2	3	4	5	6	7	8	9	10	11	12	13	14	15	16	17	18	19	20
0	4	8(1)	7(2)	4(3)	2(4)	7(4)	2(5)	5(5)	1(6)	2(6)	3(6)	4(6)	4(6)	4(6)	3(6)	3(6)	2(6)	9(5)	4(5)	8(4)	7(3)
1	7(1)	1(3)	8(3)	4(4)	1(5)	4(5)	8(5)	1(6)	2(6)	2(6)	2(6)	1(6)	2(5)	6(4)	9(5)	2(6)	3(6)	4(6)	3(6)	2(6)	8(5)
2	5(2)	7(3)	4(4)	2(5)	5(5)	1(6)	2(6)	2(6)	2(6)	1(6)	1(5)	8(4)	7(5)	1(6)	1(6)	3(5)	1(4)	8(5)	2(6)	3(6)	3(6)
3	3(3)	3(4)	1(5)	5(5)	1(6)	2(6)	2(6)	1(6)	3(5)	4(3)	4(5)	1(6)	9(5)	3(5)	1(3)	4(5)	8(5)	6(5)	8(4)	2(5)	1(6)
4	1(4)	1(5)	4(5)	1(6)	2(6)	2(6)	1(6)	1(5)	1(5)	7(5)	1(6)	5(5)	2(4)	2(5)	8(5)	7(5)	2(5)	1(4)	3(5)	5(5)	2(5)
5	4(4)	3(5)	8(5)	1(6)	2(6)	8(5)	8(4)	2(5)	8(5)	8(5)	2(5)	3(4)	5(5)	7(5)	3(5)	1(3)	3(5)	7(5)	5(5)	6(4)	3(4)
6	1(5)	5(5)	1(6)	2(6)	1(6)	9(4)	2(5)	8(5)	7(5)	1(5)	1(5)	6(5)	5(5)	7(4)	1(5)	5(5)	5(5)	6(4)	1(5)	5(5)	5(5)
7	2(5)	9(5)	2(6)	1(6)	2(5)	1(5)	8(5)	6(5)	6(5)	2(5)	6(5)	4(5)	4(3)	2(5)	5(5)	2(5)	3(3)	3(5)	5(5)	2(5)	5(3)
8	4(5)	1(6)	2(6)	4(5)	5(4)	7(5)	7(5)	6(4)	2(5)	6(5)	3(5)	5(3)	4(5)	5(5)	8(4)	8(4)	4(5)	3(5)	2(4)	1(5)	3(5)
9	8(5)	2(6)	9(5)	6(3)	5(5)	8(5)	1(5)	2(5)	6(5)	3(5)	2(4)	4(5)	4(5)	2(4)	2(5)	4(5)	2(5)	2(4)	3(5)	4(5)	8(4)
10	1(6)	2(6)	3(5)	2(5)	8(5)	3(5)	9(4)	6(5)	3(5)	2(4)	4(5)	3(5)	2(3)	3(5)	4(5)	6(4)	8(4)	4(5)	2(5)	1(2)	2(5)
11	2(6)	1(6)	1(2)	7(5)	5(5)	9(3)	5(5)	4(5)	7(3)	4(5)	3(5)	3	3(5)	3(5)	2(4)	2(5)	4(5)	1(5)	4(4)	3(5)	2(5)
12	2(6)	5(5)	3(5)	9(5)	6(4)	4(5)	5(5)	3(3)	4(5)	4(5)	2(2)	3(5)	3(5)	4(3)	2(5)	3(5)	3(4)	1(5)	3(5)	1(5)	5(3)
13	2(6)	9(4)	8(5)	5(5)	1(5)	6(5)	7(4)	3(5)	4(5)	8(3)	3(5)	3(5)	2(3)	3(5)	3(5)	6(3)	2(5)	3(5)	3(4)	9(4)	2(5)
14	2(6)	3(4)	1(6)	3(4)	6(5)	3(5)	1(5)	5(5)	5(4)	2(5)	4(5)	4(3)	3(5)	3(5)	6(2)	2(5)	3(5)	5(3)	2(5)	3(5)	5(4)
15	2(6)	4(5)	7(5)	1(5)	7(5)	8(2)	5(5)	2(5)	1(5)	4(5)	2(4)	2(5)	3(5)	1(2)	2(5)	2(5)	2(2)	2(5)	2(5)	3(3)	1(5)
16	1(6)	9(5)	2(5)	6(5)	3(5)	3(5)	4(5)	2(4)	5(5)	8(4)	2(5)	3(5)	2(3)	2(5)	2(5)	3(3)	2(5)	2(5)	3(3)	2(5)	2(5)
17	9(5)	1(6)	4(1)	8(5)	0.1	6(5)	5(4)	4(5)	2(5)	9(4)	4(5)	2(4)	2(5)	2(5)	4(3)	3(5)	1(5)	2(4)	2(5)	1(5)	1(3)
18	6(5)	1(6)	2(5)	5(5)	3(5)	4(5)	1(5)	4(5)	5(3)	4(5)	7(4)	2(5)	3(5)	7(2)	3(5)	1(5)	3(4)	3(5)	9(4)	3(4)	2(5)
19	3(5)	1(6)	7(5)	1(5)	7(5)	3(4)	5(5)	8(4)	3(5)	2(5)	9(4)	3(5)	4(3)	2(5)	1(5)	3(4)	3(5)	7(4)	7(4)	2(5)	6(4)
20	2(5)	1(6)	1(6)	3(4)	6(5)	1(5)	4(5)	8(4)	4(5)	6(3)	4(5)	4(4)	2(5)	2(5)	2(4)	2(5)	7(4)	8(4)	2(5)	2(4)	7(4)

[a]Numbers in parenthesis are exponents.

Source: Derouard [1987].

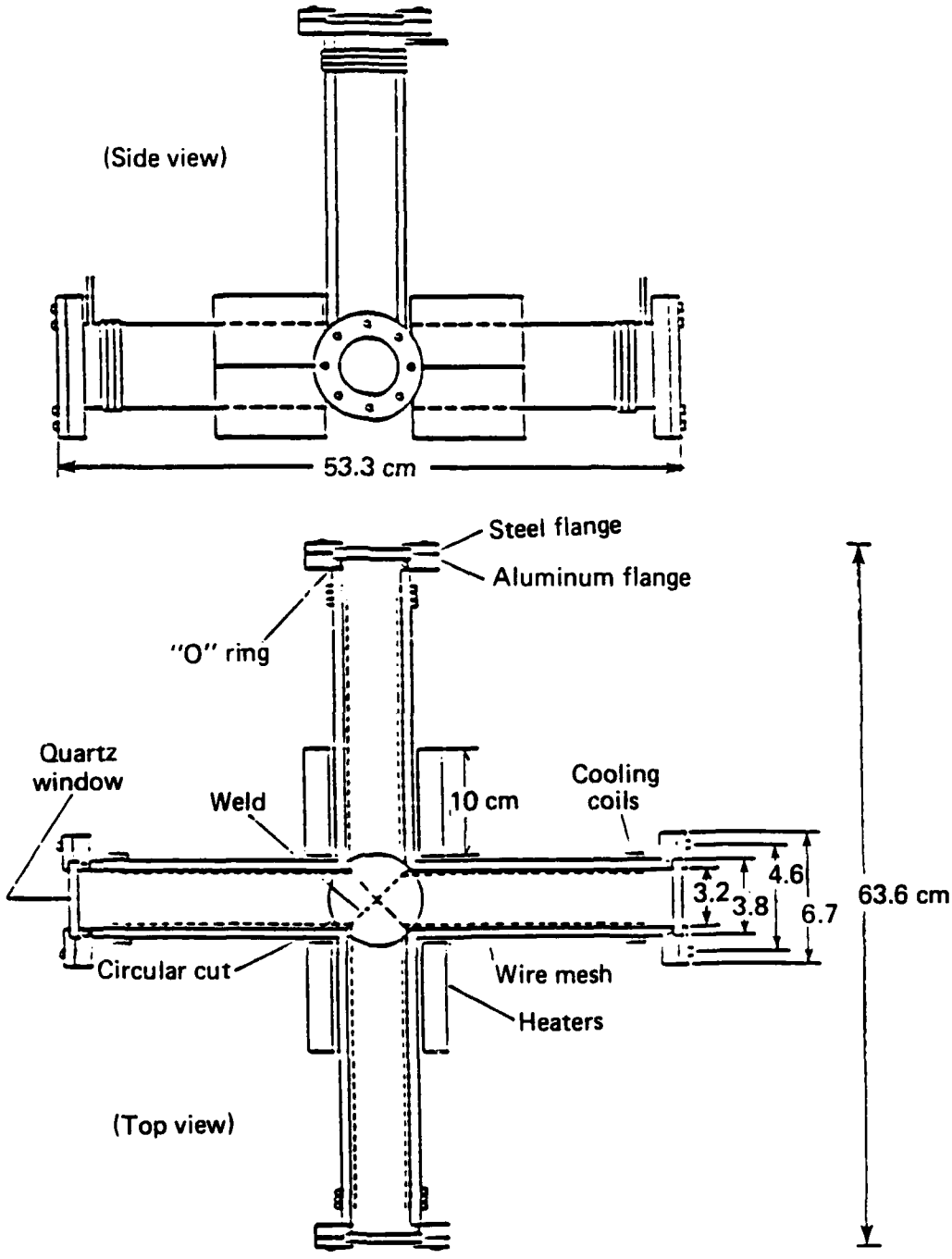

Figure 6. Heat-pipe oven for NaK experiments.

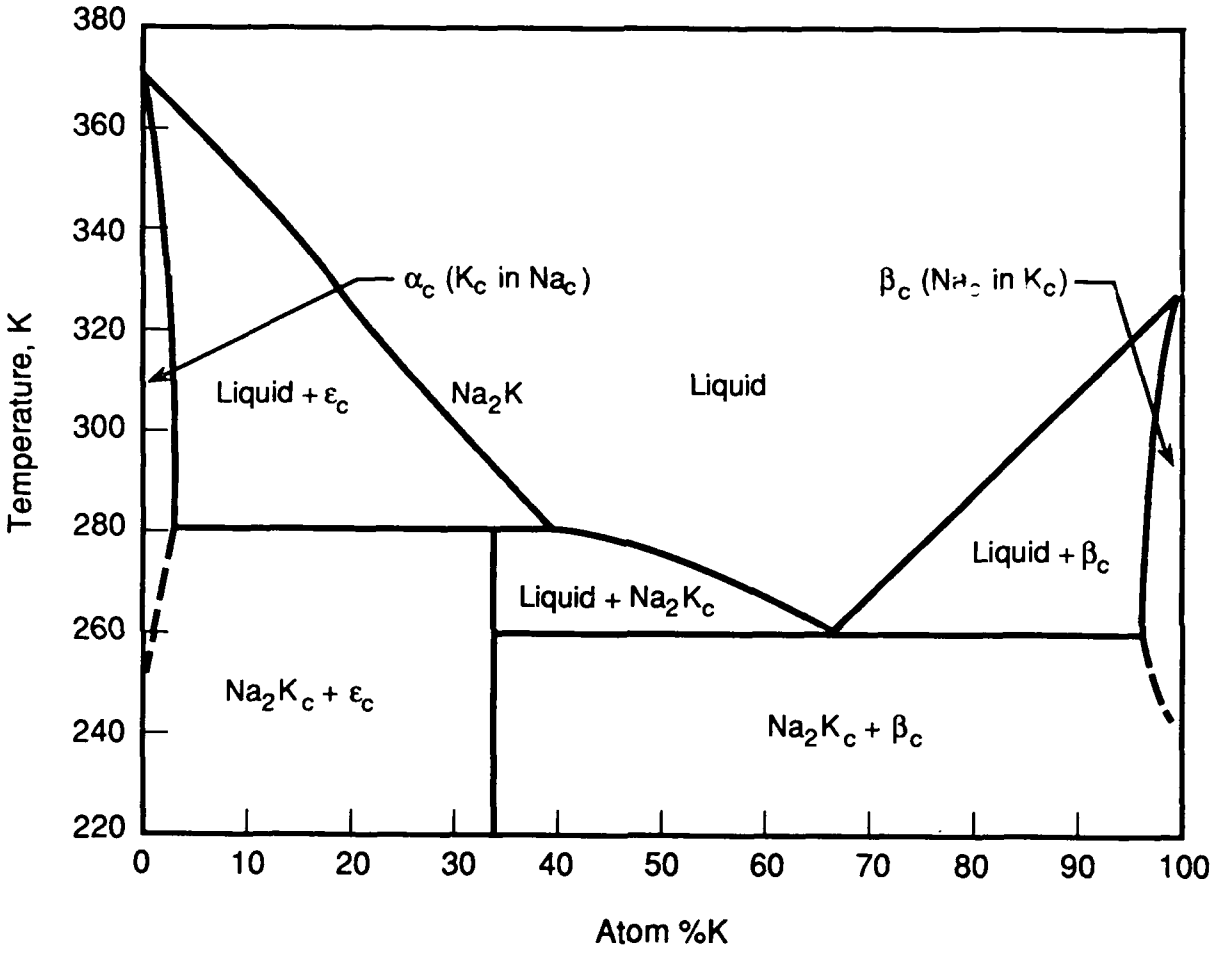

Figure 7. Phase diagram of Nak.

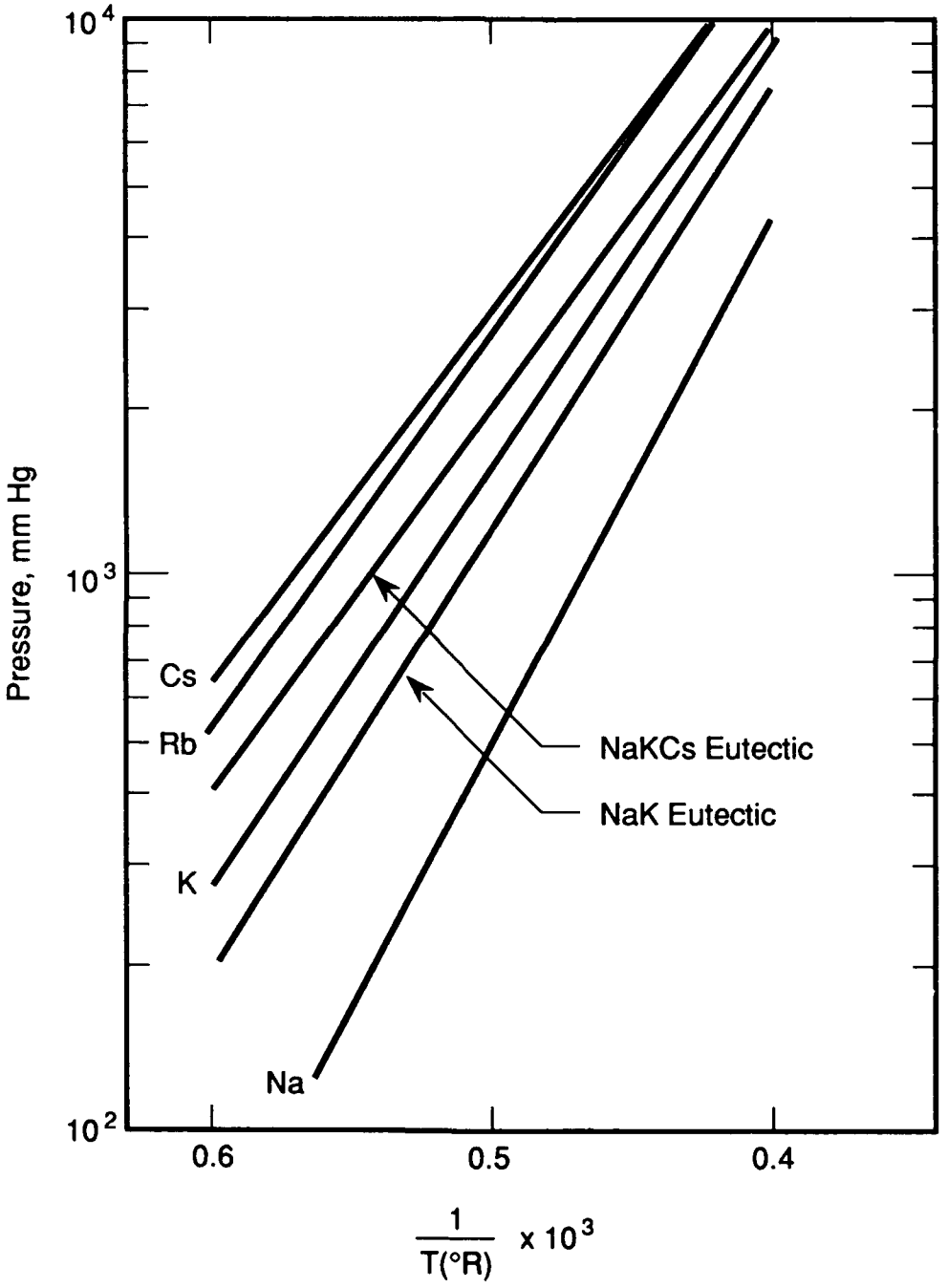

Source: Mausteller, Tepper, and Rodgers [1967].

Figure 8. Vapor pressure of the alkali metals and Nak above the eutectic.

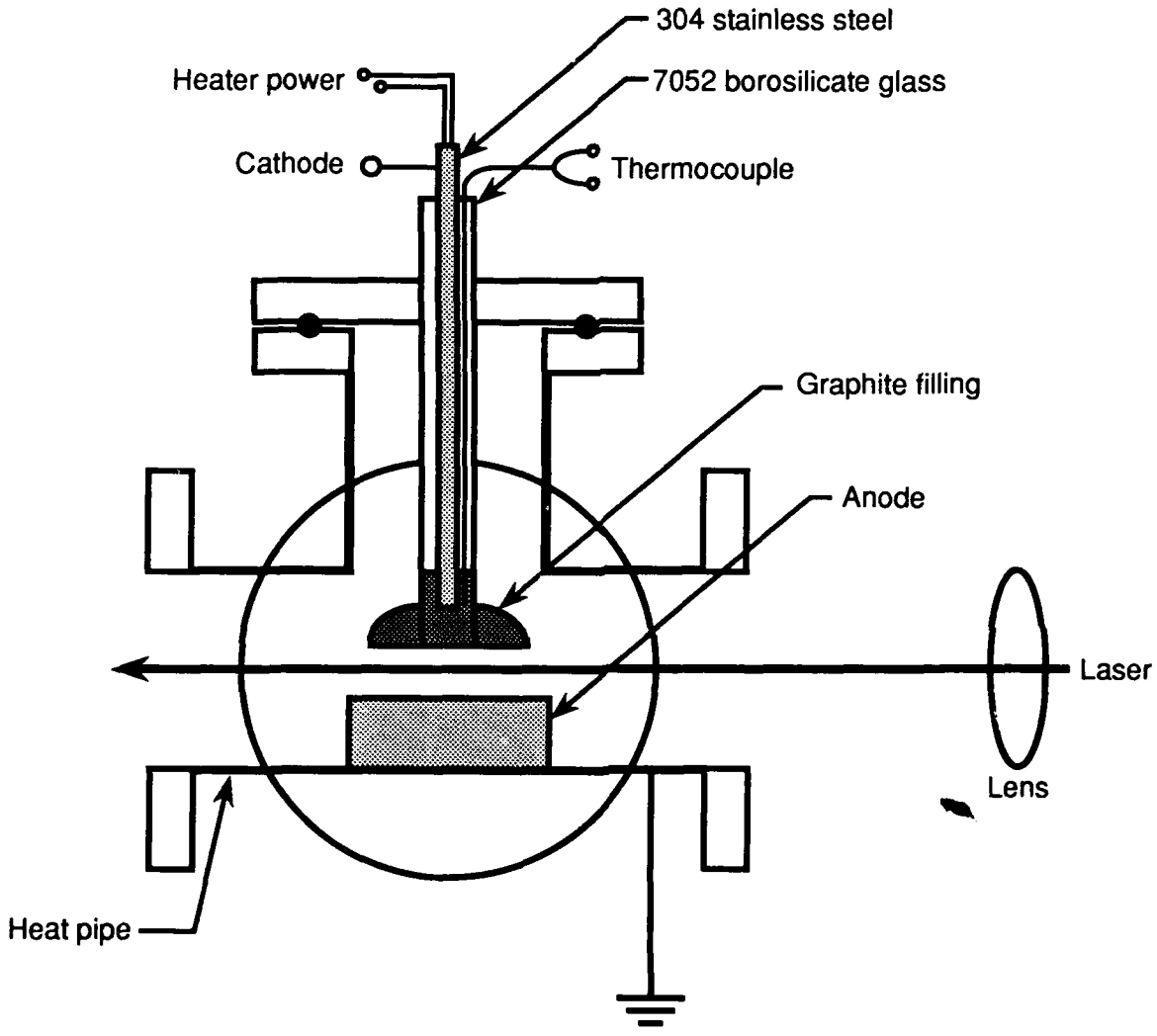

Figure 9. Electrode arrangements used in the NaK heat pipe (cathode diameter = 1.5 cm, anode diameter = 2.5 cm, and electrode gap = 1 cm).

cathode was electrically heated with an electrically insulated stainless steel heater (ARI Industries Model BXX13B7-11K). The temperature of the cathode (with heater power on) or the NaK vapor (with heater power off) was monitored with an electrically insulated chromel-alumel thermocouple. Potentials from 0 to 2000 V (Kepco APH 2000M) were applied directly across the stainless steel heater sheath and the grounded heat pipe. The electrode gap was 1 cm. The probe was operated at a temperature slightly above that of the NaK vapor. This completely eliminated metal vapor condensation on the cathode.

The experimental setup is shown schematically in Fig. 10. A 10 Hz, doubled Nd:YAG laser (Quantel Model 581) pumped a tunable dye laser (TDL-50) containing Rhodamine 6G dye for the excitation. The dye laser beam was focussed with a 50 cm focal length lens at the center of the electrode gap. The fluorescence was collected with a 25 cm focal length lens and imaged onto the slit of a 0.75 m monochromator (Spex 1702/04) equipped with an EMI 9813QB photomultiplier. The signals were processed with a boxcar integrator (SRS 250), analog to digital converter (SR 245) and timing amplifier (Ortec 574). The spectra were displayed and stored on an IBM PC.

6.4 RESULTS AND DISCUSSION.

The excitation spectrum for the experiment is shown in Fig. 11. This was taken by scanning the laser wavelength and monitoring the P(41) fluorescence to V" = 13 at 6431.8 Å. Next, the laser was set at 5942.376 Å and the monochromator scanned, thus obtaining the spectrum in Fig. 12. In these studies fluorescence to V" = 13 was monitored (indicated by the arrows). With 300 V applied to the electrodes, a scan of the region 6425 to 6433 Å is shown in Fig. 13. The forbidden Q(40) transition can be clearly seen at 6428.818 Å. With the laser set to pump the P(41) transition at 5947.722 (see Fig. 11), scans of the fluorescence in the region 6425 to 6433 Å were performed repetitatively with increasing voltage, the result is shown in Fig. 14. The ratios of the intensities I(Q)/I(R) and I(Q)/I(P) are shown plotted in Fig. 15. The sensitivity (S) of the electric field measurement is defined (for the R branch) as

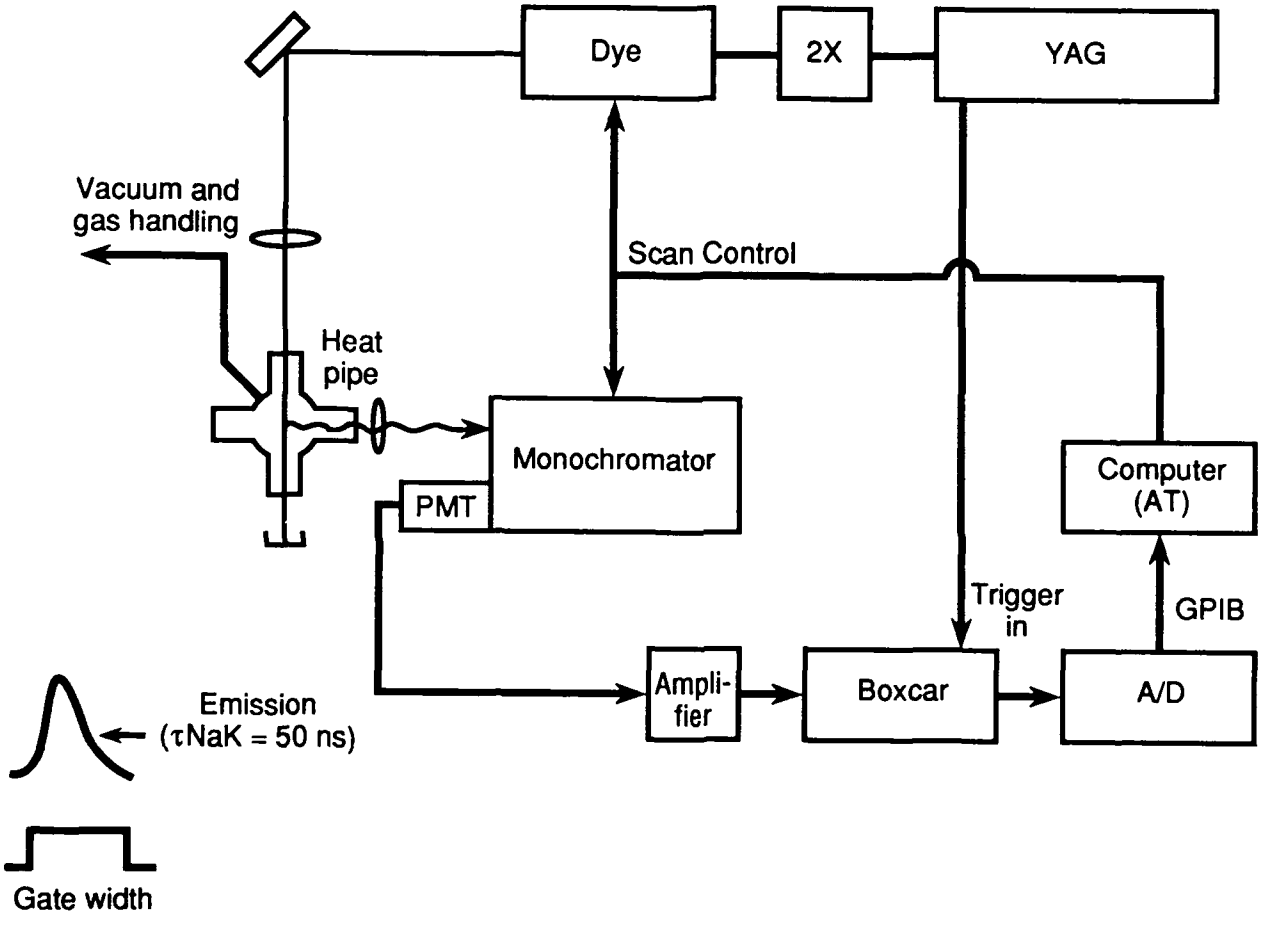

Figure 10. Experimental setup.

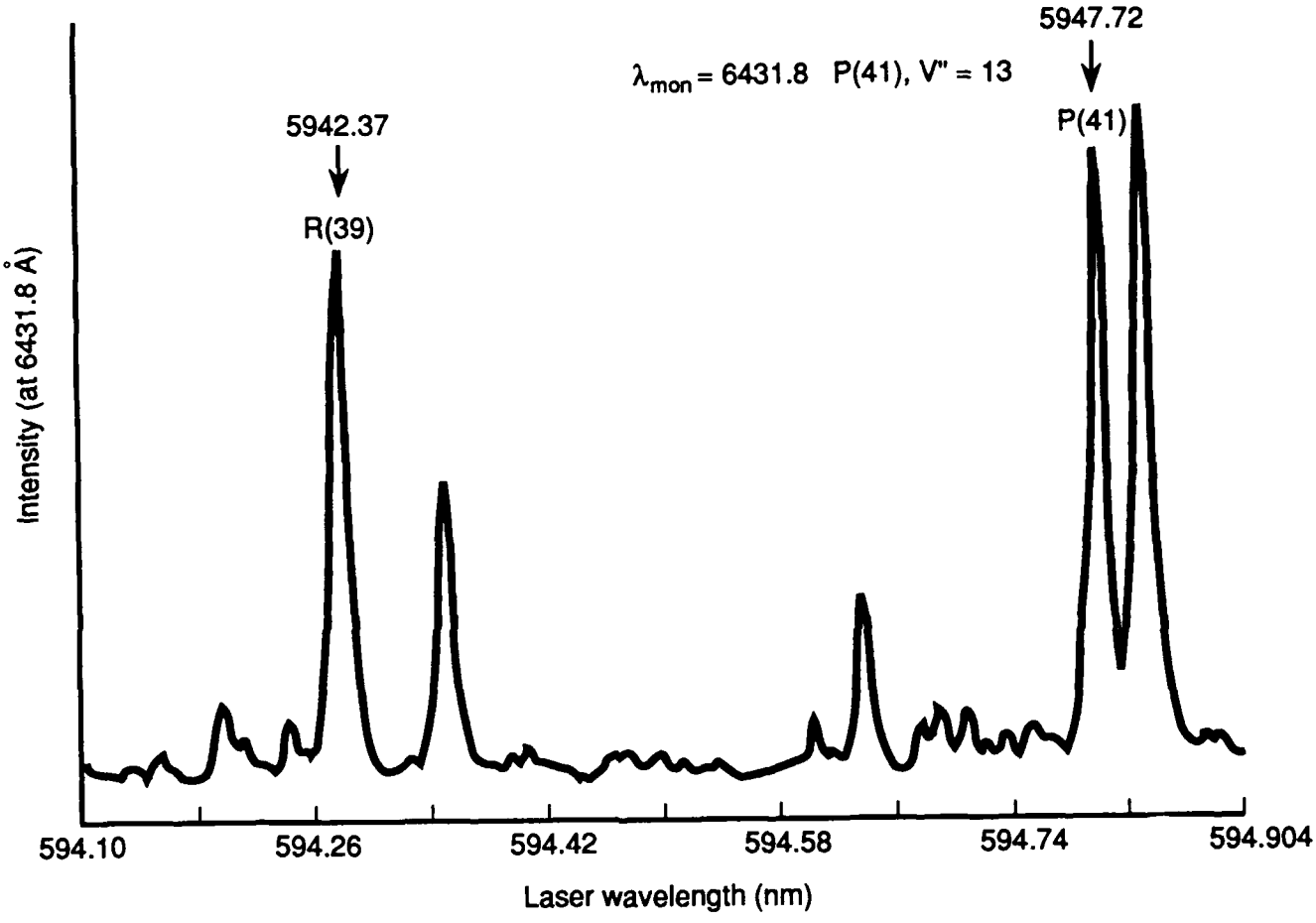

Figure 11. NaK excitation spectrum for the V" = 2 → V' = 2 transitions.

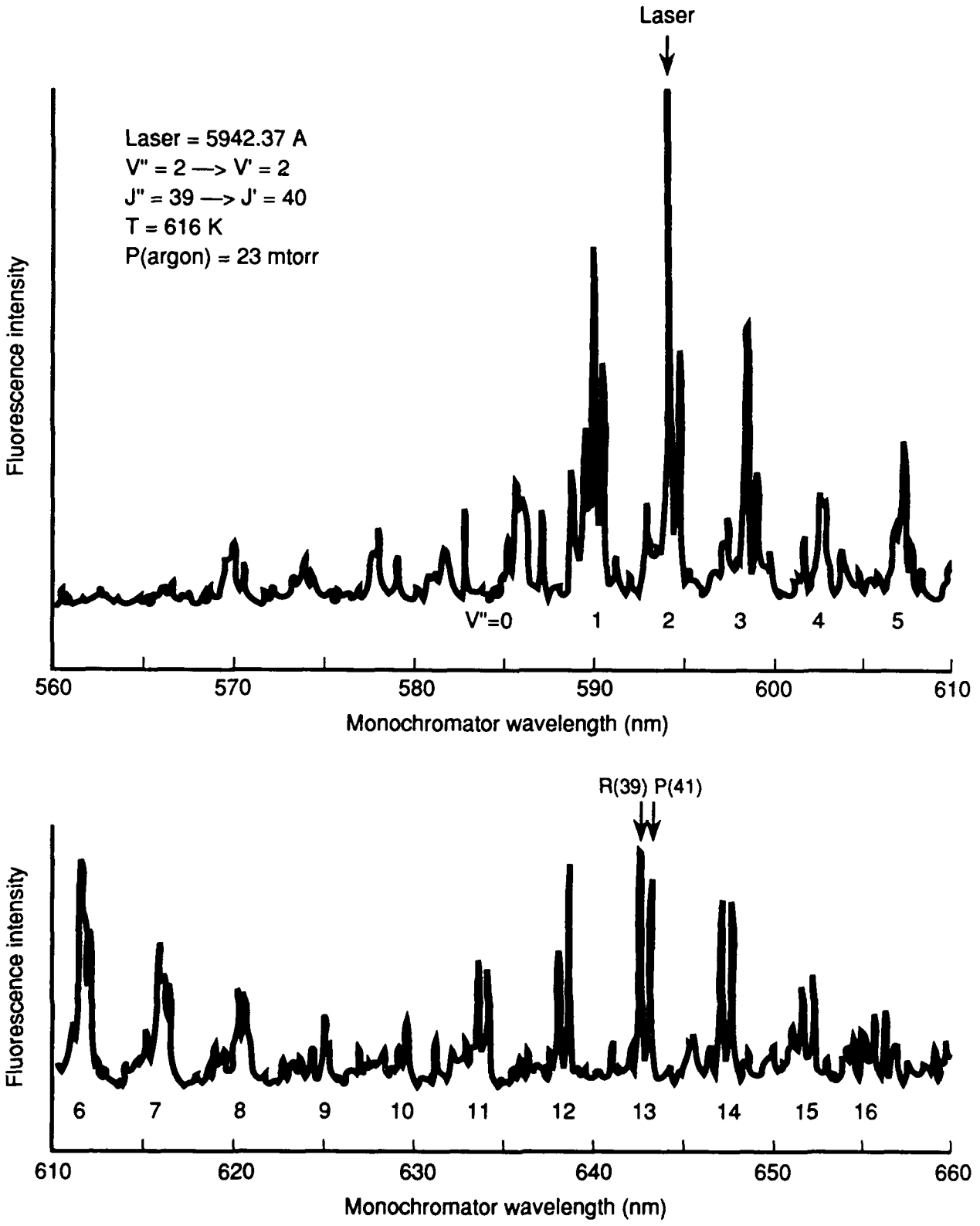

Figure 12. NaK laser-induced fluorescence spectrum for the transitions V' = 2, J' = 40 → V", J" = 39, 40, 41.

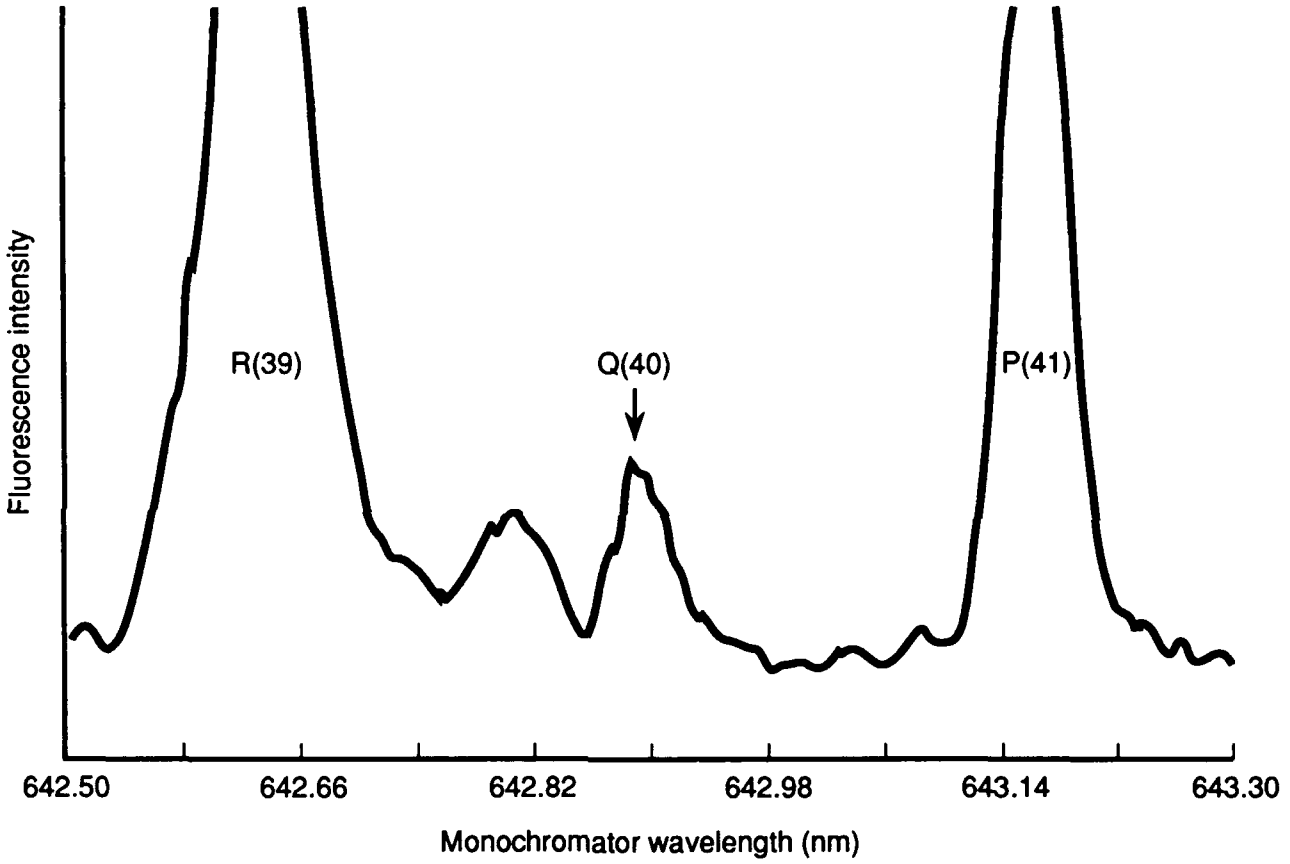

Figure 13. Close-up of fluorescence RP doublets to V" = 13 with 300 V applied to the electrodes.

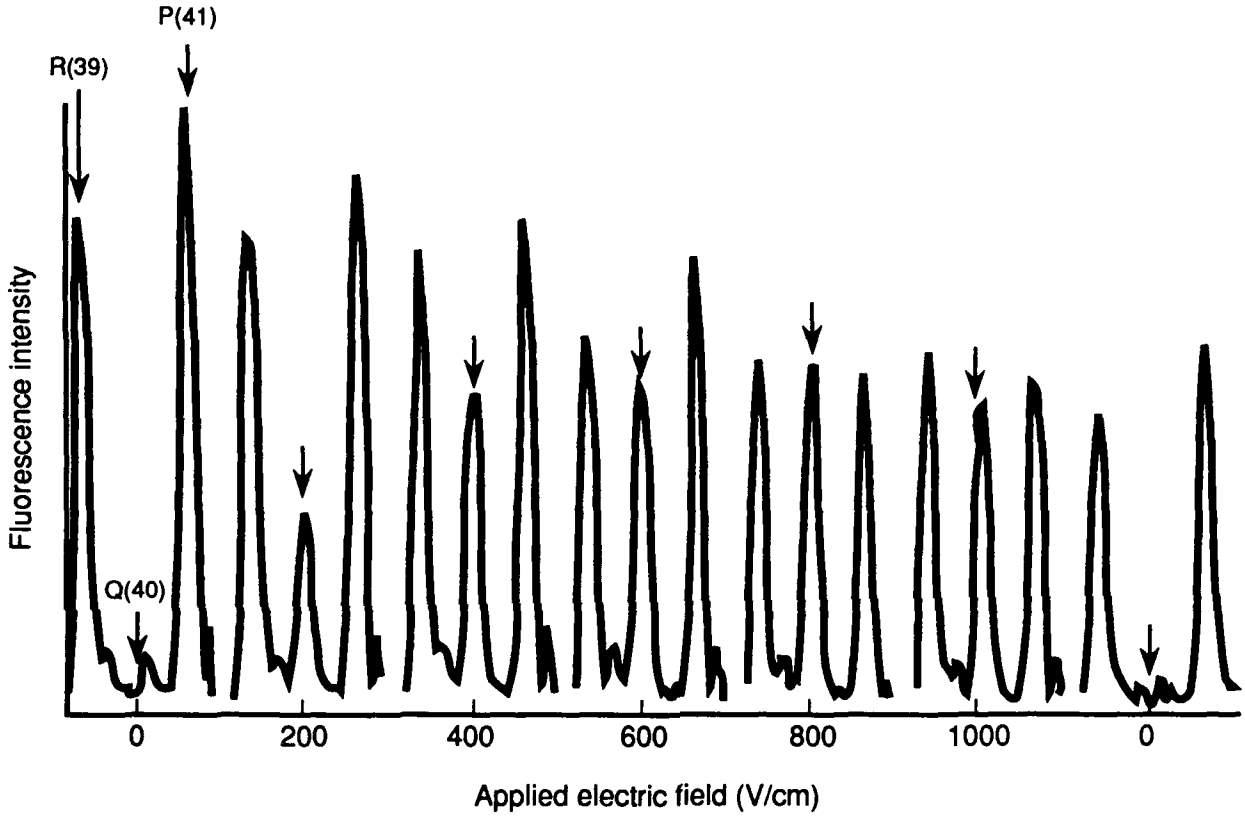

Experimental conditions:
Power (laser) = 6 mW
Pressure (argon) = 20 mtorr
Temperature = 662 K
Slits = 160/160 μ
Boxcar sensitivity = 0.2 V

Figure 14. A succession of electric field measurements.

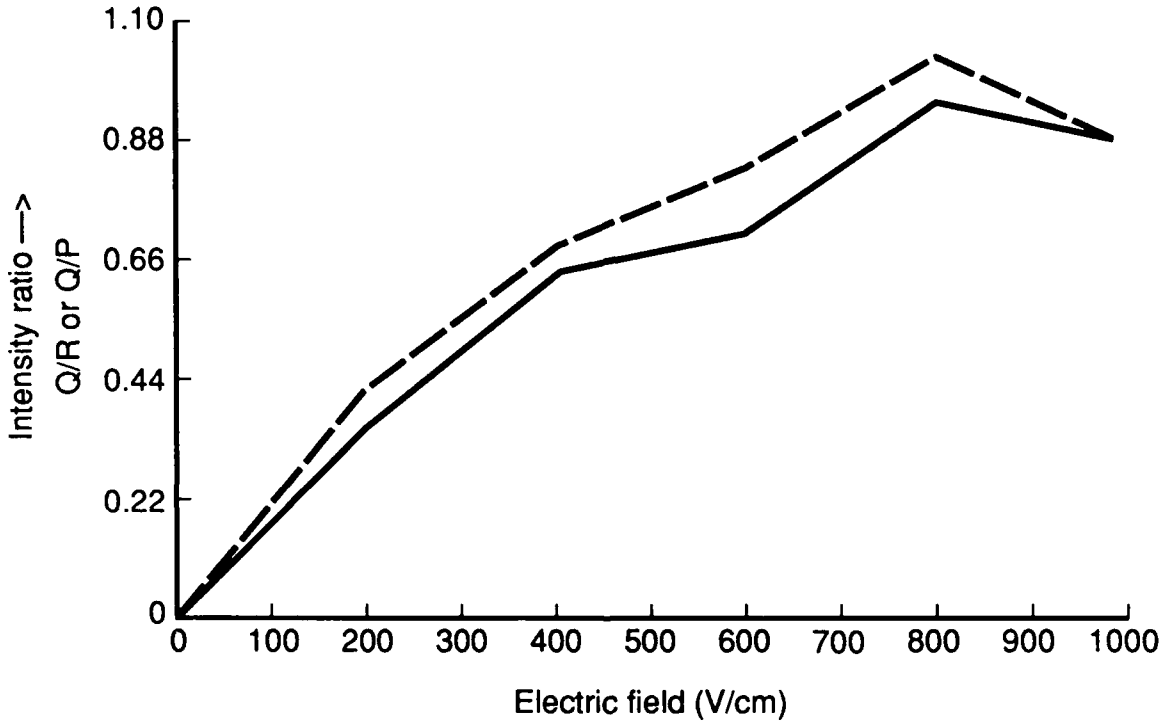

Note: Dashed and solid lines are for the Q/R and Q/P intensity ratios, respectively.

Figure 15. Ratios of forbidden to allowed intensities versus electric potential (taken from data given in Fig. 11).

$$S_R = d[I(Q)/I(R)]/dV \quad .$$

For the data point at 800 V/cm in Table 9, the sensitivity is 0.00125 cm V^{-1}. By direct comparison, this is the **same** sensitivity (± 10 percent) reported by Derouard and Sadeghi [1987] for their measurements with the same level (V' = 2, J' = 40) at an electric field strength of 1000 V cm^{-1}.

Fluorescence intensity was found to increase with temperature as shown in Fig. 16. The temperature indicated is of the NaK vapor with an Argon buffer gas pressure of 24 mtorr. The gradual increase in fluorescence intensity is presumably due to the increasing thermal population of V" = 2.

The variation of fluorescence intensity with Argon pressure at a fixed temperature (710 K) is shown in Fig. 17. Strong collisional quenching of the fluorescence is seen for pressures above 100 mtorr.

The variation in sensitivity versus laser power is shown in Fig. 18. At a fixed temperature of 680 K, and argon pressure of 70 mtorr, an electric field of 1000 V cm^{-1} was applied to the electrodes. The laser power was decreased while the monochromator repetitively scanned over the region 6425 to 6433 Å. It is noteworthy that the sensitivity is a strong function of laser power. This observation has not been reported in the literature. Several repeats of

Table 9. Data points used in Fig. 15.

V/cm	Q/R	Q/P	S_R(cm V^{-1})	S_p(cm V^{-1})
0	0	0	--	--
200	0.41	0.35	2.0×10^{-3}	1.75×10^{-3}
400	0.68	0.65	1.7×10^{-3}	1.63×10^{-3}
600	0.83	0.70	1.38×10^{-3}	1.17×10^{-3}
800	1.00	0.95	1.25×10^{-3}	1.18×10^{-3}
1000	0.88	0.88	0.88×10^{-3}	0.88×10^{-3}

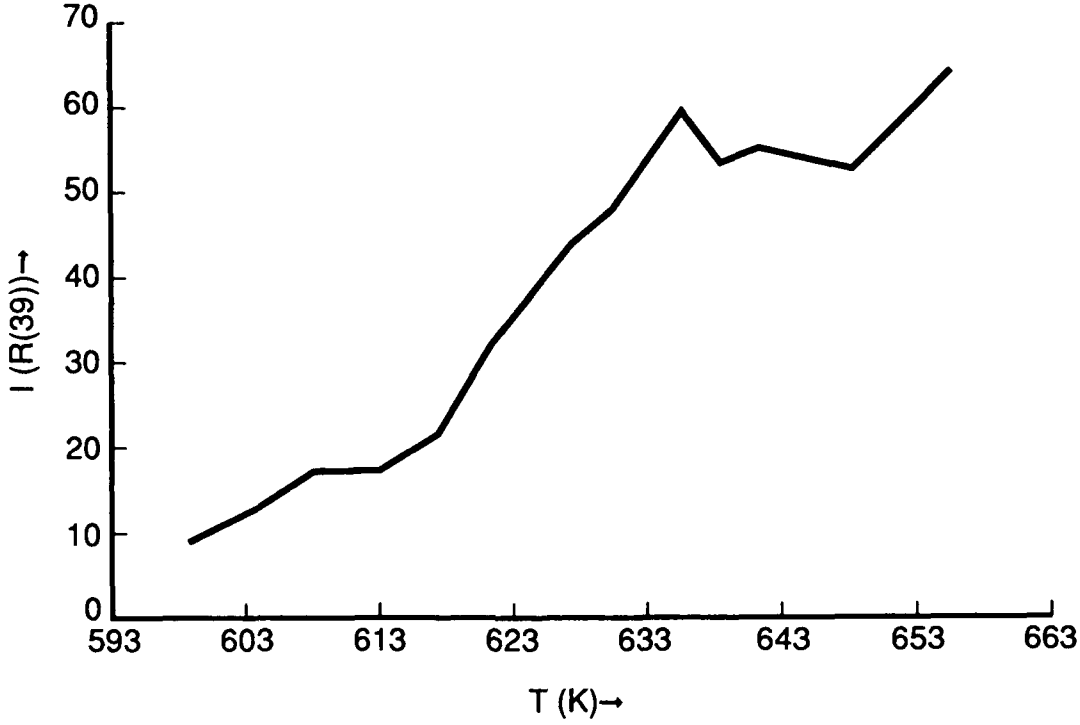

Figure 16. Intensity of the R(39) fluorescence line versus temperature.

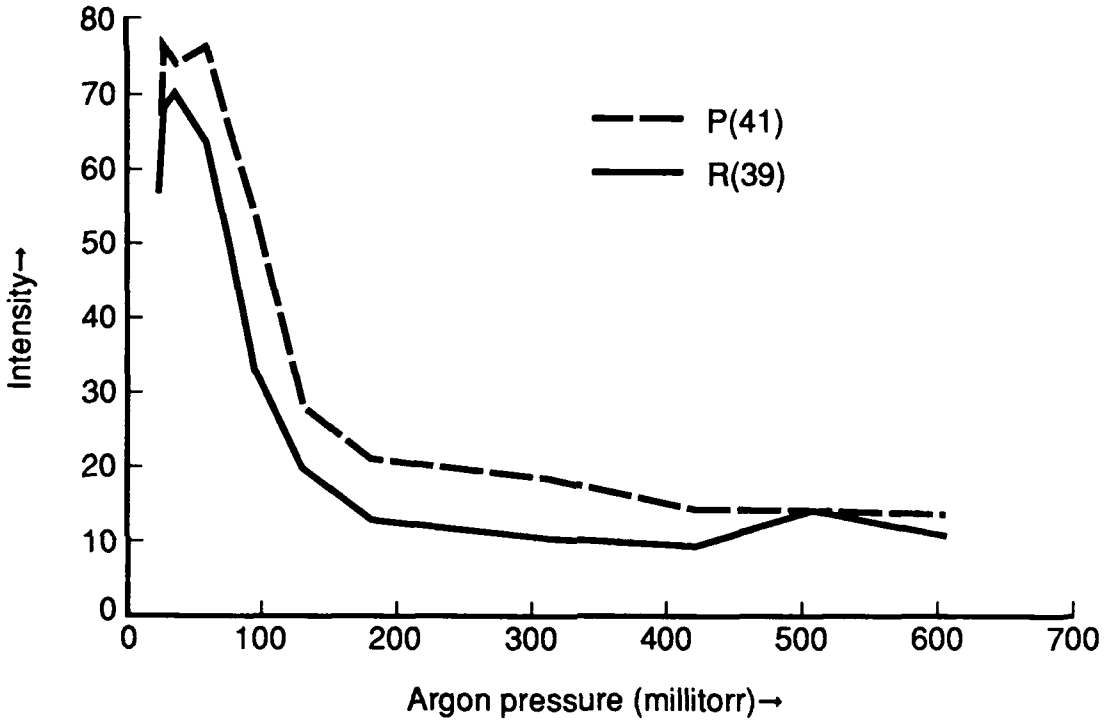

Figure 17. Fluorescence intensity of the R(39) and P(41) transitions versus buffer gas pressure, T ≈ 710°K.

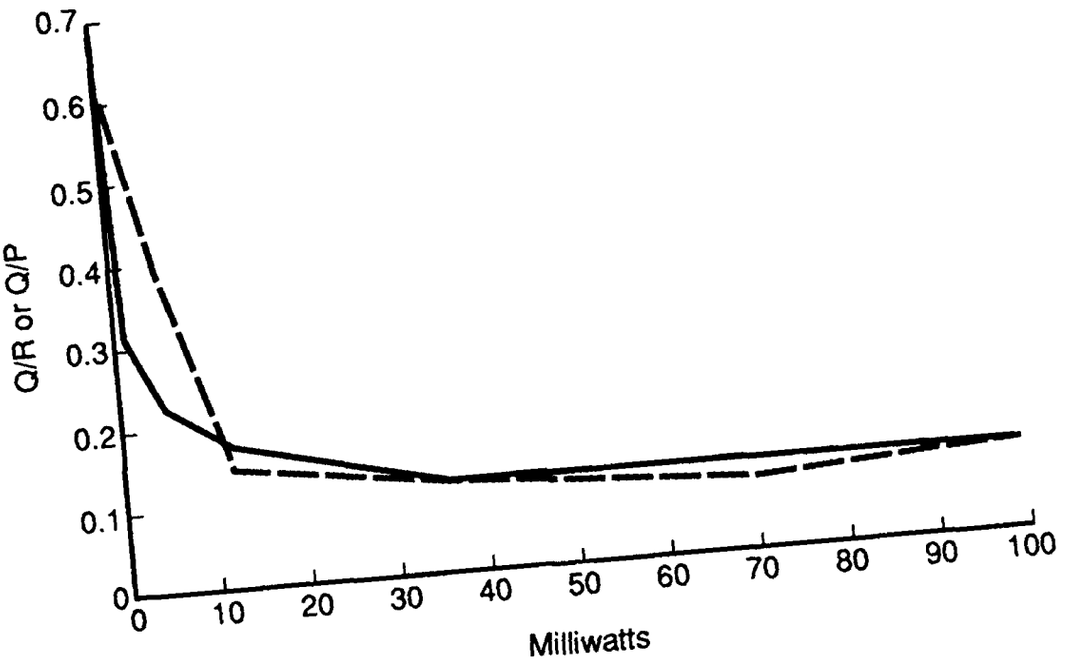

Figure 18. Forbidden to allowed intensity ratios versus laser power. (The dashed and solid lines give the I(Q)/I(R) and I(Q)/I(P) dependencies on laser power, respectively.)

the experiment have confirmed that the phenomenon is real. Presumably, at high laser power the gas becomes partially ionized by resonant multiphoton absorption through the molecular manifold of the dimers present in the vapor. This ionization then reduces the magnitude of the electric field in the immediate vicinity of the laser beam leading to a decrease in sensitivity. More work would be required to determine the mechanism of this effect.

6.5 CONCLUSIONS.

The measurement of a steady state electric field using NaK prepared in the perturbed level $V' = 2$, $J' = 40$ was successful. The sensitivity (0.00125 cm V^{-1}) was found to be the same as with experiments done in cells using low power continuous lasers. However, the lowest electric field that could be measured was roughly 50 V cm^{-1}, this an order of magnitude higher than the results obtained by Derouard and Sadeghi [1986a]. The optimum buffer gas pressure is roughly 50 mtorr. No optimum temperature was found. The dramatic decrease in sensitivity with increasing laser power implies that the laser is beginning to seriously perturb the medium at intensities above 10^6 to 10^7 W cm^{-2}.

SECTION 7
ICl EXPERIMENTS

Following the conclusion of the NaK experiments, a second search for other heteronuclear diatomic molecules that could serve as electric field sensors was conducted. The interhalogens were considered on the bases of having the correct electronic states with convenient absorption and emission wavelengths, favorable vapor pressure characteristics, and well characterized potential energy curves. The interhalogens have ground $X^1\Sigma^+$ states and optically accessible $A^3\Pi_1$ first excited states. ICl was determined to be the best candidate. Hybrid potential curves were constructed and intensity calculations were performed for the lowest 16 vibrational levels of the X state and the lowest 36 levels of the A state. The intensity computations resulted in a complete table of FCFs and the X to A bands. A cell was constructed and successfully tested. An excitation spectrum of low signal to noise was obtained.

7.1 INTRODUCTION.

The interhalogens all have dipole moments in their ground states as shown in Table 10 [Moody and Thomas, 1971]. The relevant potential

Table 10. Dipole moments of the interhalogens.

Interhalogen	Dipole Moment (Debye)
BrF	1.29
ClF	0.88
ICl	0.60
IBr	1.30
BrCl	0.57

Source: Moody and Thomas [1971, p. 37].

energy curves [Hulthén, Järlsäter, and Koffman, 1960] for ICl are shown in Fig. 19. The A-X band system of ICl is in a convenient region of the spectrum and hence laser-induced fluorescence may be excited using Rhodamine 6G dye in the region 5800 to 6050 Å. Electronic transitions between these states results in the same spectral features (RP and Q branches) and the selection rules as in the case of NaK on its $X^1\Sigma^+$ to $B^1\Pi$ band system. As shown in Fig. 20 (left side), one obtains a Q branch "forbidden" transition for R(J) [or P(J)] excitation and (right side) RP branch "forbidden" transitions for Q(J) excitation.

7.2 RELEVANT PROPERTIES.

Measured properties of the ICl $A^3\Pi_1$ state from the literature have been compiled in Table 11. The rather long radiative lifetimes and large collisional self-quenching coefficients of the A state are the main disadvantages. These two properties put an upper limit to the pressure in the cell of about 5 torr [Clyne and McDermid, 1976]. The cell can be operated at larger pressures provided a noble gas is used. Neon was found to have the smallest quenching coefficient. The Lambda doubling constant, q_o is reported to be 1.4×10^{-5} cm^{-1} [Hulthén, Järlsäter, and Koffman, 1960]. Measured line widths are quite narrow due to the low temperature and long radiative lifetimes, and these compare favorably with the laser linewidth. Gaseous ICl exists in equilibrium with I_2 and Cl_2; the small equilibrium constant is favorable since it indicates that ICl is the major constituent in the vapor. The presence of I_2 is of concern since it absorbs strongly on its $B^3\Pi^+_{ou}$-$X^1\Sigma^+$ system that overlaps the A-X band system of ICl. This seems to be a serious disadvantage primarily because the B-X system of I_2 absorption is roughly 50 times stronger than the ICl A-X system [Holleman and Steinfeld, 1971]. However, because of the radiative lifetime of the I_2 $B^3\Pi^+_{ou}$ state is only 1 to 1.5 μs [Holleman and Steinfeld, 1971], I_2 fluorescence has ceased 10 μs after the laser pulse, ICl continues to radiate for considerably longer times (~100 μs) (at sufficiently low pressure). Consequently, I_2 fluorescence can be completely eliminated by delaying the gated detection

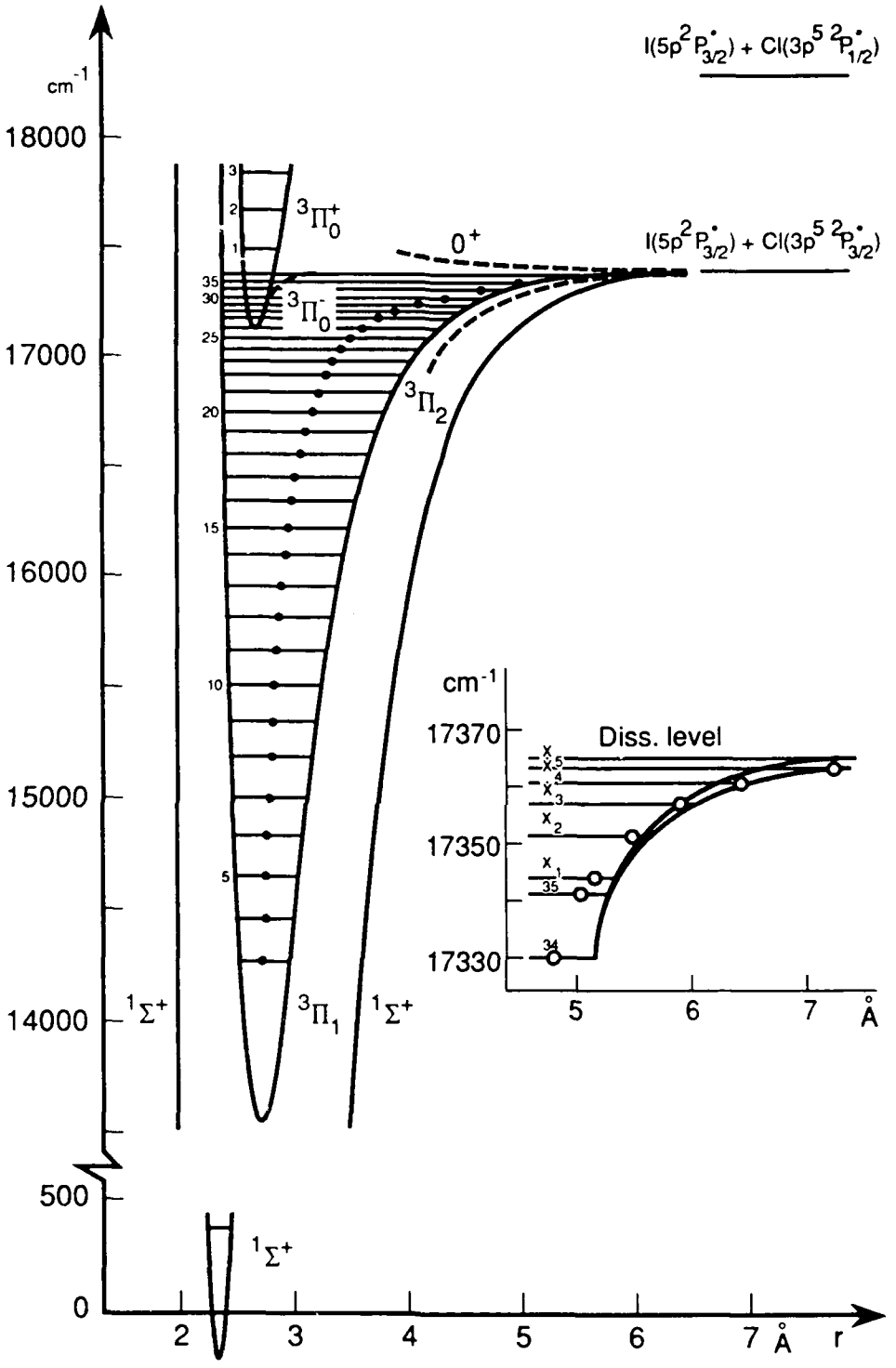

Source: Hulthén, Järlsäter, and Koffman [1960].

Figure 19. Potential energy curves of ICl $X^1\Sigma^+$ and $A'\Pi_1$ states.

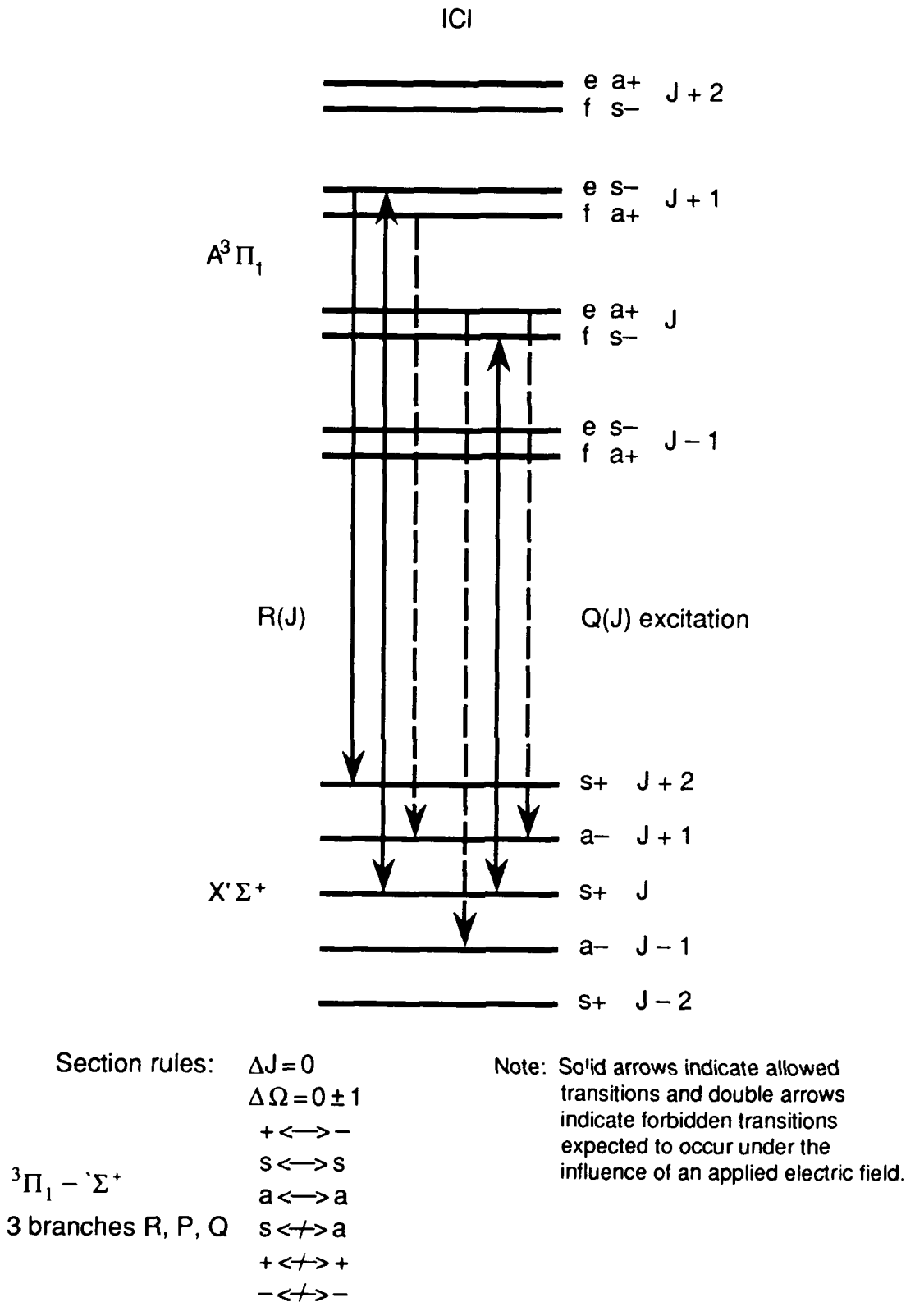

Figure 20. Rotational structure and selection rules for the A-K band of ICl.

Table 11. Relevant properties of ICl.

Property	Value	Source
Radiative lifetime	405 to 460 ± 40 μs	Harris, Natzle, and Moore, 1979
Self-collision quenching coefficient	$3.1 \times 10^{-10} \pm 0.5$ cm^3 s^{-1}	Harris, Natzle, and Moore, 1979
Cross section	110×10^{-16} cm^2	Harris, Natzle, and Moore, 1979
Neon-collision quenching coefficient	4.5×10^{-12} cm^3 s^{-1}	Harris, Natzle, and Moore, 1979
cross section	0.76×10^{-16} cm^2	Harris, Natzle, and Moore, 1979
Einstein A	1.55×10^3 s^{-1}	Harris, Natzle, and Moore, 1979
Lambda doubling constant	2.7×10^{-5} cm^{-1}	Hansen, Thompson, Western, and Howard, 1983
Perturbed levels in A state	V' = 28, J' = 2,9 29, 3,6,9 30, ~35 31, ~30 32, --	Coxon, Gordon, and Wickramaaratchi, 1980
Room temperature line width	0.02 Å	Harris, Natzle, and Moore, 1979
Equilibrium constant key for $2ICl = I_2 + Cl_2$	1.8×10^{-3} at T = 25°C	Holleman and Steinfeld, 1971
	2.2×10^{-3} at T = 30°C	Harris, Natzle, and Moore, 1979

system by this amount. Cl_2 has no interferring electronic bands in the spectral region of interest. The main disadvantage of ICl is the low absorption, resulting in low fluorescence yield.

7.3 ICl VAPOR PRESSURE.

The main advantage of ICl (over NaK) is that is may be kept indefinitely in a pyrex cell at room temperature requiring only a cold finger (a part of the cell kept cold by immersion in a cold material) for pressure control. The ICl vapor pressure curve is shown in Fig. 21. Curves for the other interhalogens lie in much less convenient regions of temperature and pressure. At convenient temperatures (close to room temperature), the vapor pressure should be low enough that quenching of the fluorescence is minimized, yet high enough that good fluorescence signals may be recorded. The typical working pressure range is from 0.01 to 5.0 torr [King and McFadden, 1978; Clyne and McDermid, 1976]. At pressures above 5.0 torr, ICl A-X fluorescence is almost completely quenched by selfcollisions. Using a thermoelectric cooler to control the temperature of a cold finger between -50°C and -20°C, the pressure in the pyrex cell could be varied from 0.036 to 1.0 torr. This capability was confirmed by measuring the vapor pressure directly with a capacitance manometer and comparing it with the vapor pressure curve at the measured temperature.

7.4 INTENSITY CALCULATIONS.

Although FCFs are reported in the literature [Coxon and Wickramaaratchi, 1980; Coxon, Gordon, and Wickramaaratchi, 1980], many levels of interest are left out.

Hybrid potential curves (Fig. 22) for the X and A states were constructed (Table 12). A simple exponential was used in region I. In region II, the Ryberg Klein Rees (RKR) part, the potentials were obtained from spectroscopic constants [Coxon and Wickramaaratchi, 1980] and are given in Table 13. The outer part of the potentials (region III) were constructed by fitting the outer wall of the RKR to a polynomial. A C_5 coefficient [King and McFadden, 1978] for the A

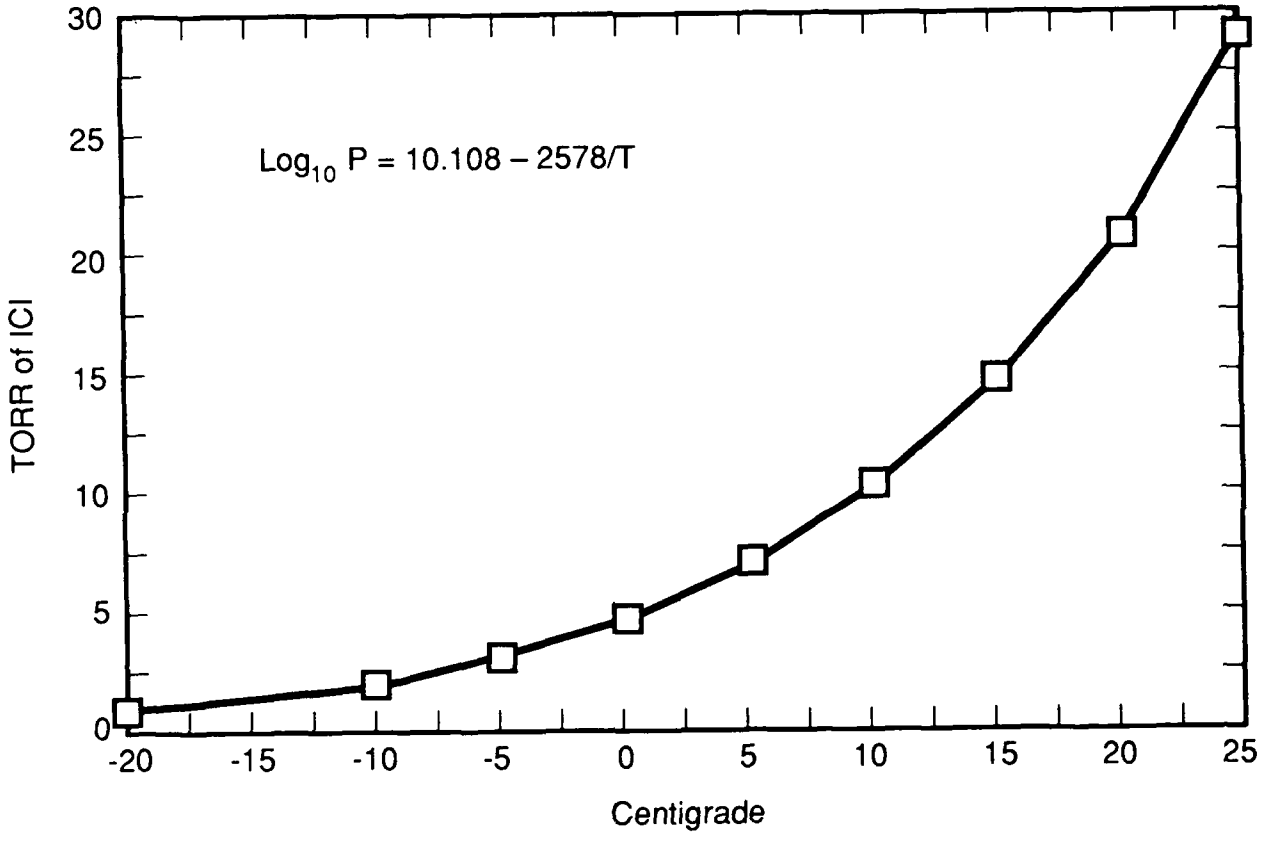

Source: Greenwood [1951].

Figure 21. Partial pressure of ICl versus temperature.

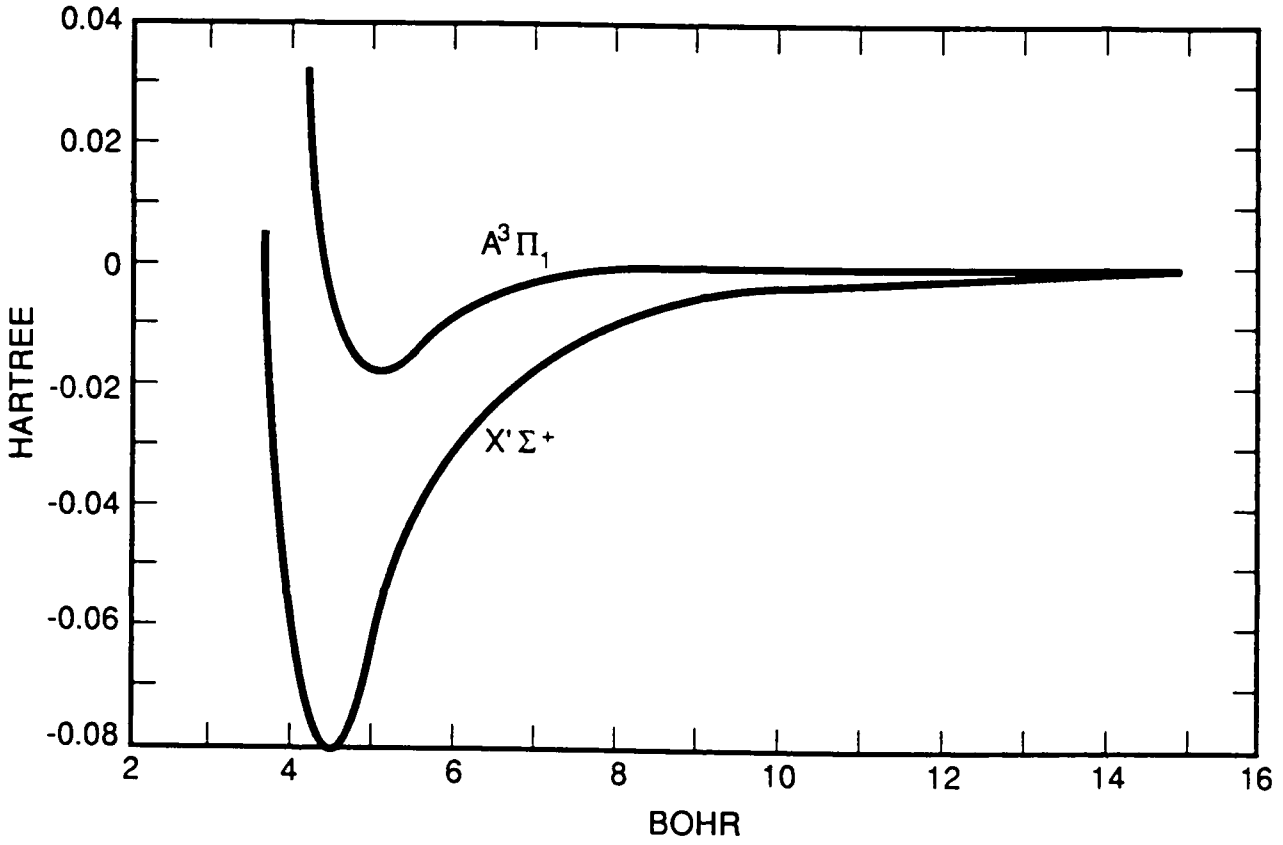

Figure 22. Plot of the hybrid potential curves for the $X^1\Sigma^+$ and $A^3\Pi_1$ states of ICl used in the calculation of Franck-Condon factors.

Table 12. Hybrid potential data for the $X^1\Sigma^+$ and $A^3\Pi_1$ states.

State	Region	R[a]	Function[a]	Constants
X	I	$R \leq 3.9$	$A\, e^{-BR} + C$	$A = 9.344184 \times 10^4$ $B = 3.780389$ $C = -8.951235 \times 10^{-2}$
	II	$3.9 < R < 5.5$	RKR	
	III	$5.5 \leq R$	$C_3R^{-3} + C_6R^{-6} + C_8R^{-8}$	$C_3 = -4.104763$ $C_6 = -787.004$ $C_8 = 8144.573$
A	I	$R \leq 4.4$	$A\, e^{-BR} + C$	$A = 3.003334 \times 10^9$ $B = 5.930834$ $C = -1.210713 \times 10^{-2}$
	II	$4.4 < R < 12.0$	RKR	
	III	$12.0 \leq R$	$C_3R^{-3} + C_6R^{-6} + C_8R^{-8}$	$C_3 = -0.188135$ $C_6 = 366.8663$ $C_8 = -51932.98$

[a]Atomic units.

Table 13. Spectroscopic constants.

Constant	$X^1\Sigma^+$	$A^3\Pi_1$
T_e	0.0	13742.9(5)
D_e	17557.6(2)	3814.7(6)
ω_e	384.27(5)	211.0(3)
$\omega_e x_e$	1.49(2)	2.12(1)
$\omega_e y_e$	$-3.3(15) \times 10^{-2}$	$-2.4(8) \times 10^{-2}$
$\omega_e z_e$	--	$0.2(3) \times 10^{-3}$
B_e	0.114157(2)	0.08529(7)
α_e	$5.32(2) \times 10^{-4}$	$7.4(4) \times 10^{-4}$
γ_e	$-0.13(5) \times 10^{-5}$	$-1.0(8) \times 10^{-5}$
r_e (Å)	2.32091(2)	2.685(1)
$V'' \leq 9$		
$V' \leq 14$		

Source: Coxon and Wickramaaratchi, 1980.

state was used. No long range coefficients were found for the X state. The resulting outer walls were considered good enough for the purpose at hand. The resulting hybrid potentials for the X and A states are given in Tables 14 and 15. These were used in a program (INTENSITY) to obtain a complete table of FCFs (see Table 16) for $0 \leq V'' \leq 15$, $0 < V' \leq 35$, and $J'' = J' = 30$.

The table shows a continual drop in FCF overlap for excitation from low V" to every increasing V' levels. Since the perturbed levels are very high in the A states (see Table 17), this suggests that one try to excite the lowest available perturbed level. If that is not experimentally realizable, excitation of lower V' states of low J would have to be tried.

Table 14. Hybrid potential for the $X^1\Sigma^+$ state of ICl.

R (Bohr)	V(R) (Hartrees)	R (Bohr)	V(R) (Hartrees)
1.0000000	2131.6750000	4.8002830	-0.0705770
2.0000000	48.5441800	4.8429909	-0.0689095
2.9999990	1.0200120	4.8838086	-0.0672561
3.0499990	0.8289195	4.9229259	-0.0656170
3.0999990	0.6707383	4.9609098	-0.0639923
3.1499990	0.5398006	4.9979482	-0.0623821
3.1999990	0.4314143	5.0340419	-0.0607864
3.2499990	0.3416953	5.0693803	-0.0592053
3.2999990	0.2674291	5.5000000	-0.0433766
3.3499990	0.2059532	6.0000000	$-3.102269\ 10^{-2}$
3.3999990	0.1550652	6.5000000	$-2.282589\ 10^{-2}$
3.4499990	0.1129417	7.0000000	$-1.724385\ 10^{-2}$
3.4999990	$7.807316\ 10^{-2}$	7.5000000	$-1.333818\ 10^{-2}$
3.5499990	$4.920997\ 10^{-2}$	8.0000000	$-1.053384\ 10^{-2}$
3.5999990	$2.531788\ 10^{-2}$	8.5000000	$-8.471743\ 10^{-3}$
3.6499990	$5.540714\ 10^{-3}$	9.0000000	$-6.922360\ 10^{-3}$
3.6999990	$-1.083013\ 10^{-2}$	9.5000000	$-5.735447\ 10^{-3}$
3.7499980	$-2.438155\ 10^{-2}$	10.0000000	$-4.810321\ 10^{-3}$
3.7999980	$-3.559899\ 10^{-2}$	10.5000000	$-4.077997\ 10^{-3}$
3.8499980	$-4.488448\ 10^{-2}$	11.0000000	$-3.490218\ 10^{-3}$
3.8999980	$-5.257071\ 10^{-2}$	11.5000000	$-3.012567\ 10^{-3}$
3.9523628	-0.0592053	12.0000000	$-2.620066\ 10^{-3}$
3.9665358	-0.0607864	12.5000000	$-2.294283\ 10^{-3}$
3.9816537	-0.0623821	13.0000000	$-2.021413\ 10^{-3}$
3.9979055	-0.0639923	13.5000000	$-1.790975\ 10^{-3}$
4.0154800	-0.0656170	14.0000000	$-1.594908\ 10^{-3}$
4.0343771	-0.0672561	14.5000000	$-1.426941\ 10^{-3}$
4.0549750	-0.0689095	15.0000000	$-1.282140\ 10^{-3}$
4.0778408	-0.0705770	15.5000000	$-1.156591\ 10^{-3}$
4.1035409	-0.0722587	16.0000000	$-1.047152\ 10^{-3}$
4.1332097	-0.0739544	16.5000000	$-9.512869\ 10^{-4}$
4.1687365	-0.0756640	17.0000000	$-8.669276\ 10^{-4}$
4.2140899	-0.0773875	17.5000000	$-7.923772\ 10^{-4}$
4.2836318	-0.0791247	18.0000000	$-7.262344\ 10^{-4}$
4.3858848	-0.0799984	18.5000000	$-6.673329\ 10^{-4}$
4.4977379	-0.0791247	19.0000000	$-6.146981\ 10^{-4}$
4.5861769	-0.0773875	19.5000000	$-5.675096\ 10^{-4}$
4.6508060	-0.0756640	20.0000000	$-5.250742\ 10^{-4}$
4.7056074	-0.0739544	30.0000000	$-1.530954\ 10^{-4}$
4.7547407	-0.0722587		

Table 15. Hybrid potential for the $A^3\Pi_1$ state of ICl.

R (Bohr)	V(R) Hartrees)	R (Bohr)	V(R) (Hartrees)
1.0000000	7977657.0000000	5.3564296	-0.0159617
2.0000000	21190.7800000	5.4528055	-0.0150405
3.0000000	56.2762500	5.5378432	-0.0141403
3.1000000	31.0940000	5.6168342	-0.0132618
3.2000000	17.1777900	5.6924229	-0.0124058
3.3000000	9.4873890	5.7663112	-0.0115730
3.4000000	5.2375180	5.8392544	-0.0107642
3.5000000	2.8889440	5.9123869	-0.0099801
3.6000000	1.5910760	5.9862752	-0.0092215
3.6999990	0.8738462	6.0611086	-0.0084893
3.7999990	0.4774884	6.1382093	-0.0077845
3.8999990	0.2584539	6.2175779	-0.0071079
3.9999990	0.1374107	6.3001590	-0.0064608
4.0999990	0.0705196	6.3863301	-0.0058439
4.1999990	$3.355417\ 10^{-2}$	6.4772263	-0.0052584
4.2999990	$1.312622\ 10^{-2}$	6.5736022	-0.0047051
4.3999990	$1.837358\ 10^{-3}$	6.6764035	-0.0041852
4.4261174	-0.0001638	6.7871413	-0.0036998
4.4268732	-0.0002256	6.9069500	-0.0032496
4.4280066	-0.0003004	7.0380974	-0.0028353
4.4293299	-0.0003892	7.1822829	-0.0024575
4.4308419	-0.0004928	7.3419652	-0.0021163
4.4325418	-0.0006131	7.5186543	-0.0018109
4.4346209	-0.0007512	7.7157531	-0.0015403
4.4368887	-0.0009101	7.9323153	-0.0013021
4.4395342	-0.0010934	8.1715555	-0.0010934
4.4427471	-0.0013021	8.4240227	-0.0009101
4.4463372	-0.0015403	8.7178745	-0.0007512
4.4504943	-0.0018109	9.0175858	-0.0006131
4.4550300	-0.0021163	9.3528223	-0.0004928
4.4606996	-0.0024575	9.7232094	-0.0003892
4.4665575	-0.0023797	10.1266661	-0.0003004
4.4733601	-0.0032496	10.5970182	-0.0002256
4.4811082	-0.0036998	11.1321898	-0.0001638
4.4896116	-0.0041852	11.7799873	-0.0001141
4.4988718	-0.0047051	12.0000000	$-1.067911\ 10^{-4}$
4.5090761	-0.0052584	12.5000000	$-8.728237\ 10^{-5}$
4.5202255	-0.0058439	13.0000000	$-7.329105\ 10^{-5}$
4.5323200	-0.0064608	13.5000000	$-6.293455\ 10^{-5}$
4.5457368	-0.0071079	14.0000000	$-5.502865\ 10^{-5}$
4.5600986	-0.0077845	14.5000000	$-4.881502\ 10^{-5}$
4.5759726	-0.0084893	15.0000000	$-4.379939\ 10^{-5}$
4.5931687	-0.0092215	15.5000000	$-3.965366\ 10^{-5}$
4.6124439	-0.0099801	16.0000000	$-3.615604\ 10^{-5}$
4.6336088	-0.0107642	16.5000000	$-3.315368\ 10^{-5}$
4.6570420	-0.0115730	17.0000000	$-3.053910\ 10^{-5}$
4.6836867	-0.0124058	17.5000000	$-2.823519\ 10^{-5}$
4.7141118	-0.0132618	18.0000000	$-2.618540\ 10^{-5}$
4.7498274	-0.0141403	18.5000000	$-2.434738\ 10^{-5}$
4.7932911	-0.0150405	19.0000000	$-2.268871\ 10^{-5}$
4.8503609	-0.0159617	19.5000000	$-2.118405\ 10^{-5}$
4.9395556	-0.0169033	20.0000000	$-1.981322\ 10^{-5}$
5.0741048	-0.0173809	30.0000000	$-2.727044\ 10^{-7}$
5.2290621	-0.0169033		

Table 16. Calculated FCFs for the $X^1\Sigma^+$-$A^3\Pi_1$ band system of ICl [transition wavelengths (in vacuum) are also given below each entry].

V' / V"	0	1	2	3	4	5	6	7	8
0	1.7-7[a]	1.8-6	1.0-5	3.9-5	1.1-4	2.8-4	6.1-4	1.1-3	1.9-3
	7337[b]	7228	7124	7026	6932	6843	6759	6680	6604
1	3.2-6	3.1-5	1.5-4	5.2-4	1.3-3	2.9-3	5.5-3	9.1-3	1.4-2
	7548	7433	7323	7219	7120	7027	6938	6854	6774
2	3.1-5	2.5-4	1.1-3	3.2-3	7.3-3	1.3-2	2.1-2	3.0-2	3.8-2
	7770	7647	7531	7421	7317	7218	7125	7036	6952
3	1.8-4	1.3-3	4.9-3	1.2-2	2.3-2	3.5-2	4.6-2	5.1-2	5.0-2
	8003	7873	7750	7633	7523	7419	7320	7227	7138
4	8.2-4	4.9-3	1.5-2	3.1-2	4.7-2	5.7-2	5.5-2	4.3-2	2.6-2
	8248	8110	7980	7856	7740	7629	7525	7426	7333
5	2.8-3	1.4-2	3.5-2	5.6-2	6.4-2	5.3-2	3.1-2	1.0-2	4.3-4
	8056	8360	8221	8091	7967	7850	7739	7635	7536
6	7.9-3	3.1-2	6.0-2	6.9-2	5.1-2	2.1-2	2.0-3	2.7-3	1.5-2
	8779	8623	8476	8337	8206	8082	7965	7854	7750
7	1.8-2	5.6-2	7.6-2	5.6-2	1.7-2	3.9-5	1.0-2	2.8-2	3.3-2
	9068	8902	8745	8597	8457	8325	8201	8084	7974
8	3.6-2	8.0-2	6.9-2	2.1-2	4.4-5	1.7-2	3.6-2	3.0-2	1.1-2
	9373	9196	9028	8871	8722	8582	8450	8326	8209
9	6.1-2	9.1-2	3.9-2	2.3-4	1.9-2	4.1-2	2.7-2	4.2-3	2.0-3
	9697	9507	9328	9160	9002	8853	8712	8580	8456
10	9.0-2	7.9-2	7.5-3	1.4-2	4.4-2	2.7-2	1.6-3	7.6-3	2.5-2
	10041	9837	9646	9466	9297	9138	8989	8848	8716
11	1.1-1	4.8-2	2.1-3	4.4-2	3.4-2	1.6-3	1.2-2	3.1-2	2.2-2
	10406	10187	9982	9790	9610	9440	9280	9131	8990
12	1.3-1	1.4-2	2.7-3	4.9-2	5.6-3	1.1-2	3.4-2	1.9-2	3.7-4
	10795	10560	10340	10133	9940	9759	9588	9429	9279
13	1.4-1	1.9-6	5.8-2	2.3-2	5.2-3	3.7-2	2.0-2	8.0-8	1.5-2
	11209	10956	10719	10498	10290	10096	9914	9743	9583
14	1.3-1	1.6-2	6.2-2	2.9-4	3.5-2	2.8-2	2.0-5	1.9-2	2.8-2
	11650	11377	11122	10884	10661	10452	10257	10075	9904
15	1.0-1	5.8-2	3.4-2	1.7-2	4.4-2	1.8-3	1.9-2	3.0-2	4.7-3
	12118	11823	11548	11291	11052	10828	10619	10423	10240

[a] $1.7\text{-}7 = 1.7 \times 10^{-7}$

[b] 7337 = 7337 Å

Table 16. Calculated FCFs for the $X^1\Sigma^+$-$A^3\Pi_1$ band system of ICl [transition wavelengths (in vacuum) are also given below each entry] (Continued).

V" \ V'	9	10	11	12	13	14	15	16	17
0	3.1-3[a] 6533[b]	4.6-3 6465	6.3-3 6402	8.2-3 6342	1.0-2 6286	1.2-2 6233	1.4-2 6184	1.5-2 6139	1.6-2 6096
1	1.9-2 6699	2.4-2 6628	2.9-2 6562	3.2-2 6499	3.4-2 6440	3.5-2 6385	3.5-2 6333	3.3-2 6286	3.1-2 6241
2	4.3-2 6873	4.5-2 6799	4.3-2 6728	3.9-2 6662	3.3-2 6600	2.5-2 6543	1.8-2 6489	1.2-2 6438	7.5-3 6392
3	4.3-2 7055	3.1-2 6976	1.9-2 6902	9.7-3 6833	3.2-3 6768	2.8-4 6707	3.4-4 6650	2.3-3 6598	5.0-3 6549
4	1.1-2 7245	1.9-3 7162	1.9-4 7084	3.9-3 7011	1.0-2 6942	1.5-2 6878	1.9-2 6819	1.9-2 6763	1.8-2 6712
5	2.8-3 7444	1.2-2 7356	2.1-2 7274	2.5-2 7197	2.3-2 7125	1.7-2 7057	1.1-2 6994	5.0-3 6936	1.5-3 6883
6	2.7-2 7652	2.9-2 7559	2.1-2 7473	1.1-2 7391	2.8-3 7315	4.5-6 7244	1.7-3 7178	5.7-3 7117	9.5-3 7060
7	2.2-2 7870	7.6-3 7772	2.8-4 7681	2.3-3 7595	9.3-3 7514	1.5-2 7439	1.8-2 7370	1.6-2 7305	1.1-2 7245
8	2.5-4 8099	4.4-3 7996	1.5-2 7899	2.1-2 7808	1.9-2 7723	1.2-2 7644	4.4-3 7570	4.9-4 7502	3.3-4 7439
9	1.6-2 8340	2.5-2 8230	2.0-2 8127	8.7-3 8031	9.8-4 7941	8.3-4 7858	5.7-3 7780	1.1-2 7708	1.3-2 7642
10	2.5-2 8592	1.1-2 8476	5.3-4 8367	2.9-3 8265	1.1-2 8170	1.7-2 8082	1.5-2 7999	9.9-3 7923	4.0-3 7853
11	3.2-3 8858	1.9-3 8735	1.3-2 8619	2.0-2 8511	1.6-2 8410	6.5-3 8317	5.6-4 8230	8.5-4 8149	4.8-3 8075
12	8.7-3 9139	2.2-2 9007	1.9-2 8884	6.6-3 8770	3.0-5 8663	3.8-3 8563	1.1-2 8471	1.4-2 8386	1.2-2 8307
13	2.6-2 9434	1.3-2 9294	5.2-4 9193	4.3-3 9041	1.4-2 8927	1.7-2 8822	1.1-2 8724	3.5-3 8634	7.6-5 8550
14	7.5-3 9744	8.7-4 9595	1.3-2 9456	2.0-2 9326	1.2-2 9205	2.1-3 9093	5.0-4 8989	5.7-3 8893	1.1-2 8805
15	4.6-3 10070	2.1-2 9911	1.8-2 9762	3.9-3 9624	6.8-4 9495	8.7-3 9376	1.5-2 9265	1.3-2 9163	6.1-3 9070

[a] 3.1-3 = 3.1×10^{-3}

[b] 6533 = 6533 Å

Table 16. Calculated FCFs for the $X^1\Sigma^+$-$A^3\Pi_1$ band system of ICl [transition wavelengths (in vacuum) are also given below each entry] (Continued).

V' / V"	18	19	20	21	22	23	24	25	26
0	1.7-2[a]	1.7-2	1.7-2	1.6-2	1.6-2	1.4-2	1.3-2	1.1-2	1.0-2
	6058[b]	6022	5990	5961	5936	5913	5893	5876	5861
1	2.7-2	2.4-2	2.1-2	1.7-2	1.4-2	1.2-2	9.7-3	7.8-3	6.3-3
	6201	6164	6130	6100	6073	6049	6028	6010	5994
2	4.0-3	1.8-3	5.9-4	8.7-5	8.3-6	1.5-4	3.7-4	5.8-4	7.4-4
	6350	6311	6275	6244	6215	6191	6169	6150	6133
3	7.6-3	9.5-3	1.1-2	1.1-2	1.1-2	9.8-3	8.7-3	7.6-3	6.6-3
	6504	6463	6426	6393	6364	6337	6315	6295	6278
4	1.5-2	1.1-2	8.2-3	5.5-3	3.4-3	2.0-3	1.1-3	5.3-4	2.3-4
	6665	6622	6584	6549	6518	6490	6466	6446	6428
5	6.6-5	2.9-4	1.4-3	2.7-3	3.8-3	4.4-3	4.7-3	4.7-3	4.5-3
	6833	6788	6747	6711	6678	6649	6624	6602	6584
6	1.2-2	1.2-2	1.1-2	9.9-3	7.8-3	5.9-3	4.3-3	2.9-3	2.1-3
	7008	6961	6918	6879	6845	6815	6789	6766	6746
7	6.7-3	3.0-3	8.7-4	5.5-5	1.1-4	5.7-4	1.1-3	1.5-3	1.8-3
	7191	7141	7096	7055	7019	6988	6960	6936	6915
8	2.5-3	5.3-3	7.4-3	8.3-3	8.2-3	7.4-3	6.2-3	5.1-3	4.0-3
	7382	7329	7282	7239	7201	7168	7138	7113	7091
9	1.3-2	9.8-3	6.3-3	3.4-3	1.5-3	4.4-4	4.4-5	2.0-5	1.6-4
	7581	7525	7475	7430	7390	7355	7325	7298	7275
10	6.3-4	8.8-5	1.4-3	3.1-3	4.6-3	5.3-3	5.4-3	5.1-3	4.5-3
	7789	7731	7678	7630	7588	7551	7519	7491	7466
11	8.8-3	1.1-2	9.9-3	7.9-3	5.5-3	3.4-3	1.9-3	8.8-4	3.6-4
	8007	7945	7890	7840	7795	7756	7722	7692	7667
12	7.5-3	3.0-3	5.2-4	2.5-5	7.1-4	1.8-3	2.6-3	3.1-3	3.3-3
	8235	8170	8111	8058	8011	7970	7934	7903	7876
13	1.2-3	4.5-3	7.2-3	8.2-3	7.7-3	6.2-3	4.6-3	3.1-3	2.1-3
	8474	8405	8343	8287	8237	8194	8155	8122	8094
14	1.2-2	9.2-3	5.3-3	2.1-3	4.2-4	6.5-7	2.9-4	8.1-4	1.3-3
	8724	8651	8585	8525	8473	8427	8386	8351	8321
15	1.1-3	8.3-5	1.8-3	4.2-3	5.8-3	6.2-3	5.7-3	4.7-3	3.7-3
	8984	8906	8836	8774	8718	8669	8626	8589	8558

[a] 1.7-2 = 1.7×10^{-2}

[b] 6058 = 6058 Å

Table 16. Calculated FCFs for the $X^1\Sigma^+$ - $A^3\Pi_1$ band system of ICl [transition wavelengths (in vacuum) are also given below each entry] (Continued).

V" \ V'	27	28	29	30	31	32	33	34	35
0	9.2-3[a]	7.9-3	7.0-3	5.9-3	5.1-3	4.2-3	3.4-3	2.6-3	1.4-3
	5848[b]	5837	5827	5819	5812	5806	5802	5798	5795
1	5.1-3	4.1-3	3.4-3	2.7-3	2.2-3	1.8-3	1.4-3	1.0-3	5.5-4
	5981	5969	5959	5951	5944	5938	5933	5929	5926
2	8.6-4	8.9-4	9.1-4	8.7-4	8.2-4	7.3-4	6.2-4	4.9-4	2.8-4
	6119	6107	6097	6088	6080	6074	6069	6065	6062
3	5.6-3	4.7-3	4.0-3	3.3-3	2.8-3	2.2-3	1.8-3	1.3-3	7.2-4
	6263	6250	6239	6230	6222	6215	6210	6206	6203
4	8.7-5	2.1-5	1.3-6	2.1-6	1.1-5	2.0-5	2.5-5	2.6-5	1.7-5
	6412	6399	6387	6377	6369	6362	6356	6352	6349
5	4.1-3	3.7-3	3.3-3	2.8-3	2.4-3	2.0-3	1.6-3	1.3-3	6.9-4
	6567	6553	6541	6531	6522	6515	6509	6504	6501
6	1.4-3	9.4-4	6.5-4	4.3-4	2.9-4	1.9-4	1.2-4	8.0-5	3.9-5
	6729	6714	6701	6691	6682	6674	6668	6663	6659
7	2.0-3	1.9-3	1.9-3	1.8-3	1.6-3	1.4-3	1.1-3	9.1-4	5.1-4
	6897	6881	6868	6857	6847	6839	6833	6828	6824
8	3.1-3	2.4-3	1.8-3	1.4-3	1.1-3	7.9-4	5.8-4	4.1-4	2.1-4
	7072	7056	7042	7030	7020	7012	7005	6999	6996
9	3.4-4	4.8-4	5.9-4	6.4-4	6.5-4	6.2-4	5.4-4	4.5-4	2.6-4
	7255	7238	7223	7211	7200	7191	7184	7178	7174
10	3.9-3	3.2-3	2.7-3	2.2-3	1.8-3	1.4-3	1.1-3	7.9-4	4.2-4
	7445	7427	7412	7399	7388	7378	7371	7365	7361
11	1.0-4	1.2-5	2.1-6	2.7-5	5.8-5	8.3-5	9.4-5	9.1-5	5.7-5
	7644	7625	7609	7596	7584	7574	7566	7560	7556
12	3.2-3	2.9-3	2.7-3	2.3-3	2.0-3	1.7-3	1.3-3	9.9-4	5.4-5
	7852	7832	7815	7801	7789	7779	7770	7764	7759
13	1.3-3	7.6-4	4.5-4	2.2-4	1.1-4	5.5-5	2.4-5	9.6-6	2.9-6
	8069	8048	8030	8017	8004	7993	7984	7977	7972
14	1.6-3	1.7-3	1.8-3	1.8-3	1.6-3	1.4-3	1.1-3	9.1-4	5.1-4
	8295	8273	8254	8242	8228	8216	8207	8200	8195
15	2.8-3	2.0-3	1.5-3	9.4-4	6.5-4	4.4-4	2.9-4	1.9-4	9.2-5
	8530	8506	8486	8477	8462	8450	8440	8432	8427

[a] 9.2-3 = 9.2×10^{-3}

[b] 5848 = 5848 Å

Table 17. Perturbed levels in the $A^3\Pi_1$ state and excitation line positions.

V"	J"	V'	J'	ν	λ
0	31	30	32	17181.75	5820.129[a]
0	33			17166.96	5825.144
1	31			16800.99	5952.031[b]
1	33			16786.27	5957.251
2	31			16423.23	6088.936
2	33			16408.58	6094.374
0	26	29	27	17180.02	5820.715[a]
0	28			17167.50	5824.960[c]
1	26			16799.11	5952.698[b]
1	28			16786.65	5957.117
2	26			16421.19	6089.692
2	28			16408.79	6094.295
0	31	31	32	17201.74	5813.367
0	33			17186.94	5818.371
1	31			16820.98	5944.959[b]
1	33			16806.25	5950.167[b]
2	31			16443.22	6081.535
2	33			16428.56	6086.960
0	28	31	29	17216.37	5808.426[a]
0	30			17202.94	5812.960[a]
1	28			16835.51	5939.825[b]
1	30			16822.15	5944.545[b]
2	28			16457.66	6076.199
2	30			16444.36	6081.115
0	27	31	28	17212.90	5806.898[c]
0	29			17207.92	5811.277[c]
1	27			16840.01	5938.238[b,c]
1	29			16827.10	5942.795[b,c]
2	27			16462.13	6074.589
2	29			16449.28	6079.295

[a]Few I_2 coincidences
[b]Uncongested
[c]No I_2 coincidences

7.5 PERTURBED LEVELS.

A number of perturbed levels have been reported in vibrational levels of the A state close to the dissociation limit. These levels are ideally suited for use in electric field measurements because (as demonstrated with the V' = 2, J' = 40 level in the $B^1\Pi$ state of NaK) the lambda doubling can be very small and at the same time the fluorescence well separated. Some perturbed levels were determined from the analysis given by Coxon, Gordon, and Wickramaaratchi [1980]. A table of perturbed levels with small lambda doublet splittings and line positions is presented in Table 17. This was taken from the work of Hulthén, Järlsäter, and Koffman [1980].

7.6 EXPERIMENTAL.

The pyrex cell used in the experiments is shown in Fig. 23. A two stage thermoelectric (TE) cooler (Marlow Industries Model MI2021T-02AC) was epoxied to a metal heat sink. The cold side of the TE cooler made thermal contact (silicone grease) with the end of the cell cold finger in an evacuated enclosure. Thermocouple leads were attached directly to the cold finger. Temperature measurements were accurate to ± 1.0°C. ICl was prepared by placing I_2 crystals (certified, Fisher) in the cold finger, evacuating the cell, then adding a few torr of Cl_2 vapor (Matheson). ICl formed readily; an excess of Cl_2 was evidenced by the appearance of yellow crystals of ICl_3 [Buckles and Bader, 1971]. The cell was then briefly pumped on, and then sealed with a teflon valve. The laser beam passed through the Brewster windows and fluorescence was observed at right angle.

7.7 RESULTS AND CONCLUSION.

Figure 24 shows an excitation spectrum of the ICl vapor taken at -15°C which corresponds to an ICl pressure of 1.3 torr. Here, the laser is exciting the states near the perturbed level V' = 29, J' = 27 by absorption from V" = 0, J" = 26 (see Table 17), and the detection system is recording the fluorescence to V' = 1. The two slightly shifted scans show the reproducibility and approximate signal to noise obtained. The largest features are likely due to ICl fluorescence.

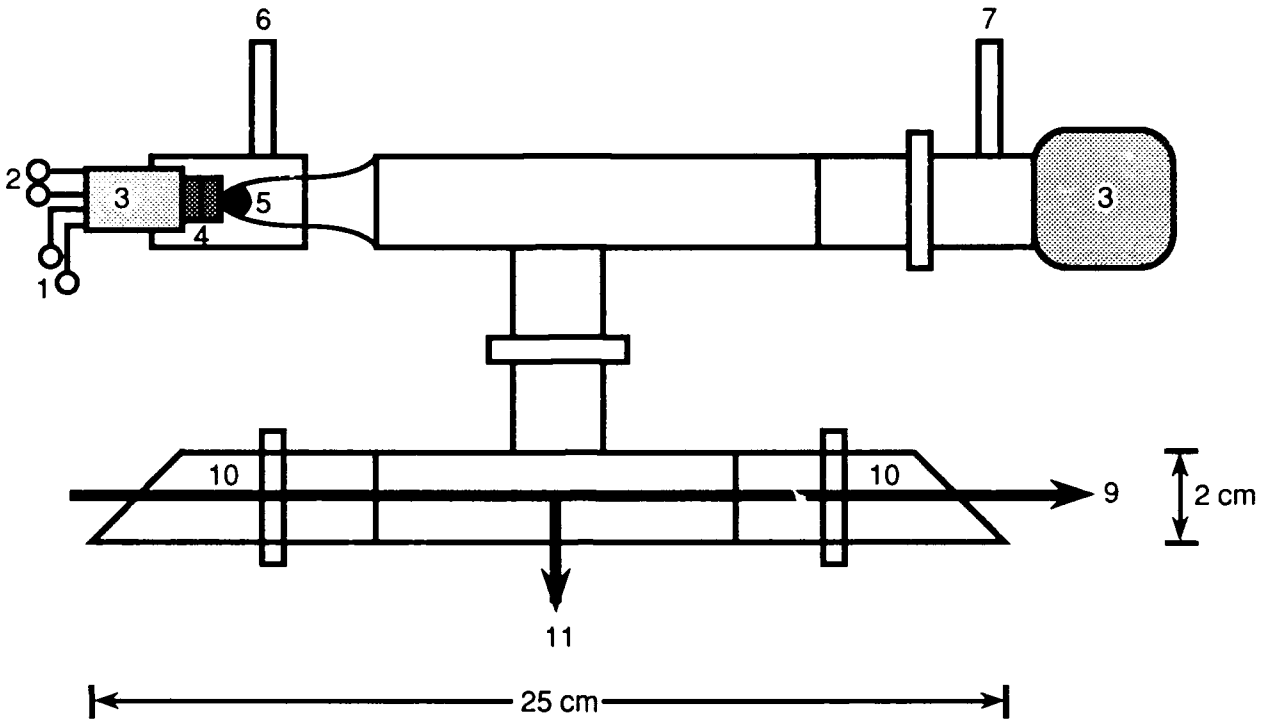

1 Thermoelectric cooler power
2 Thermocouple leads
3 Heat sink
4 Thermoelectric cooler
5 ICl crystals
6 To vacuum
7 To vacuum
8 Teflon valve
9 Laser beam
10 Brewster windows
11 Fluorescence

Figure 23. Schematic of the cell used to generate ICl vapor.

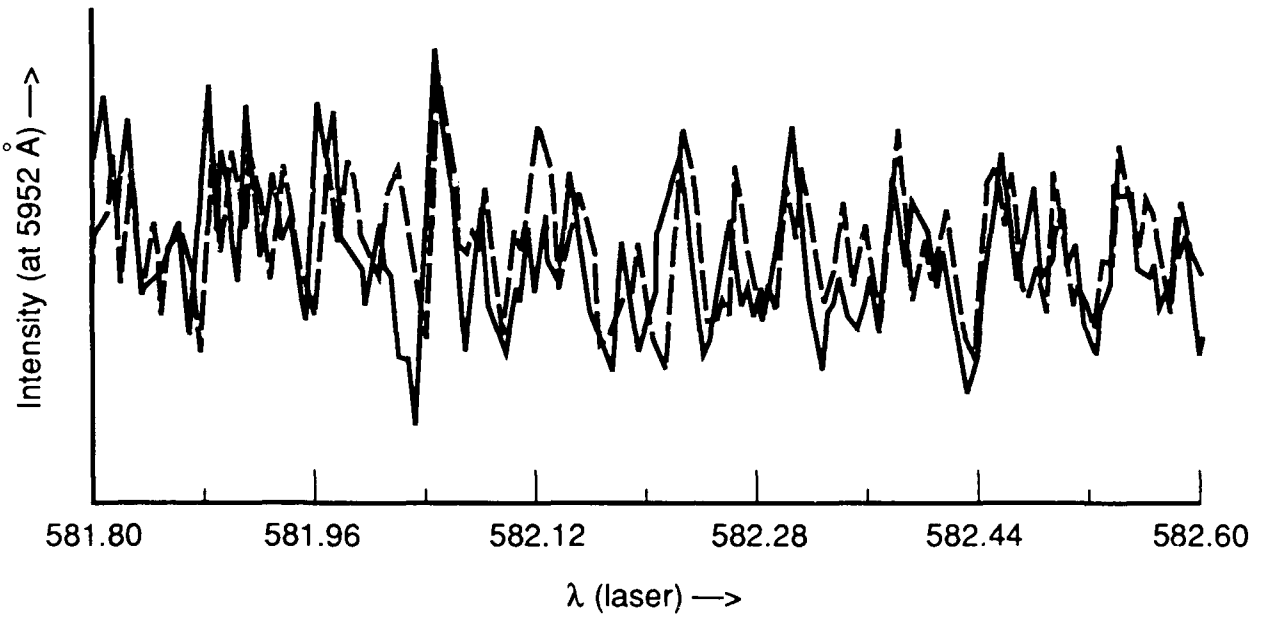

Experimental Conditions:

Temperature = -15°C
$\lambda_{monitor}$ = 5952.0
λ_{laser} = 5818–5826
Gate = 15 μs
Delay = 30 μs
Slits = 300/300 μm
Sensitivity = 0.1 V

Figure 24. Excitation spectrum of ICl vapor.

The main contribution to noise was scattered light from the inside of the cell. More work was needed to improve the system response. Though it was clear that considerable improvements in the spectrum were possible, we decided to use the remaining research effort for CO experiments, for several reasons. CO is the only molecule identified which could possibly be used as a sensor without being enclosed in some sort of glass container. Other reasons include the poor signal to noise in the ICl excitation spectrum and the fact that ICl is very caustic.

SECTION 8
CO EXPERIMENTS AND RESULTS

8.1 INTRODUCTION.

Being of great importance in atmospheric, combustion, and interstellar studies the CO molecule has been extensively studied both theoretically and experimentally. A compilation of relevant parameters and representative values with sources used in these studies is presented in Table 18.

The combination of moderate quenching coefficient with short radiative lifetime allowed studies of CO at considerably higher pressures (to 150 torr) than with NaK of ICl.

Unfortunately, the ground state diple moment (in V" = 0) is rather small compared with NaK (0.112 versus 2.67 debye). Since the sensitivity for measuring the electric field scales linearly with this quantity, one can predict a factor of 20 reduction in the sensitivity of the technique relative to NaK. To overcome this reduction, one must seek vibration rotation states in the $A^1\Pi$ state with small lambda-doublet splittings. The potential energy curves for CO are shown in Fig. 25 [Krupenie, 1986]. The $A^1\Pi$ state is located in a particularly conjested region where perturbations due to the nearby sigma states ($a'^3\Sigma^+$, $e^3\Sigma^-$, and $I^1\Sigma^-$) cause shifts in the lambda doublet splittings. Lambda doublet splittings and perturbation information were used to select target levels in the $A^1\Pi$ state. Accurate line positions were taken from the sources given or calculated from spectroscopic constants. Laser-induced fluorescence experiments by two photon resonant absorption have been reported for excitation from V" = 0 to V' = 0 through 9.

A number of multiphoton resonant ionization studies have been performed, implying that ionization of the medium may significantly compete with fluorescence. The particular mechanism by which it is occurring in these experiments (two-photon resonant, four-photon

Table 18. Compilation of relevant parameters and sources used in this work.

Quantity	Typical Value	Reference
Radiative life times ($A\,^1\Pi$):		
$\Gamma_{Rad} = 10^8\ s^{-1}$		Girard, Billy, Vigue, and Lehmann, 1982
V = 0 J = 10 to 30 $\tau_{Rad} \approx$ 10 to 20 ns		Provorov, Stoicheff, and Wallace, 1977
Quenching rate constants and cross sections:		
$A\,^1\Pi$ (V = 9)	$K(X = self) = 8.7 \times 10^{-10}\ cm^3\ s^{-1}$	Melton and Yiin, 1975
K's also given for X = He, Ne, Ar, Kr, Xe, H_2, D_2, and SF_6		
$A\,^1\Pi$ (V = 9, J = 22)	$K(self) \approx 4 \times 10^{-10}\ cm^3\ s^{-1}$	Girard, Billy, Vigue, and Lehmann, 1982
$A\,^1\Pi$ (V = 0 to 8)	$\sigma_{vib}(X = He, V = 1) = 0.45\ Å^2$	Fink and Comes, 1974
X = He, Ne, Ar, Kr, Xe,	$K(X = He, V = 1) = 0.0021\ torr^{-1}$	
$A\,^1\Pi$ (V = 13, J = 13)	$\sigma_{Rot}(X = He) = 23\ Å^2$	Vikis, 1983
X = H_2, D_2, He, Ne, N_2, Ar, Xe, CO		
$A\,^1\Pi$ (V = 0, 9, 13, 14)	$\sigma_{(Fl.\ quench)}(X = self) = 57.1\ Å^2$	Vikis, 1978
X = H_2, D_2, He, Ne, Ar, Kr, Xe, CO, CO_2, O_2, N_2		
$A\,^1\Pi$ (V = 0, 1)	$\sigma_{vib}(X = He) = 0.37\ Å^2$	Comes and Fink, 1972
X = He, Ne, Ar, Kr, H_2, D_2, N_2	$K_{vib}(X = He) = 0.0017\ torr^{-1}$	
	$\sigma_{(Fl.\ quench)}(X = He) = 0.035\ Å^2$	
	$K(Fl.\ quench)(X = He) = 0.00016\ torr^{-1}$	

Table 18. Compilation of relevant parameters and sources used in this work (Continued).

Quantity	Typical Value	Reference
$X\,^1\Sigma^+$ (V = 1)	$\sigma_{Rot}(H_2, T = 293\ K) = 34\ bohr^2$ $K_{Rot}(H_2, \Delta J = 1, T = 293) = 0.38\ s^{-1}\ torr^{-1}$	Bréchignac et al., 1980
Dipole moments: (T) = Theoretical, (E) = Experimental		
(E) $X\,^1\Sigma^+$ (V ≈ 0)	$\mu = 0.112 \pm 0.005$ debye	Burrus, 1958
(E) $A\,^1\Pi$ (V = 0)	$\mu \leq 0.15 \pm 0.05$ debye	Fisher and Dalby, 1976
(T) $A\,^1\Pi$ (R = 2.05 to 2.40 bohr)	$\mu(R) = 0.61$ to 1.46 debye	Norbeck, Merkel, and Certain,
(E) $X\,^1\Sigma^+$ (R = 0.87 to 1.91 Å, V = 1 to 38) also gives transition moments	$\mu(R)$	Chackerian et al., 1984
(T) $X\,^1\Sigma^+$ (R = 1.4 to 30 bohr)	$\mu(R)$	Kirby-Docken and Liu, 1977
(TE) $X\,^1\Sigma^+$ (R = 0.8 to 1.9 Å) also gives transition matrix elements	$\mu(R)$	Chackerian, 1976
(T) $X\,^1\Sigma^+$ (R = 1.5 to 6.0 bohr)	$\mu(R)$	Werner, 1981
Perturbation analysis ($A\,^1\Pi$ state):		
(V = 1 to 6, J = 1 to 6)	$\delta_{ef}(V = 1, J = 6) = 16$ MHz	Field, 1971
(V = 6, J = 1 to 22) line positions (6 to 13 band)		Onaka, 1957
(V = 0 to 18) perturbation parameters		Field, Wicke, Simmons, and Tilford, 1972
(V = 0, J = 1 to 75)	$\delta_{ef}(V = 0, J = 1) = 0.016\ cm^{-1}$	Le Floch, 1987
(V = 0 to 7, J = 1 to 29)		Simmons, Bass, and Tilford, 1969
Accurate line positions in the $X\,^1\Sigma^+ - A\,^1\Pi$ **band:**		Krupenie, 1986 Tilford and Simmons, 1972 Simmons, Bass, and Tilford, 1969

Table 18. Compilation of relevant parameters and sources used in this work (Continued).

Quantity	Typical Value	Reference
Oscillator strengths:		
	$(X\,^1\Sigma^+ - A\,^1\Pi,\ V' = 0)$ f = 0.02	Aarts and DeHeer, 1970
	$(X\,^1\Sigma^+ - A\,^1\Pi,\ V' = 0$ to 12)	Lassettre and Skerbele, 1971
Laser induced fluorescence studies by two photon absorption (X-A bands):		
	$V'' = 0 \rightarrow V' = 1$	Bernheim, Kittrell, and Veirs, 1978
	$V'' \rightarrow V'$: 0-0 to 0-9	Bernheim, Kittrell, and Veirs, 1977
	$V'' \rightarrow V'$: 0-3 and 0-9	Filseth, Wallenstein, and Zacharias, 1977
Resonant multiphoton ionization studies:		
	$CO(X\,^1\Sigma^+) \xrightarrow{2\,h\nu} CO(A\,^1\Pi) \xrightarrow{2\,h\nu} CO^+(X\,^2\Sigma^+) + e^-$	Jones et al., 1982
	$CO(X\,^1\Sigma^+) \xrightarrow{3\,h\nu} CO(A\,^1\Pi) \xrightarrow{2,3\,h\nu} CO^+(X\,^2\Sigma^+) + e^-$	Pratt, Poliakoff, Dehmer, and Dehmer, 1983
	$CO(X\,^1\Sigma^+) \xrightarrow{1\,h\nu}{}^1 CO(A\,^1\Pi) \xrightarrow{1\,h\nu}{}^2 CO^+(X\,^2\Sigma^+) + e^-$	Zacharias, Rottke, and Welge, 1980
Spectroscopic constants:		
	$X\,^1\Sigma^+$	Huber and Herzberg, 1979
	$A\,^1\Pi$	Tilford and Simmons, 1972

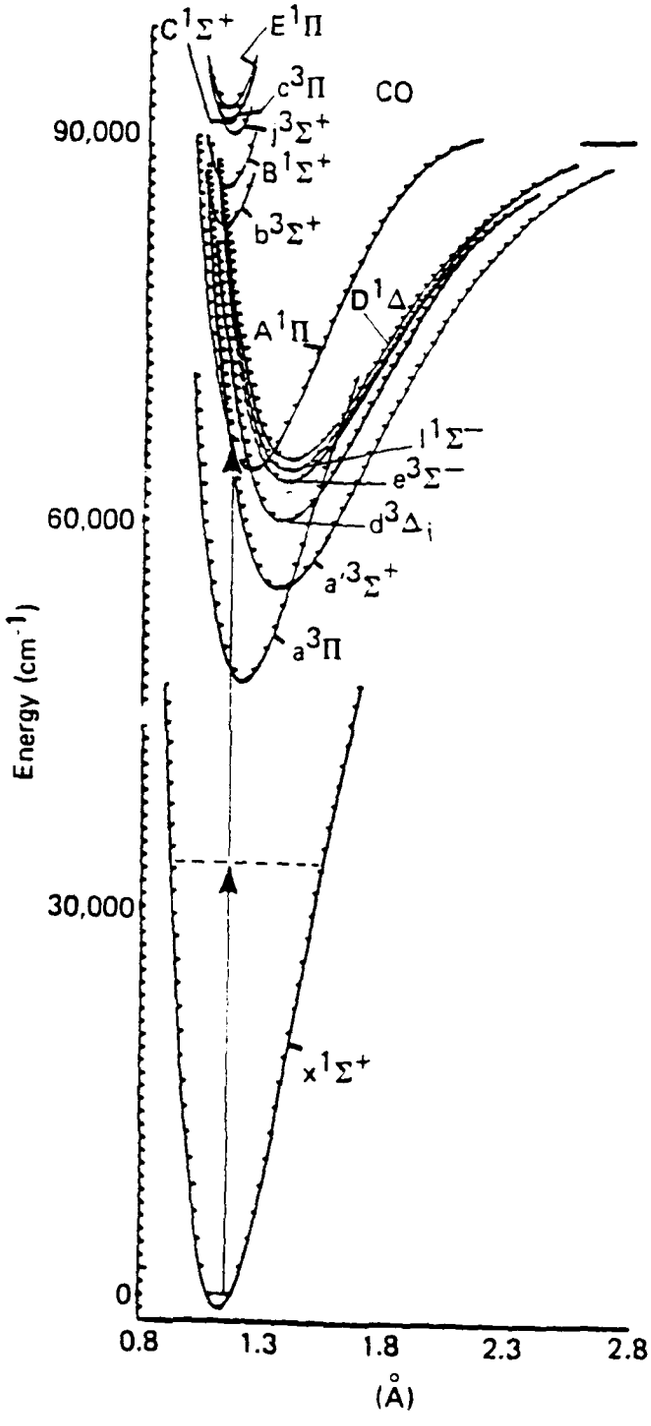

Source: Krupenie [1986].

Figure 25. Potential energy curves of the lowest electronic states of CO.

ionization)* have been reported previously by Jones et al. [1982]. Three-photon resonant, four- or five-photon ionization have also been reported by Pratt, Poliakoff, Dehmer, and Dehmer [1983], as well as one-photon resonant, two-photon ionization [Zacharias, Rottke, and Welge, 1980]. Excessive ionization must be avoided in these experiments because of the possibility of space-charge shielding of the applied electric field in the vicinity of the laser beam. Unfortunately, no determination of absolute percentage ionization was found in the literature.

Spectroscopic constants for the $X^1\Sigma^+$ and $A^1\Pi$ states were obtained from Huber and Herzberg [1979] and Tilford and Simmons [1972] and are given in Tables 19 and 20. Franck-Condon Factors are given in Table 21.

8.2 PERTURBED LEVELS.

As noted in the previous section, only states with small lambda-doublet splittings were sought. A list of target levels for the experiments was prepared. The intent was to find the level with the smallest lambda doublet splitting with the added constraint of having rotational angular momentum at the thermal maximum (J_{max} = 7, 300°K). From information provided by R. W. Field [1971] shown in Table 22 the best level was found to be V' = 1, J' = 6 with a splitting of 16.0 MHz (± 10 percent). Other potential levels, not investigated in these experiments, are listed in Table 23.

The relative approximate intensities, wavelengths, priorities, and laser dyes needed for exciting the target levels of Table 22 are given in Table 24. Unfortunately, remaining time only allowed for studies of V' = 3, 4, and 1; hence, more work is required for the rigorous testing of all known candidate levels. For excitation of V' = 1 target levels, the transitions and line positions are given in Table 25. The maximum signal intensity was experimentally found for fluorescence termination at V' = 7. The corresponding fluorescence line positions are given in Table 26. For excitation to target levels

*This notation means that two of the four photons needed to ionize, add together to connect two real resonances (states) of the molecule.

Table 19. Molecular constants of ground state $X^1\Sigma^+$ of CO (in wavenumbers).

$Y_{10} = 2169.81358$	$Y_{21} = 5.487 \times 10^{-7}$
$Y_{20} = -13.28831$	$Y_{31} = 2.54 \times 10^{-8}$
$Y_{30} = 0.010511$	$Y_{02} = -6.12147 \times 10^{-6}$
$Y_{40} = 5.74 \times 10^{-5}$	$Y_{12} = 1.153 \times 10^{-9}$
$Y_{50} = 9.83 \times 10^{-7}$	$Y_{22} = -1.805 \times 10^{-10}$
$Y_{60} = -3.166 \times 10^{-8}$	$Y_{03} = 5.83 \times 10^{-12}$
$Y_{01} = 1.93128087$	$Y_{13} = -0.1738 \times 10^{-12}$
$Y_{11} = -0.01750441$	

Table 20. Molecular constants of state $A^1\Pi$ of CO (in wavenumbers).

$T_e = 65075.77$[a]	$Y_{11} = -2.3251 \times 10^{-2}$
$Y_{10} = 1518.24$	$Y_{21} = 1.5911 \times 10^{-3}$
$Y_{20} = -19.40$	$Y_{31} = -5.7160 \times 10^{-4}$
$Y_{30} = 7.6584 \times 10^{-1}$	$Y_{41} = 8.2417 \times 10^{-5}$
$Y_{40} = -1.4117 \times 10^{-1}$	$Y_{51} = -5.9413 \times 10^{-6}$
$Y_{50} = 1.434 \times 10^{-2}$	$Y_{61} = 2.1149 \times 10^{-7}$
$Y_{60} = -8.051 \times 10^{-4}$	$Y_{71} = -2.991 \times 10^{-9}$
$Y_{70} = 2.36 \times 10^{-5}$	$Y_{02} = -7.29 \times 10^{-6}$
$Y_{80} = -2.90 \times 10^{-7}$	$Y_{12} = -1.05 \times 10^{-7}$
$Y_{01} = 1.6115$	

[a] T_e is the energy difference between the $X^1\Sigma^+$ and $A^1\Pi$ lowest states potential minima.

Table 21. Franck-Condon Factors for the $A^1\Pi$ - $X^1\Sigma^+$ fourth positive system.

V'		0	1	2	3	4	5	6	7	8
V"	0	1.1319-1	2.6087-1	2.8477-1	1.9629-1	9.6040-2	3.5535-2	1.0340-2	2.4282-3	4.6859-4
	1	2.1614-1	1.5487-1	3.0508-3	7.6435-2	1.9313-1	1.8569-1	1.0829-1	4.4465-2	1.3804-2
	2	2.2997-1	1.2179-2	9.0126-2	1.1607-1	5.0832-3	5.7179-2	1.6502-1	1.6681-1	9.9629-2
	3	1.8128-1	2.0493-2	1.1704-1	6.4536-4	8.9569-2	8.4157-2	4.7128-4	6.7660-2	1.5884-1
	4	1.1879-1	8.7285-2	3.4433-2	5.7630-2	6.6561-2	6.1711-3	9.8034-2	5.1406-2	2.7202-3
	5	6.8846-2	1.2304-1	3.2357-4	9.1254-2	1.3841-5	8.2359-2	2.2684-2	3.1553-2	9.4377-2
	6	3.6675-2	1.1603-1	3.2109-2	4.2201-2	4.2898-2	4.2265-2	2.1776-2	7.2885-2	5.9304-4
	7	1.8429-2	8.8057-2	7.3469-2	2.2336-3	7.3886-2	4.2668-5	6.9877-2	2.9021-3	5.8181-2
	8	8.8974-3	5.8371-2	9.0972-2	9.8994-3	4.4622-2	3.2779-2	2.9742-2	3.0612-2	4.2672-2
	9	4.1842-3	3.5370-2	8.4527-2	4.0627-2	7.9687-3	6.0808-2	3.8286-5	5.8344-2	1.6689-5
	10	1.9367-3	2.0162-2	6.6327-2	6.4755-2	1.4618-3	4.5052-2	2.4181-2	2.3731-2	3.2522-2
	11	8.8941-4	1.1024-2	4.6641-2	7.1751-2	1.9480-2	1.4504-2	4.9695-2	1.1030-5	4.9442-2
	12	4.0787-4	5.8643-3	3.0446-2	6.5086-2	4.1768-2	1.7143-4	4.4180-2	1.6298-2	2.1594-2
	13	1.8773-4	3.0666-3	1.8881-2	5.2041-2	6.5313-2	6.7201-3	2.0995-2	3.9190-2	4.2287-4
	14	8.7084-5	1.5891-3	1.1304-2	3.8223-2	5.7629-2	2.3102-2	3.3642-3	4.1680-2	9.2001-3
	15	4.0846-5	8.2117-4	6.6118-3	2.6471-2	5.1936-2	3.7973-2	7.3801-4	2.6615-2	2.8617-2
	16	1.9425-5	4.2525-4	3.8121-3	1.7597-2	4.2528-2	4.5927-2	9.4788-3	9.4220-3	3.6896-2
	17	9.3867-6	2.2157-4	2.1816-3	1.1373-2	3.2596-2	4.6731-2	2.1795-2	6.1450-4	3.0143-2
	18	4.6172-6	1.1653-4	1.2459-3	7.2159-3	2.3851-2	4.2574-2	3.1818-2	1.6937-3	1.6581-2

Table 21. Franck-Condon Factors for the $A^1\Pi$ - $X^1\Sigma^+$ fourth positive system (Continued).

V'		9	10	11	12	13	14	15	16
V"	0	7.5264-5	1.0151-5	1.1568-6	1.1181-7	9.1869-9	6.4215-10	3.7782-11	1.8874-12
	1	3.3745-3	6.6637-4	1.0812-4	1.4579-5	1.6462-6	1.5635-7	1.2525-8	8.4721-10
	2	4.1314-2	1.2831-2	3.1152-3	6.0724-4	9.6710-5	1.2731-5	1.3957-6	1.2800-7
	3	1.4862-1	8.4545-2	3.3725-2	1.0112-2	2.3717-3	4.4621-4	6.8445-5	8.6524-6
	4	8.9110-2	1.5679-1	1.2914-1	6.7610-2	2.5283-2	7.1696-3	1.5970-3	2.8572-4
	5	2.1092-2	1.8021-2	1.1299-1	1.5095-1	1.0784-1	5.1173-2	1.7696-2	4.6884-3
	6	6.3519-2	7.2827-2	2.4331-3	4.5471-2	1.3211-1	1.3855-1	8.5849-2	3.6707-2
	7	3.7499-2	1.0104-2	8.2806-2	4.0479-2	2.7402-3	7.8643-2	1.4142-1	1.2017-1
	8	9.8388-3	6.8218-2	6.0762-3	4.0752-2	7.7972-2	1.1842-2	2.2424-2	1.0892-1
	9	5.8879-2	5.9671-3	4.3499-2	4.4543-2	2.4546-3	6.9276-2	5.2619-2	1.8350-5
	10	2.3741-2	2.4797-2	4.1697-2	4.7082-3	6.2178-2	1.2255-2	2.6202-2	7.6757-2
	11	1.0943-3	4.9911-2	5.7511-6	5.1872-2	8.4925-3	3.3523-2	4.8135-2	1.3307-4
	12	3.0204-2	1.4383-2	3.1435-2	2.0623-2	2.0729-2	4.0979-2	1.9786-3	5.6287-2
	13	4.2877-2	1.7179-3	4.1004-2	2.1272-3	4.4591-2	6.1243-6	4.6549-2	1.1148-2
	14	2.1882-2	2.5544-2	1.0672-2	3.1550-2	1.0101-2	2.9406-2	1.9578-2	1.6848-2
	15	1.9365-3	3.7613-2	1.2081-3	3.4831-2	4.0014-3	3.5446-2	2.3548-3	4.1117-2
	16	3.5232-3	2.3565-2	1.9485-2	1.0192-2	2.8332-2	6.0848-3	3.0450-2	8.6642-3
	17	1.8049-2	5.1274-3	3.2376-2	2.6912-4	3.1077-2	3.7993-3	2.9198-2	4.8212-3
	18	2.9379-2	3.2516-4	2.5475-2	1.2637-2	1.1864-2	2.3360-2	5.3800-3	2.7723-2

Table 21. Franck-Condon Factors for the $A^1\Pi$ - $X^1\Sigma^+$ fourth positive system (Continued).

V'		17	18	19	20	21	22	23	24
V"	0	9.6394-14	1.9682-15	1.7458-16	6.9579-16	8.4461-18	4.7739-16	2.2078-16	2.3198-17
	1	4.8179-11	2.2816-12	8.8683-14	3.5241-15	5.5781-16	1.8542-16	1.2590-16	7.7682-16
	2	9.8388-9	6.3250-10	3.4137-11	1.5954-12	5.3403-14	8.4261-16	2.1479-16	5.7173-19
	3	9.0748-7	7.9258-8	5.7731-9	3.5084-10	1.7696-11	7.0676-13	2.3445-14	2.0941-15
	4	4.1658-5	4.9963-6	4.9572-7	4.0797-8	2.7859-9	1.5695-10	7.2888-12	3.0316-13
	5	9.8077-4	1.6515-4	2.2666-5	2.5551-6	2.3757-7	1.8248-8	1.1565-9	6.0027-11
	6	1.1654-2	2.8628-3	5.5819-4	8.7798-5	1.1256-5	1.1833-6	1.0227-7	7.2653-9
	7	6.4922-2	2.4980-2	7.2532-3	1.6441-3	2.9713-4	4.3394-5	5.1631-6	5.0252-7
	8	1.3911-1	9.8285-2	4.6607-2	1.6147-2	4.2794-3	8.9197-4	1.4877-4	2.0069-5
	9	5.4755-2	1.2915-1	1.2656-1	7.5863-2	3.1782-2	9.9277-3	2.3987-3	4.5850-4
	10	2.1822-2	1.0029-2	8.9341-2	1.3590-1	1.0721-1	5.5381-2	2.0615-2	5.8141-3
	11	5.7040-2	6.0094-2	2.2404-3	3.7582-2	1.1661-1	1.2977-1	8.5100-2	3.8334-2
	12	1.8132-2	1.6192-2	7.2885-2	3.1097-2	3.3754-3	7.2539-2	1.3088-1	1.1416-1
	13	2.5596-2	5.0261-2	4.4292-4	4.5885-2	6.4819-2	6.9871-3	2.4538-2	1.0405-1
	14	4.0913-2	4.4129-4	5.0304-2	2.4094-2	8.8213-3	6.7352-2	3.9879-2	3.6765-4
	15	1.5983-4	4.1675-2	1.4535-2	1.8411-2	5.1503-2	2.7558-3	3.5154-2	6.7555-2
	16	2.6350-2	2.0329-2	1.2562-2	4.1355-2	2.6062-5	4.3585-2	3.0498-2	3.4547-3
	17	3.2361-2	1.7042-3	3.8687-2	8.6115-4	3.6321-2	1.9083-2	1.1515-2	5.1596-2
	18	4.6775-3	2.7916-3	9.2564-3	2.2094-2	2.2721-2	7.8327-3	4.1710-2	1.2774-3

Table 22. Predicted lambda doub[illegible]ransitions: CO $A^1\Pi$.*

Priority	V	J	δ (MHz)	Dominant Σ Perturber (low J)
4	0	1	156	
		2	508	
		3	1150	$e^3\Sigma^-(1)$
		4	2281	
		5	4330	
		6	8291	
1	1	5	10	$a'\ ^3\Sigma^+(10)$
		6	16	
3	2	2	25	
		3	57	
		4	115	$I^1\Sigma^-(3)$
		5	234	
		6	558	
2	3	1	10	
		2	30	
		3	56	$e^3\Sigma^-(5)$
		4	87	
		5	119	
		6	150	
6	4	1	537	
		2	1352	
		3	2100	$a'\ ^3\Sigma^+(14)$
		4	2551	
		5	2654	
		6	2497	
-	5	-	---	$e^3\Sigma^-(8)$
5	6	1	10	
		2	31	
		3	68	$a'\ ^3\Sigma^+(17)$
		4	130	
		5	233	
		6	405	

*The uncertainty in all predicted frequencies is at least 10 percent.

Source: Field [1971].

Table 23. Other perturbed levels of the $A^1\Pi$ state.

V'	J'	δ_{e-f} (cm^{-1})*	Reference
6	7,8,11,13,14		Onaka, 1957
0	9,12,13,16,17,27		Simmons, Bass, and Tilford, 1969
1	0,1,23,26,29		
2	7,8,25,28,29		
3	18,22,26,28		
4	0,1		
5	15,18,21,22		
6	7,11,13,14,16		
0	1	0.016	Le Floch et al., 1987
0	2	0.029	
0	3	0.050	
0	4	0.090	
0	19	0.651	
0	20	0.400	
0	21	0.260	
0	22	0.181	
0	23	0.114	
0	24	0.123	
0	25	0.105	
0	26	0.093	
0	27	0.034	
0	28	0.009	
0	29	0.004	

*δ(MHz) = δ (cm^{-1}) × C × 10^{-6} where C is the speed of light.

Table 24. Calculated absorption band of the A-X transition from V" = 0 (J" = 1 to J' = 1) with approximate frequencies and wavelengths.*

V'	Relative Intensity	ν (cm-1)	λ J"=1 → J'=1 (Å)	J'	Priority	Laser Dye
0	1.00	64746.30	1544.49	1,2	4	Rh: 610 + 640**
1	1.91	66227.60	1509.94	5,6	1	Rh: 610 + 640
2	2.02	67673.92	1477.67	2,3	3	Rh 610
3	1.60	69085.91	1477.47	1 to 4	2	Rh 590
4	1.04	70463.59	1419.17	1	6	Rh 590
5	0.61	71806.77	1392.63	-	-	Rh 575
6	0.32	73115.34	1367.70	1 to 3	5	Fluorescein

*Target levels from Table 22 are given with priorities and laser dye.

**Optimize dye mixture (mg/L):

Rhodamine:	610	640
Oscillator	23.4	50.9
Amplifier	6.4	14.5

Table 25. Transitions and wavelengths for V" = 0 → V' = 1 excitation of target levels J' = 5 and J' = 6.

Excitation	J'	λ(vacuum)
S(3)	5	1509.380[b]
R(4)	5	1509.648[a]
Q(5)	5	1510.083[a]
P(6)	5	1510.609[a]
O(7)	5	1511.300[b]
S(4)	6	1509.290[b]
R(5)	6	1509.659[a]
Q(6)	6	1510.183[a]
P(7)	6	1510.799[a]
O(8)	6	1511.570[b]

[a]See Tilford and Simmons [1972], p. 173.
[b]Calculated from spectroscopic constants.

Table 26. Fluorescence transitions and wavelengths from target levels V' = 1, J' = 5, and J' = 6.

V'	V"	J'	J"	λ(vacuum)	λ(air)
1	7	5	R(4)	1930.86	1930.22
1	7	5	Q(5)	1931.53	1930.89
1	7	5	P(6)	1932.33	1931.70
1	7	6	R(5)	1930.82	1930.18
1	7	6	Q(6)	1931.63	1930.99
1	7	6	P(7)	1932.57	1931.93

of V' = 3 and 4, the corresponding maximum signal transitions (fluorescence to V" = 9 and 11) and wavelengths are given in Tables 27 through 30, respectively.

8.3 EXPERIMENTAL.

The experimental setup is shown in Fig. 26. In order to transmit the maximum amount of fluorescence through the optical system a MgF_2 (focal length = 6.3 cm) lens (Oriel) also served as a window. Special aluminum UV grade mirrors (Acton Research) were found to be necessary because of excessive absorption due to aluminum oxide on the initial uncoated first surface mirrors. A 50 cm focal length UV grade fused silica lens was used to focus the fluorescence on the slit of the monochromator. A photomultiplier tube (PMT) with bialkali photocathode coating was found to be the most sensitive to the fluorescence (EMI 9813QB). The entire monochromator and optical system (except the PMT) was enclosed by a clear plastic glove bag and purged with Argon. The remainder of the system is the same as described previously by Chan [1988].

The cell for the experiments is shown in Fig. 27. Extended Brewster angle windows (Acton Research, FS-2D) were used in order to minimize scattered laser light. Except for the Brewster windows, the entire cell (pyrex) was coated with black vinyl tape. The electrodes were 5.5 cm in diameter with a 1 cm spacing.

8.4 RESULTS AND DISCUSSION.

The excitation spectrum for excitation of V' = 1 is shown in Fig. 28. This spectrum was taken by monitoring the fluorescence terminating at V' = 7 at 1931 Å while scanning the laser. Note that the laser wavelength shown is of the dye fundamental, the actual laser wavelength is half of that shown. The wavelength scales in these spectra are approximate (± 1 Å). The peaks assigned with an asterisk are those that terminate on one of the two target levels of V' = 1 (i.e., J' = 5 and 6). These transitions are listed in Table 28. The resulting laser-induced fluorescence signal to noise was rather weak and could not be adequately resolved in these experiments. Hence, a

Table 27. Transitions and wavelengths for V" = 0 → V' = 3 excitation of target levels J' = 3 and J' = 4.

Excitation	J'	λ(vacuum)
S(1)	3	1447.150[b]
R(2)	3	1447.278[a]
Q(3)	3	1447.515[a]
P(4)	3	1447.841[a]
O(5)	3	1448.28[b]
S(2)	4	1447.060[b]
R(3)	4	1447.263[a]
Q(4)	4	1447.584[a]
P(5)	4	1447.987[a]
O(6)	4	1448.510[b]

[a]Tilford and Simmons [1972].
[b]Calculated from spectroscopic constants.

Table 28. Fluorescence transitions and wavelengths from target levels V' = 3, J' = 3, and J' = 4.

V'	V"	J'	J"	λ(vacuum)	λ(air)
3	9	3	R(2)	1970.34	1969.70
3	9	3	Q(3)	1970.75	1970.11
3	9	3	P(4)	1971.30	1970.66
3	9	4	R(3)	1970.28	1969.63
3	9	4	Q(4)	1970.82	1970.18
3	9	4	P(5)	1971.51	1970.86

Table 29. Transitions and wavelengths for V" = 0 → V' = 4 excitation of target level J' = 1.

Excitation	J'	λ(vacuum)
R(0)	1	1419.044[a]
Q(1)	1	1419.125[a]
P(2)	1	1419.277[a]
O(3)	1	1419.560[b]

[a]Tilford and Simmons [1972].
[b]Calculated from spectroscopic constants.

Table 30. Fluorescence transitions and wavelengths from target levels V' = 4 and J' = 1.

V'	V"	J'	J"	T(vacuum)	T(air)
4	11	1	R(0)	2068.83	2068.17
4	11	1	Q(1)	2068.98	2068.32
4	11	1	P(2)	2069.28	2068.61

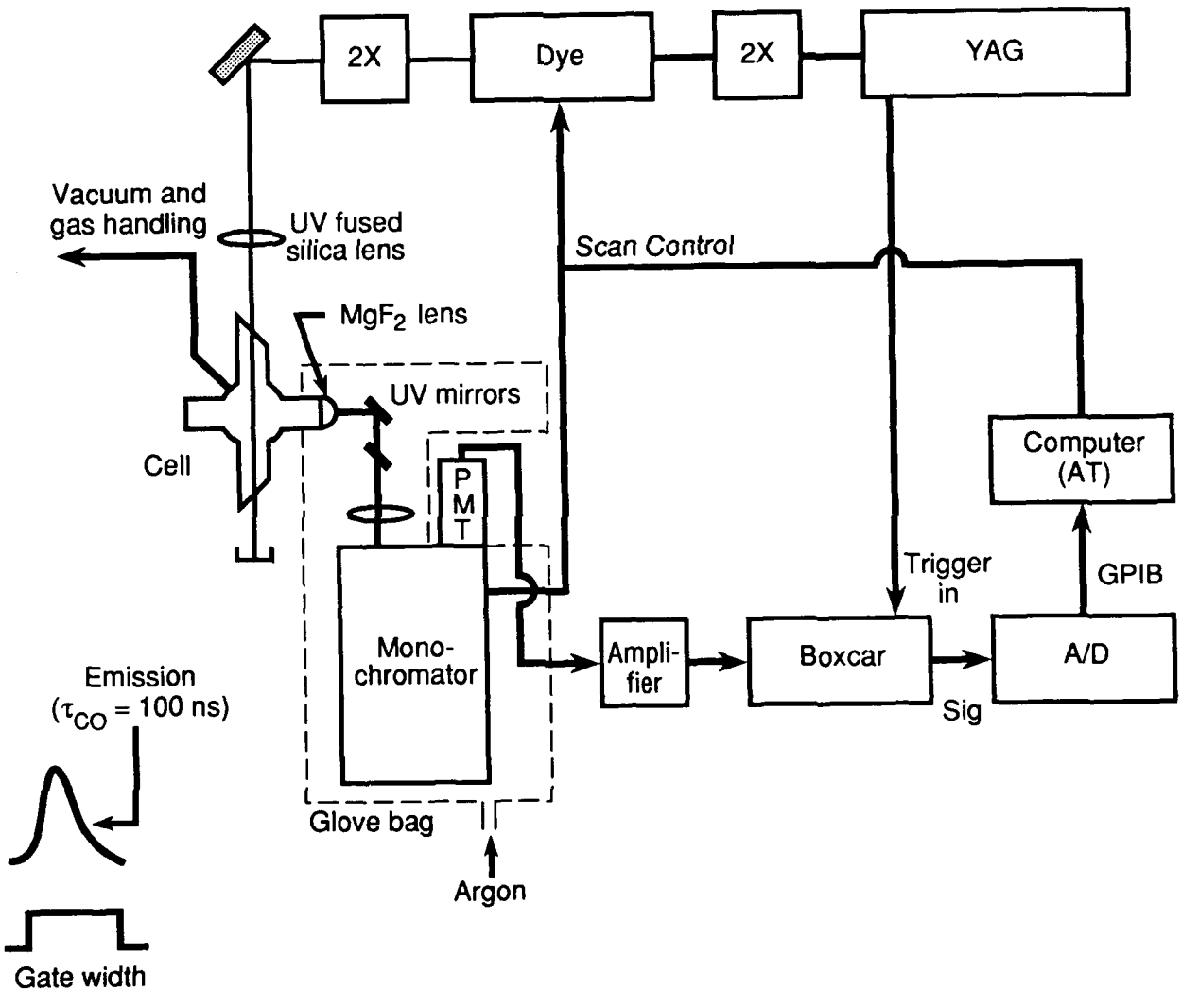

Figure 26. CO experimental setup.

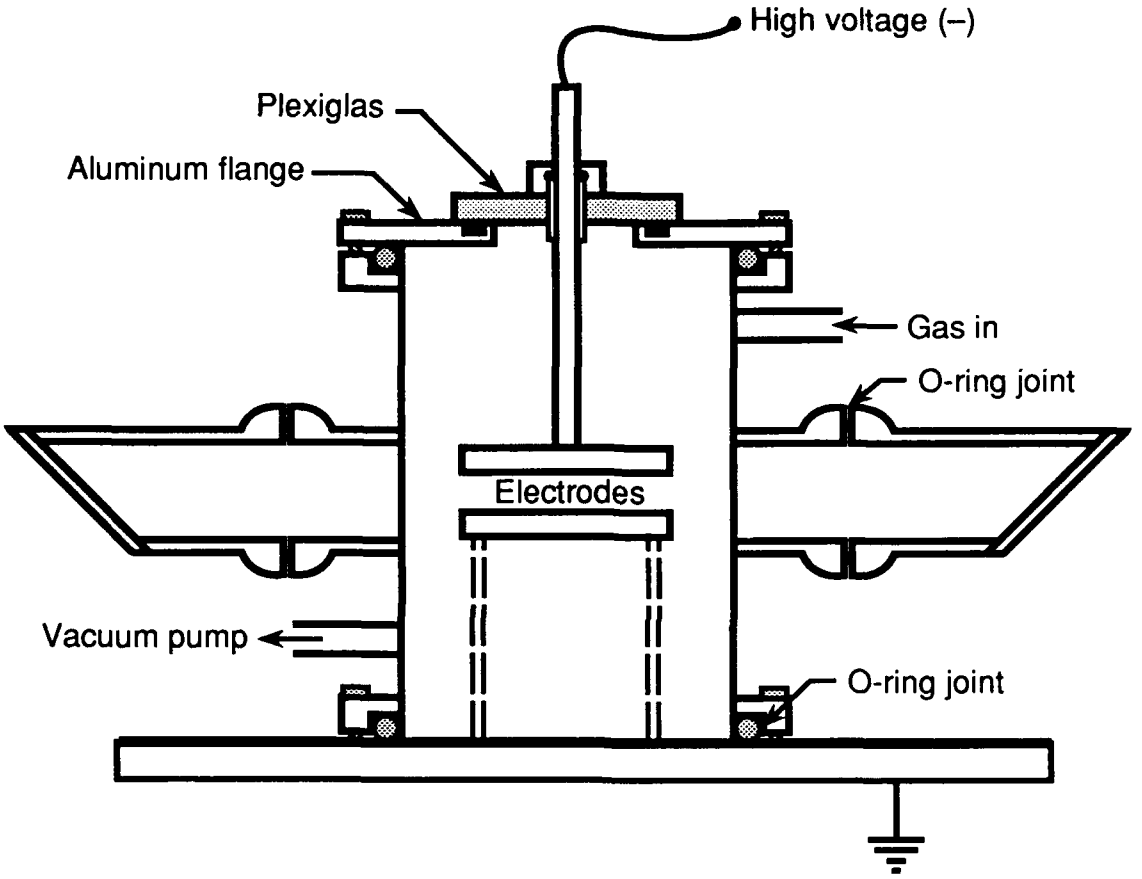

Figure 27. Cell for CO experiments.

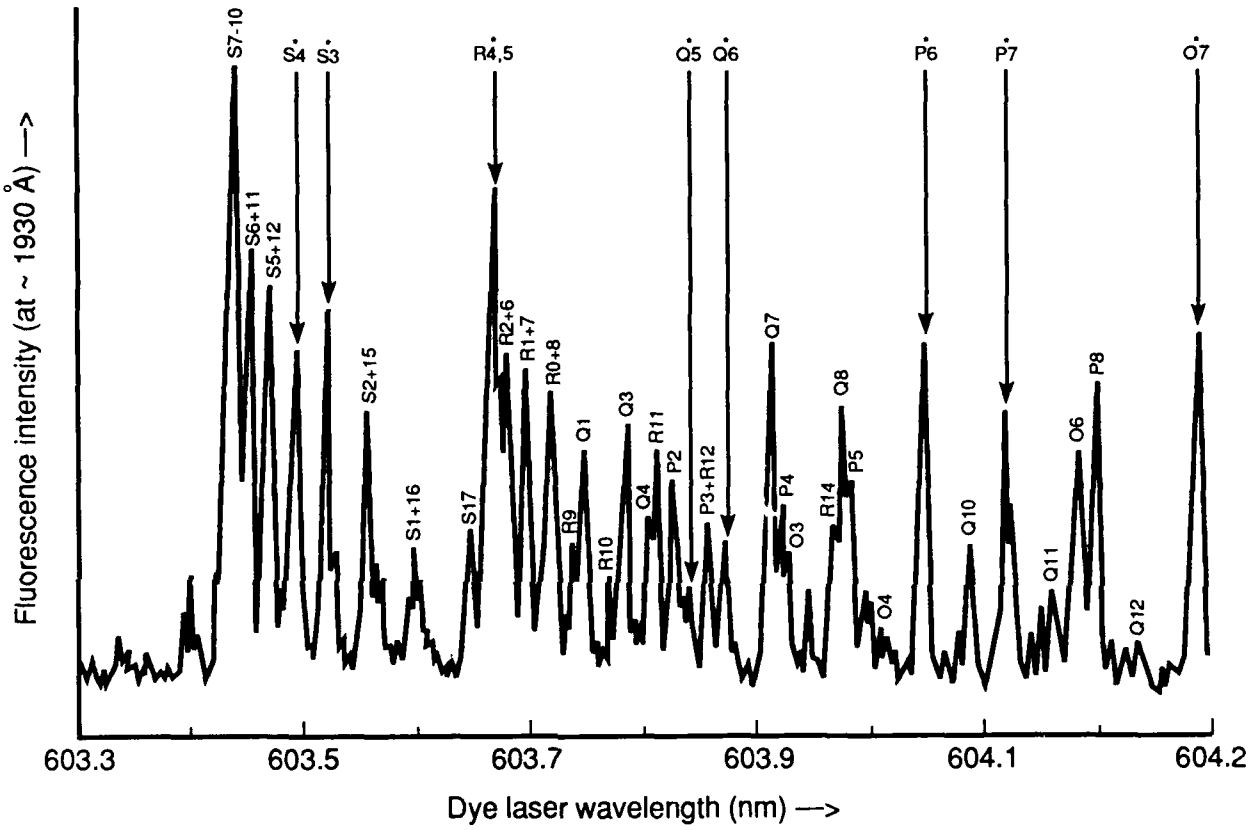

Figure 28. CO excitation spectrum for V" = 0 → V' = 1.

reliable check of the electric field sensitivity of the highest priority levels could not be made.

The excitation spectrum of V' = 3 is shown in Fig. 29. This spectrum was obtained by monitoring the fluorescence terminating at V" = 9 at 1969 Å while scanning the laser. The target levels are marked with an asterisk (transitions listed in Table 27). Fluorescence features were adequately resolved for many of the levels shown in this spectrum, none were found to exhibit forbidden transitions due to an applied electric field (1 KV/cm).

The excitation spectrum of V' = 4 is shown in Fig. 30 (target transitions are given in Table 27). This spectrum was obtained by monitoring fluorescence terminating at V" = 11 at 2068 Å. The largest fluorescence signal to noise was obtained in this case. Adequately resolved fluorescence was obtained in most cases. All of the resolvable transitions in this spectrum were checked, none were found to produce forbidden transitions in an applied electric field (~1 KV/cm).

Fluorescence spectra obtained by scanning the monochromator from 2066 to 2073 Å for five different excitations (fluorescence from V' = 4) are shown in Figs. 31 through 35. The experimental conditions for all of the spectra (Figs. 28 through 34) are recorded in Table 31. In Figs. 28 through 31, the RP doublets are scanned repetitively while the slit width is decreased (resolving power increased). The instrument resolution is shown for each scan. Anomalous behavior, suggesting an electric field effect can be seen in Fig. 35 when an electric field of 1 KV/cm is applied in some cases. However, this behavior could not be due to forbidden transitions, because the RP doublets were not resolved, and anomalous splittings do not replicate.

Since the transitions in these spectra are known, the spacings of the RP doublets may be determined. A relative figure of merit for the resolution of the fluorescence is the ratio of the RP doublet splittings [$\Delta_2 f(J)$] to the instrumental bandwidth ($\Delta\lambda$). These have been tabulated for each fluorescence spectrum in Table 32. It is found that not all RP doublets could be adequately resolved and a merit ratio of 15 or more was required.

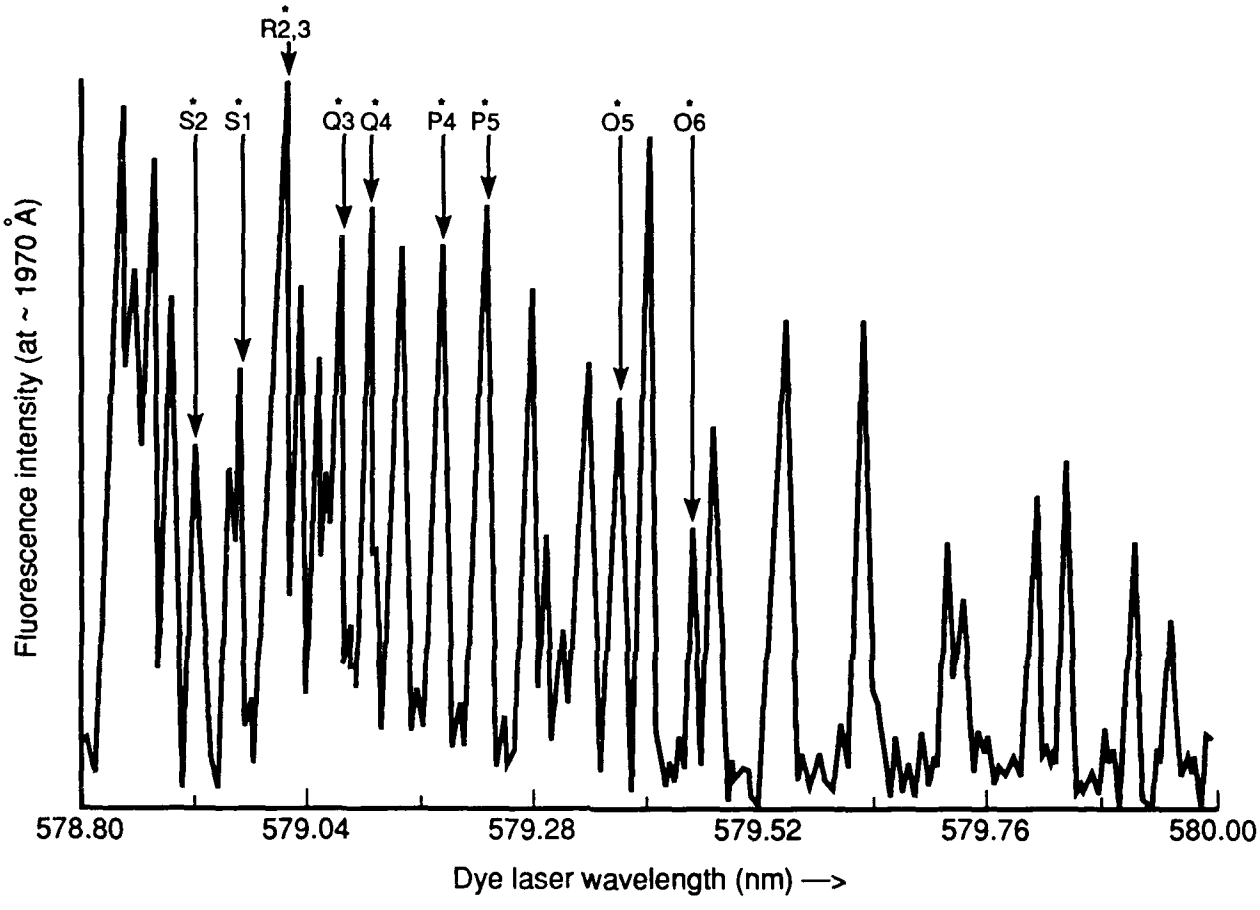

Figure 29. CO excitation spectrum for V" = 0 → V' = 3.

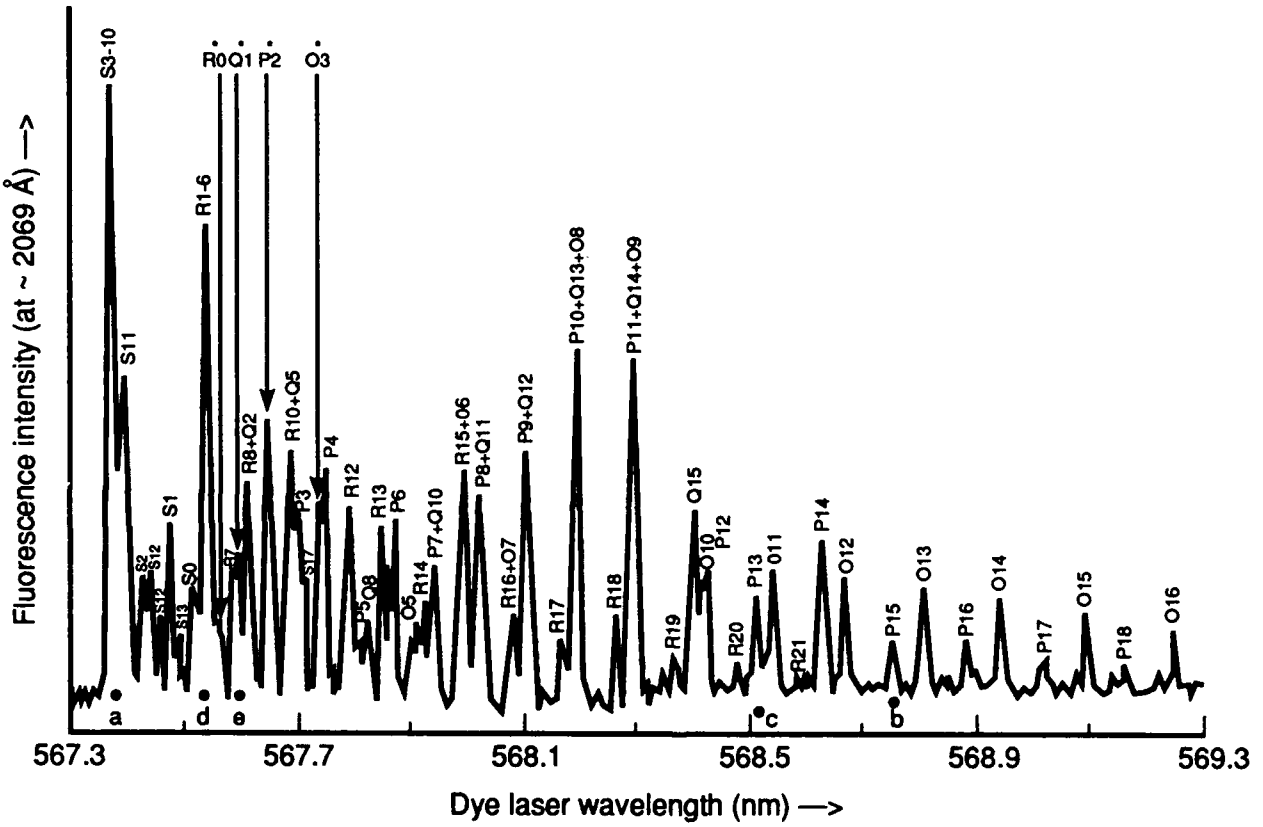

Figure 30. CO excitation spectrum for V" = 0 → V' = 4.

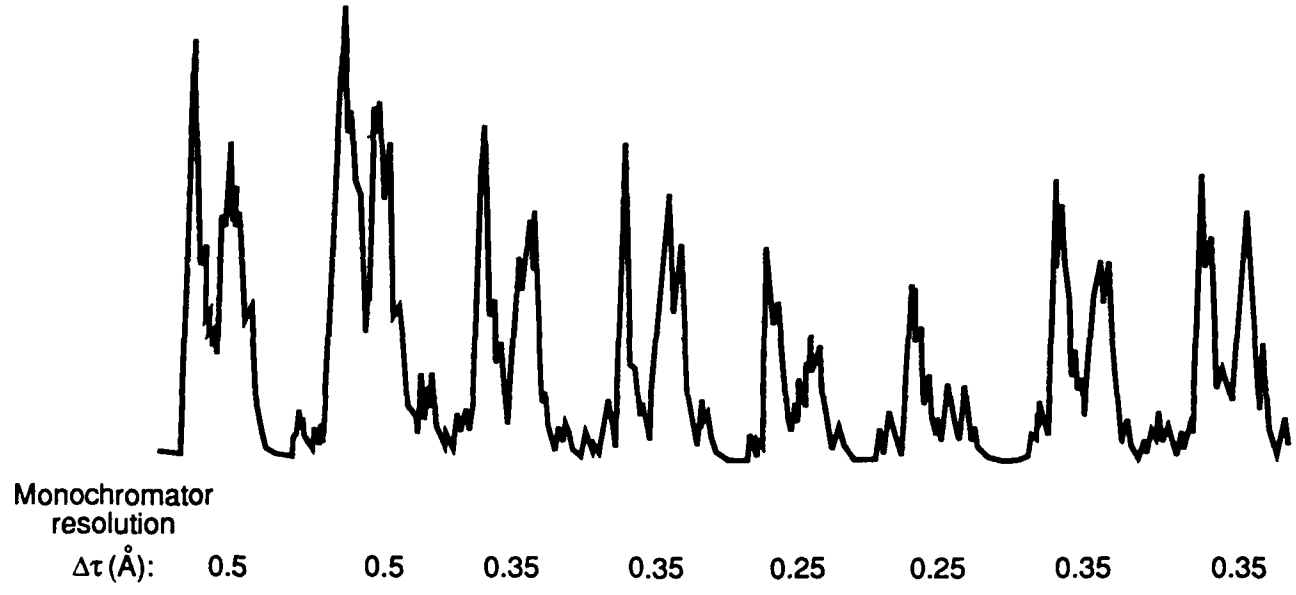

Figure 31. Laser-induced fluorescence from V' = 4, J' ~ 12 to V" = 11. (RP doublets are shown as a function of instrument resolution.)

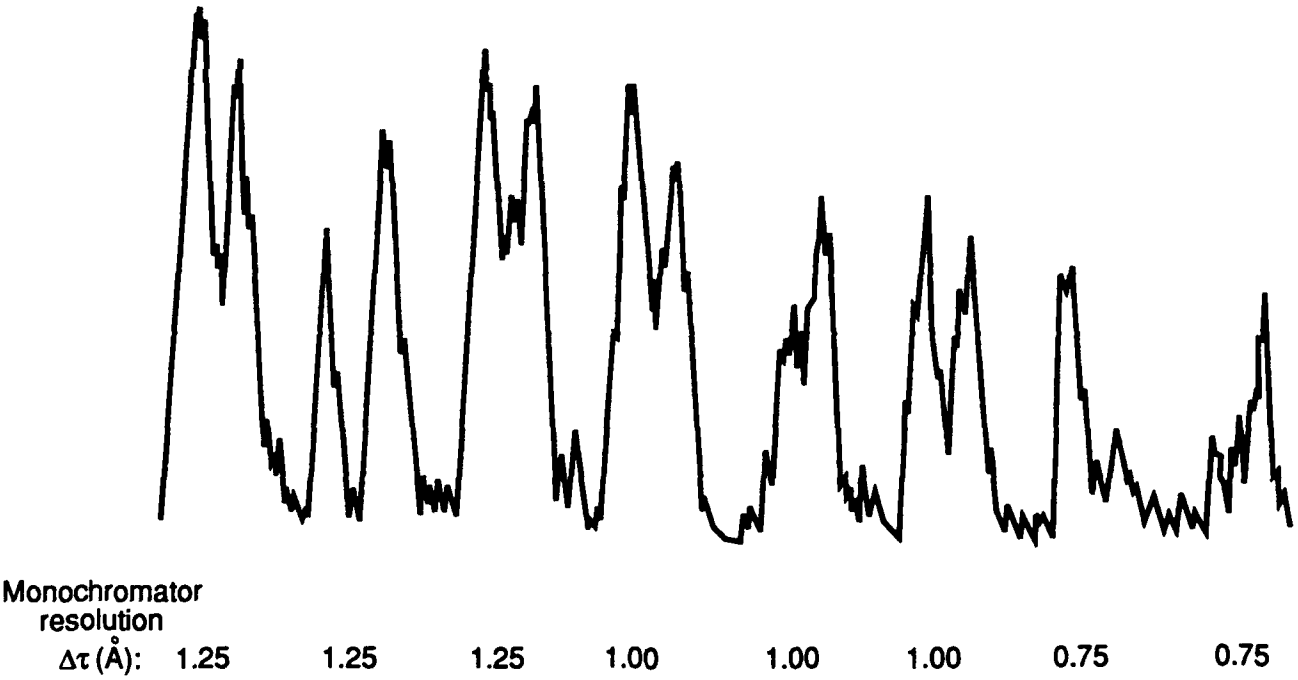

Figure 32. Laser-induced fluorescence from V' = 4, J' = 14 to V" = 11. [The R(13) and P(15) doublets are shown as a function of instrument resolution.]

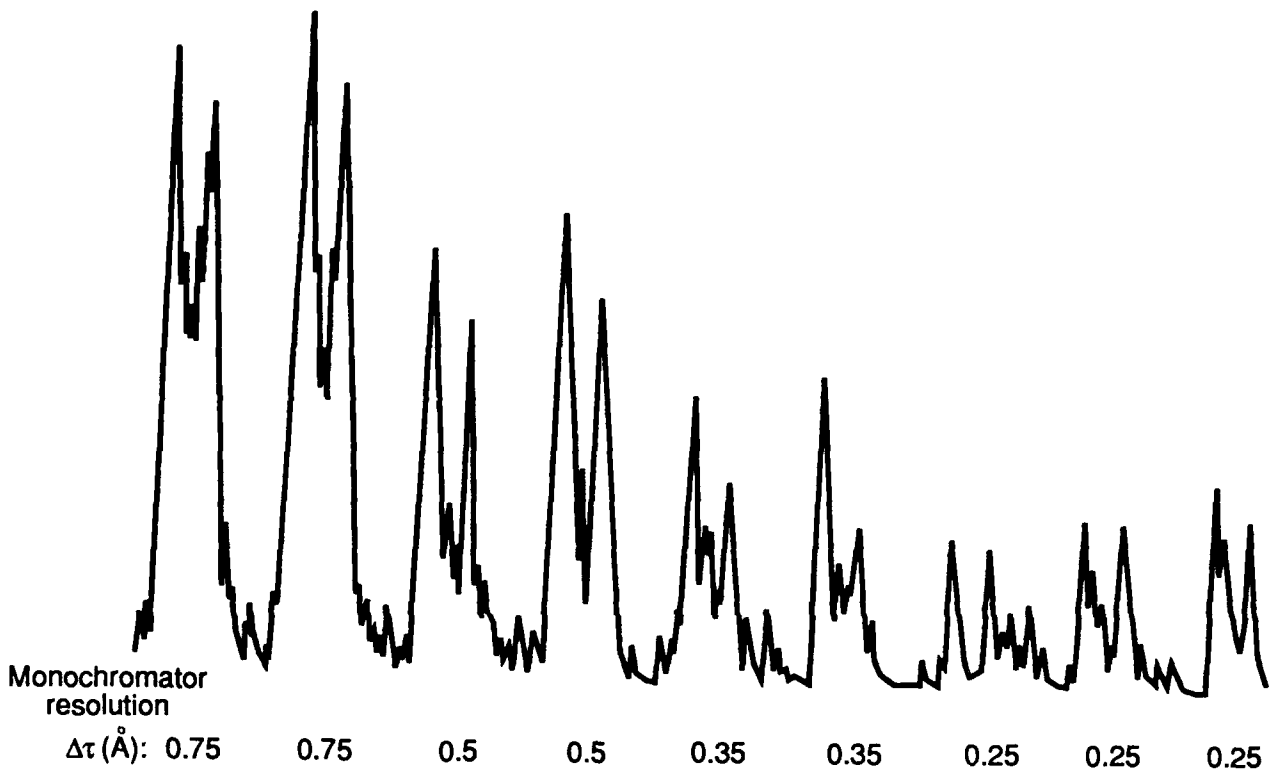

Figure 33. Laser-induced fluorescence from V' = 4, J' = 12. [The R(11) and P(13) doublets are shown as a function of instrument resolution.]

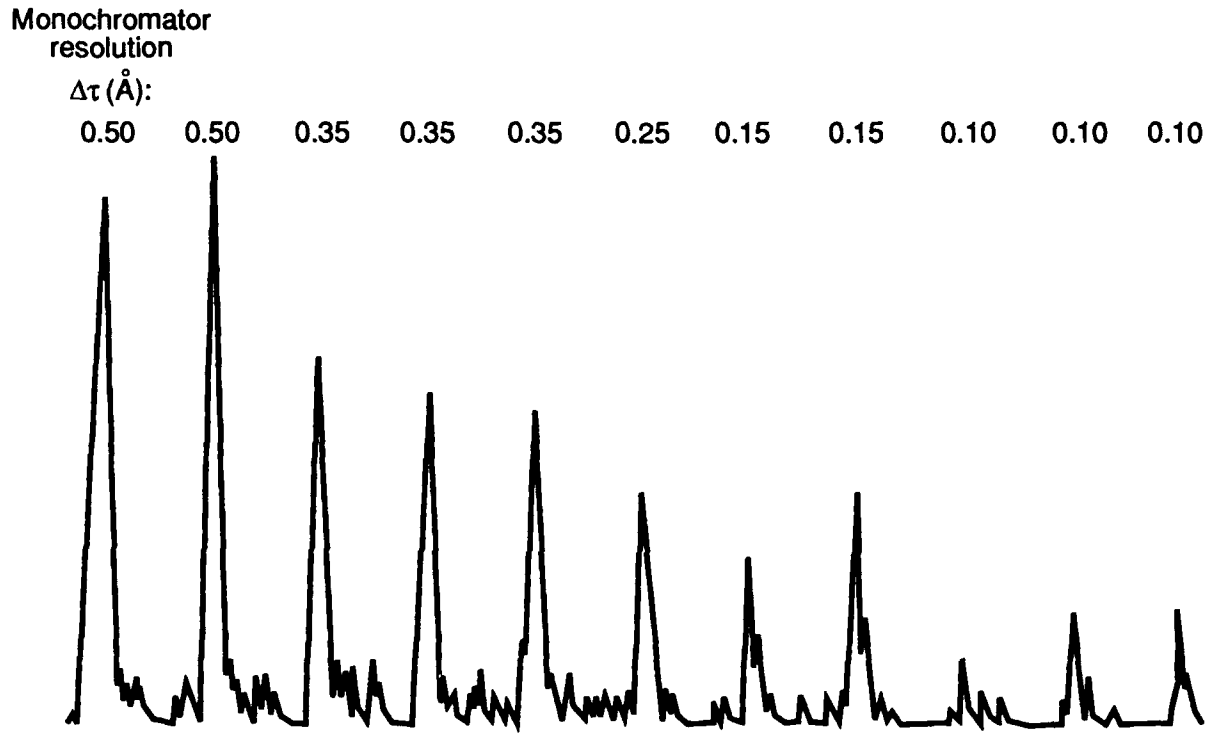

Figure 34. Laser-induced fluorescence from V' = 4, J' = 1. [The R(0) and P(2) doublets are shown to be unresolved.]

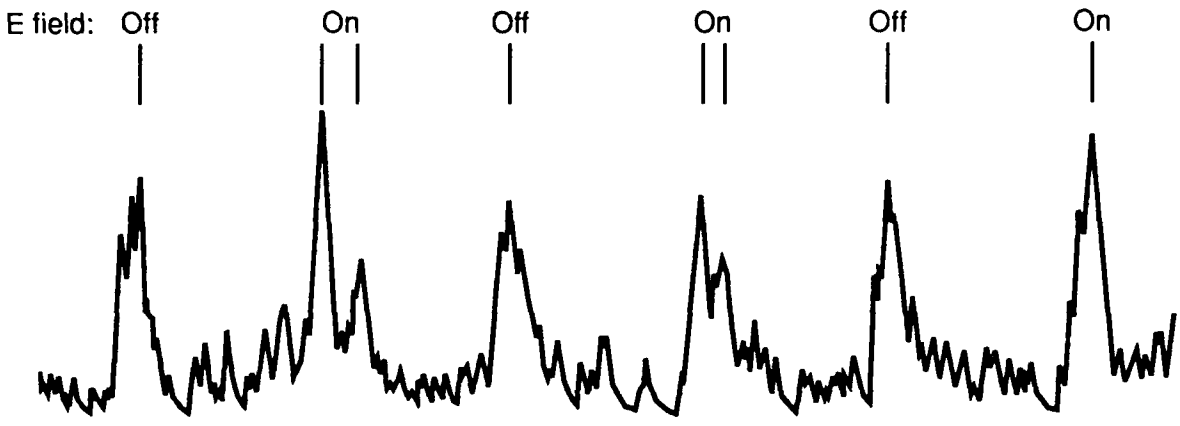

Figure 35. Laser-induced fluorescence from V' = 4, J' = 1. [The R(0) and P(2) doublets are unresolved. Anomalous behavior is shown in two cases with an applied electric field of 1 KV/cm.]

Table 31. Experimental conditions for specrtra in Figs. 31 through 35.

Transition: V" → V' J" → J'	0 → 1	0 → 3	0 → 4	0 → 4 ~10 → 12	0 → 4 15 → 14	0 → 4 13 → 12	0 → 4 -0 → 1	0 → 4 1 → 1
Laser wavelength (Å)	3016.5 to -3017	2894 to -2902.5	2836.5 to -2846.5	~2836.1	2824.92	2841.72	~2838	2838.25
Laser power* (mW)	100	35	50	100	95	150	140	150
CO pressure (torr)	50	50	50	66	63	71	68	20
Monochromator wavelength (Å)	1931	1970	2070	2066 to -2073	2066 to -2073	2066 to -2073	2066 to -2073	2066 to -2073
Slit width (μm)	400	500	1000	100 to -50	250 to -150	150 to -50	100 to -20	150
Boxcar sensitivity (mV)	50	20	50	5	10	5	5	5

*This is the power of the doubled dye laser at 10 Hz.

Table 32. Relative resolution figure of merit for the fluorescence scans shown in Figs. 31 through 35.

LIF Spectrum	$\Delta_2F(j)$(Å)	$\Delta\tau$(Å)	$\Delta_2F(j)/\Delta\tau$	Adequately Resolved
Fig. 31	3.70	0.25	15.0	Yes
Fig. 32	4.30	0.75	5.7	No
Fig. 33	3.70	0.25	15.0	Yes
Fig. 34	0.45	0.10	4.5	No
Fig. 35	0.45	0.75	0.6	No

The fluorescence signal excitation of V' = 4 was found to be stronger than fluorescence from V' = 3, which in turn was stronger than that from V' = 1. This is explainable with the data given in Table 33. The increase could not be accounted for from the products of the FCFs for absorption and fluorescence. Laser power is not considered a factor since the transitions are saturated in each case. However, atmospheric absorption due to O_2 was found to be significant

Table 33. Franck-Condon products for absorption and fluorescence and O_2 absorption.

	Excitation		
	0 → 1	0 → 3	0 → 4
$\langle 0 \mid V' \rangle$	0.26080	0.19629	0.9604
Fluorescence	1 → 7	3 → 9	4 → 11
$\langle V' \mid V'' \rangle$	0.44465	0.14862	0.12914
FCF Product	0.01159	0.02917	0.01240
O_2 Absoption* V" → V'	0-4 and 1-6	0-2	3-6 and 4-8
λ*	1923.5 and 1938	1971.4	2060 and 2079.7
I*	4 and 0	1	--

*$X^3\Sigma_g^-$ - $B^3\Sigma_u^-$ Schumann-Runge system (from Pearse and Gaydon, 1963).

due to nearby absorption bands of the $X^3\Sigma_g^-$ to $B^3\Sigma_u^+$ band (Schumann-Runge System) [Pearse and Baydon, 1963]. Although the entire optical system was purged with Argon, it is still possible that sufficient residual O_2 remained to account for the inadequate signal from V' = 1. Additional increases in the signal from V' = 4 are due to increased optical system component throughput and photomultiplier sensitivity at 2069 Å.

In summary, forbidden transitions could not be observed. The highest priority levels (V' = 1, J" = 5 and 6) were not resolved and hence not checked for forbidden transitions. Absorption of the fluorescence by atmospheric oxygen was probably a contributing problem. The small dipole moment of CO is also a potential explanation. Finally, multiphoton ionization of CO by the high laser powers needed for the two-photon excitation may have contributed by "shorting out" the electric field in the measurement region.

SECTION 9
CONCLUSIONS

Electric field measurements using NaK were successful. The sensitivity achieved was the same as reported in the literature. The field detection limit was an order of magnitude higher than published results. The strategy of using a perturbed level (V' = 2, J' = 40) was successfully demonstrated. Unfortunately, NaK is difficult to use and no way of putting it to practical use was found.

The ICl results are incomplete. A practical cell was constructed and tested but the experiments were abandoned due to time constraints before any useful spectroscopic information could be obtained.

The most promising molecule, CO, gave negative results for all of the levels tested. The highest priority levels (V' =1, J' = 5 and 6) could not be tested because of experimental difficulties associated with signal to noise and resolution. Three potential causes identified were: small dipole moment in the $A'\Pi$ state, excessive ionization of the medium due to the high laser power needed for the two-photon excitation, and signal to noise reduction due to atmospheric absorption and optical system efficiency. No definitive conclusion can be made concerning the suitability of CO as a sensor.

SECTION 10

LIST OF REFERENCES

Aarts, J. F. M., and F. J. DeHeer, "Emission of Radiation in the Vacuum Ultraviolet by Impact of Electrons on Carbon Monoxide," *J. Chem. Phys.*, Vol. 52, No. 10, 15 May 1970, pp. 5354-5360.

Auzin'sh, M. P., R. S. Ferbert, Ya. A. Harya, and I. Ya. Pirags, "The Effect of Collisions on the Intensity and Polarization of Laser-Induced $D^1\Pi \rightarrow X^1\Sigma^+$ Fluorescence from NaK," *Chem. Phys. Lett.*, Vol. 124, No. 2, 14 February 1986, pp. 116-120.

Bernheim, R. A., C. Kittrell, and D. K. Veirs, "Doppler-Free Two-Photon Laser Excitation of the Vacuum Ultraviolet Absorption Spectrum of CO," *J. Chem. Phys.*, Vol. 69, No. 3, 1 August 1978, pp. 1308-1309.

-----, "Two-Photon Excitation of the Vacuum Ultraviolet Fluorescence of Carbon Monoxide," *Chem. Phys. Lett.*, Vol 51, No. 2, 15 October 1977, pp. 325-328.

Bréchignac, Ph., A. Picard-Bersellini, R. Charneau, and J. M. Launay, "Rotational Relaxation of CO by Collisions with H_2 Molecules: A Comparison between Theory and Experiment," *Chem. Phys.*, Vol. 53, 1980, pp. 165-183.

Buckles, R. E., and J. M. Bader, "34. Iodine (I) Chloride," *Inorganic Syntheses*, Vol. 9, No. 130, 1971, pp. 130-133.

Burrus, C. A., "Stark Effect from 1.1 to 2.6 Millimeters Wavelength: PH_3, PD_3, DI, and CO," *J. Chem. Phys.*, Vol. 28, No. 3, March 1958, pp. 427-429.

Chackerian, C., "Electric Dipole Moment Function of the $X^1\Sigma^+$ State of CO: Vibration-Rotation Matrix Elements for Transitions of Gas Laser and Astrophysical Interest," *J. Chem. Phys.*, Vol. 65, No. 10, 15 November 1976, pp. 4228-4233.

Chackerian, C., et al., "Experimental Determination of the $^1\Sigma^+$ State Electric Dipole Moment Function of Carbon Monoxide up to a Large Internuclear Separation," *Canadian J. Phys.*, Vol. 62, 1984, pp. 1579-1585.

Chan, Y., *Quantum Electric Field Sensor Development--Year 1*, Pacific-Sierra Research Corporation, PSR Note 88106, March 1988.

Clyne, A. A., and I. S. McDermid, "$B^3\Pi(0^+)$ States of IF, ICl, and IBr, Part 2. Observation and Analysis of the Excitation of spectra and IF and ICl," *J. C. S. Faraday II*, Vol. 72, 1976, pp. 2252-2268.

Comes, F. J., and E. H. Fink, "Deactivation of CO($A^1\Pi$) in Individual Vibrational Levels," *Chem. Phys. Lett.*, Vol. 14, No. 4, 15 June 1972, pp. 433-437.

Coxon, J. A., R. M. Gordon, and M. A. Wickramaaratchi, "The $A^3\Pi(1) \leftarrow X^1\Sigma^+$ Absorption Spectrum of ICl," *J. of Mol. Spectrosc.*, Vol. 79, 1980, pp. 363-379.

Coxon, J. A., and M. A. Wickramaaratchi, "The $A^3\Pi(1) \rightarrow X^1\Sigma^+$ Emission Spectrum of ICl in the Near Infrared," *J. Mol. Spectrosc.*, Vol. 79, 1980, pp. 380-395.

Derouard, J., Universite Scientifique, Technologique et Medicale de Grenoble, Saint Martin d'Heres Cedex, France, private communication, 1987.

Derouard, J., and N. Sadeghi, "Observation and Characterization of a New $c(2)^3\Sigma^+$ Electronic State Using Stark Effect and Perturbation Analysis in NaK($B^1\Pi$)," *J. Chem, Phys.*, Vol. 88, No. 5, 1 March 1988, pp. 2891-2897,

-----, "Application of the Stark Effect in NaK Molecule to the Determination of the Local Electric Field in Plasmas," *IEEE Trans. on Plasma Sci.*, Vol. PS-14, No. 4, August 1986a, pp. 515-517.

-----, "Effects of a Weak Electric Field on the Fluorescence of a Polar Molecule in a $^1\Pi$ Electronic State: e-f Zero Field Anticrossings in NaK ($B^1\Pi$)," *Optics Comm.*, Vol. 57, No. 4, 15 March 1986b, pp. 239-243.

Field, R. W., Ph.D. Thesis, Harvard University, Cambridge, Massachusetts, 1971.

Field, R. W., B. G. Wicke, J. D. Simmons, and S. G. Tilford, "Analysis of Perturbations in the $a^3\Pi$ States of CO," *J. Mol. Spectros.*, Vol. 44, 1972, pp. 383-399.

Filseth, S. V., R. Wallenstein, and H. Zacharias, "Two Photon Excitation of CO ($A^1\Pi$) and N_2 ($a^1\Pi_g$)," *Optics Comm.*, Col. 23, No. 2, November 1977, pp. 231-235.

Fink, E. H., and F. J. Comes, "Vibrational Relaxation and Quenching of CO($A^1\Pi$, V = 0-8) in Collisions with Rare Gas Atoms," *Chem. Phys. Lett.*, Vol. 25, No. 2, 15 March 1974, pp. 190-196.

Fisher, N. J., and F. W. Dalby, "On the Dipole Moments of Excited Singlet States of Carbon Monoxide, *Canadian J. Phys.*, Vol. 54, 1976, pp. 258-261.

Girard, B., N. Billy, J. Vigue, and J. C. Lehmann, "Two-Photon Optical Pumping of CO($A^1\Pi$)," *Chem. Phys. Lett.*, Vol. 92, No. 6, 12 November 1982, pp. 615-619.

Greenwood, N. N., "Physico-Chemical Properties of the Interhalogen Compounds," *Rev. of Pure and Appl. Chem.*, Vol. 84, No. 1, 1951, pp. 84-120.

Hansen, S. G., J. D. Thompson, C. M. Western, and B. J. Howard, "Laser Spectroscopy and Microwave-Optical Duble Resonance of a Supersonic Expansion ICl $A^3\Pi(1)\nu = 19$," *Mol. Phys.*, Vol. 49, No. 5., 1983, pp. 1217-1229.

Harris, S. J., W. C. Natzle, and C. B. Moore, "Zero Pressure Lifetimes and Fluorescence Quenching of ICl($A^3\Pi_1$," *J. Chem. Phys.*, Vol. 70, No. 9, 1 May 1979, pp. 4215-4219.

Havey, M. D., and J. J. Wright, "Lifetime Measurements of $A^3\Pi_1$ Vibriational Levels of ICl," *J. Chem. Phys.*, Vol. 68, No. 10, 15 May 1978, pp. 4754-4756.

Herrmann, P. P., et al., "Stark Spectroscopy of Forbidden Two-Photon Transitions: A Sensitive Probe for the Quantitative Measurement of Small Electric Fields," *J. Phys. B: At. Mol. Phys.*, Vol. 19, No. 9, 14 May 1986, pp. 1271-1280.

Holleman, G. W., and J. I. Steinfeld, "Time-Resolved Fluorescence of Iodine Monochloride," *Chem. Phys. Lett.*, Vol. 12, No. 2, 15 December 1971, pp. 431-433.

Huber, K. P., and G. Herzberg, *Molecular Spectra and Molecular Structure*, Chapter IV. *Constants of Diatomic Molecules*, Van Nostrand Reinhold Company, New York City, 1979.

Hulthén, N. Järlsäter, and L. Koffman, "On the Absorption Spectrum of ICl, Part II. Chlorine Isotopes in Iodine Chloride," *Arkiv för Fysik*, Vol. 18, No. 35, 25 May 1960, pp. 479-512.

Hulthén, N. Johansson, and U. Pilsäter, "On the Absorption Spectrum of ICl, Part I," *Arkiv för Fysik*, Vol. 14, No. 3, 12 February 1958, pp. 31-48.

Jones, R. W., et al., "$A^1\Pi \leftarrow X^1\Sigma^+$ Resonance-Enhanced Multiphoton Ionization of Jet-Cooled CO," *Chem. Phys. Lett.*, Vol. 91, No. 4, 17 September 1982, pp. 271-272.

King, G. W., and R. G. McFadden, "Energy Levels of Iodine Monochloride Near the First Dissociation Limit," *Chem. Phys. Letters*, Vol. 58, No. 1, 1 September 1978, pp. 119-121.

Kirby-Docken, K., and B. Liu, "Theoretical Study of Molecular Dipole Moment Functions 1. The $X^1\Sigma^+$ State of CO," *J. Chem. Phys.*, Vol 66, No. 10, 5 May 1977, pp. 4309-4316.

Krupenie, P. H., *The Band Spectrum of Carbon Monoxide*, National Standard Reference Data Service, National Bureau of Standards,

Washington, DC, July 1986.

Lassettre, E. N., and A. Skerbele, "Absolute Generalized Oscillator Strengths for Four Electronic Transitions in Carbon Monoxide," *J. Chem. Phys.*, Vol. 54, No. 4, 15 February 1971, pp. 1597-1607.

Le Floch, A. C., et al., "Reinvestigation of the CO $A^1\Pi$ State and its Perturbations: The V = 0 Level," *J. Mol. Spectros.*, Vol. 121, 1987, pp. 337-379.

Mausteller, J. W., F. Tepper, and S. J. Rodgers, *Alkali Metal Handling and Systems Operating Techniques*, Gordon and Breach, New York, 1967.

Melton, L. A., and K. C. Yiin, "Energy Transfer in CO $A^1\Pi$, V' = 9. I. Quenching and Isotope Effects," *J. Chem. Phys.*, Vol 62, No. 7, 1 April 1975, p. 2860.

Moody, G. J., and J. D. R. Thomas, *Dipole Moments in Inorganic Chemistry*, Edward Arnold Publishers, Ltd., London, 1971.

Moore, C. A., G. P. Davis, and R. A. Gottscho, "Sensitive, Nonintrustive, *In-Situ* Measurement of Temporally and Spatially Resolved Plasma Electric Fields," *Phys. Rev. Lett.*, Vol. 52, No. 7, 13 February 1984, pp. 538-541.

Norbeck, J. M., R. R. Merkel, and P. R. Certain, "Dipole Moment Functions for $a^3\Pi$ Carbon Monoxide," *Mol. Phys.*, Vol. 34, No. 2, 1977, pp. 589-591.

Onaka, R., "Perturbation at V = 6 of the $A^1\Pi$ State of CO," *J. Chem. Phys.*, Vol. 26, 1957, pp. 1763-1764.

Pearse, R. W. B., and A. G. Gaydon, *The Identification of Molecular Spectra*, John Wiley and Sons, Inc., New York City, 1963.

Pratt, S. T., E. D. Poliakoff, P. M. Dehmer, and J. L. Dehmer, "Photoelectron Studies of Resonant Multiphoton Ionization of CO via the $A^1\Pi$ State," *J. Chem. Phys.*, Vol. 78, No. 1, 1 January 1983. pp. 65-72.

Provorov, A. C., B. P. Stoicheff, and S. Wallace, "Fluorescence Studies in CO with Tunable VUV Laser Radiation," *J. Chem. Phys.*, Vol. 67, No. 11, 1 December 1977, pp. 5393-5394.

Radzig, A. A., and B. M. Smirnov, *Reference Data on Atmos, Molecules, and Ions*, Springer-Verlag, New York City, 1985.

Ratcliff, L. B., D. D. Konowalow, and W. J. Stevens, "Electronic Transition Dipole Moment Functions for NaK," *J. Mol. Spectrosc.*, Vol. 110, 1985, pp. 242-255.

Simmons, J. D., A. M. Bass, and S. G. Tilford, "The Fourth Positive System of Carbon Monoxide Observed in Absorption at High Resolution in the Vacuum Ultraviolet Region," *Astrophys. J.*, Vol. 155, January 1969, pp. 345-358.

Stevens, W. J., D. D. Konowalow, and L. B. Ratcliff, "Electronic Structure and Spectra of the Lowest Five $^1\Sigma^+$ and $^3\Sigma^+$ States and Lowest Three $^1\Pi$, $^3\Pi$, $^1\Delta$, and $^3\Delta$ States of NaK," *J. Chem. Phys.*, Vol. 80, No. 3, 1 February 1984, pp. 1215-1224.

Tilford, S. G., and J. D. Simmons, "Atlas of the Observed Absorption Spectrum of Carbon Monoxide Between 1060 and 1900 Å," *J. Phys. Chem. Ref. Data*, Vol. 1, No. 1, 1972, pp. 147-187.

Vikis, A. C., "Energy Transfer in Monochromatically Excited $^{13}C^{16}O$ and $^{12}C^{18}O$ ($A^1\Pi$ $v' = 13$) Molecules," *J. Chem. Phys.*, Vol. 69, No. 2, 15 July 1978, pp. 703-709.

-----, "Rotational Relaxation of the $A^1\Pi(v' = 13, J' = 13^+)$ State of $^{13}CO^{16}O$ by Various Gases," *Canadian J. Chem.*, Vol. 61, 1983, pp. 952-955.

Werner, H. J., "MCSCF Calculation of the Dipole Moment Function of CO," *Mol. Phys.*, Vol. 44, No. 1, 1981, pp. 111-123.

Zacharias, H., H. Rottke, and K. H. Welge, "Photoionization of CO and NO by Tunable UVU Laser Radiation," *Optics Comm.*, Vol. 35, No. 2, November 1980, pp. 185-188.

Zimmerman, P., et al., "Stark Mixing Spectroscopy in Cesium," *Opt. Commun.*, Vol. 12, No. 2, October 1974, pp. 198-201.

DISTRIBUTION LIST

DNA-TR-87-244-V2

DEPARTMENT OF DEFENSE

ARMED FORCES RADIOBIOLOGY RSCH INST
ATTN: DR M R LANDAUER/BHS

ASSISTANT TO THE SECRETARY OF DEFENSE ATOMIC ENERGY
ATTN: EXECUTIVE ASSISTANT

DEFENSE COMMUNICATIONS AGENCY
ATTN: CODE DTJ DEANE PARKER

DEFENSE COMMUNICATIONS AGENCY
ATTN: COMMANDER

DEFENSE COMMUNICATIONS ENGINEER CENTER
ATTN: CODE R410

DEFENSE INTELLIGENCE AGENCY
ATTN: DT-5A (R BURGER)
ATTN: RTS-2B
ATTN: VP-TPO

DEFENSE NUCLEAR AGENCY
ATTN: DFRA
ATTN: OPNA
ATTN: OPNS
ATTN: RAAE
ATTN: RAEE
ATTN: RAEV
4 CYS ATTN: TITL

DEFENSE TECHNICAL INFORMATION CENTER
2 CYS ATTN: DTIC/FDAB

DNA PACOM LIAISON OFFICE
ATTN: DNALO

NATIONAL DEFENSE UNIVERSITY
ATTN: NWCO

NATIONAL SECURITY AGENCY
ATTN: CHIEF A4213
ATTN: Y253 (HILTON)

NET ASSESSMENT
ATTN: DOCUMENT CONTROL

STRATEGIC AND THEATER NUCLEAR FORCES
ATTN: DR E SEVIN

STRATEGIC TARGET PLANNING
ATTN: JKC (ATTN: DNA REP)
ATTN: JKCS
ATTN: JLWT (THREAT ANALYSIS)
ATTN: JPEM
ATTN: JPSS

THE JOINT STAFF
ATTN: J-3 NUC OPERATIONS BR
ATTN: J-5 NUC & CHEMICAL DIV
ATTN: J-6 F D BUTTS
ATTN: J-8 CAD

U S EUROPEAN COMMAND/ECC3S-CC
ATTN: ECC3S-CC

U S FORCES KOREA
ATTN: EACJ-TD-NS

DEPARTMENT OF THE ARMY

DEP CH OF STAFF FOR OPS & PLANS
ATTN: DAMO-ODW

HARRY DIAMOND LABORATORIES
ATTN: SLCHD-NW
2 CYS ATTN: SLCHD-NW-E
ATTN: SLCHD-NW-EA
ATTN: SLCHD-NW-EE
ATTN: SLCHD-NW-RA
ATTN: SLCHD-NW-RC
ATTN: SLCHD-NW-RH (G MERKEL)
ATTN: SLCIS-IM-TL (TECH LIB)
ATTN: W PATTERSON

OFFICE OF ASSISTANT SECRETARY OF ARMY
ATTN: SARD-ZCA

U S ARMY ATMOSPHERIC SCIENCES LAB
ATTN: SLCAS-AS

U S ARMY BALLISTIC RESEARCH LAB
ATTN: SLCBR-SS-T (TECH LIB)
ATTN: SLCBR-TB-B (G BULMASH)
ATTN: SLCBR-VL

U S ARMY ENGINEER DIV HUNTSVILLE
ATTN: CEHND-SY J LOYD
ATTN: HNDED-SY

U S ARMY MISSILE COMMAND/AMSMI-RD-CS-R
ATTN: AMSMI-RD-CS-R (DOCS)

U S ARMY NUCLEAR & CHEMICAL AGENCY
ATTN: MONA-NU

U S ARMY NUCLEAR EFFECTS LABORATORY
ATTN: DR J MEASON

U S ARMY STRATEGIC DEFENSE CMD
ATTN: CSSD-H-SAV

U S ARMY STRATEGIC DEFENSE COMMAND
ATTN: CSSD-SL

U S ARMY TEST & EVALUATION COMMAND
ATTN: TECHNICAL LIBRARY

U S ARMY WAR COLLEGE
ATTN: LIBRARY

US ARMY MATERIEL SYS ANALYSIS ACTVY
ATTN: AMXSY-CR

USA SURVIVABILITY MANAGMENT OFFICE
ATTN: SLCSM-SE J BRAND

USACACDA
ATTN: ATZL-CAC-A
ATTN: ATZL-CAD-N
ATTN: ATZL-CAN-I

DEPARTMENT OF THE NAVY

NAVAL AIR SYSTEMS COMMAND
ATTN: AIR 5161

NAVAL POSTGRADUATE SCHOOL
ATTN: CODE 1424 LIBRARY

NAVAL RESEARCH LABORATORY
ATTN: CODE 2627 (TECH LIB)

NAVAL SURFACE WARFARE CENTER
ATTN: CODE R41
ATTN: CODE R43
ATTN: CODE 425

NAVAL SURFACE WARFARE CENTER
ATTN: CODE H-21

OFFICE OF CHIEF OF NAVAL OPERATIONS
ATTN: NOP 098
ATTN: NOP 503
ATTN: NOP 551
ATTN: NOP 941F
ATTN: OP 654
ATTN: OP 981

THEATER NUCLEAR WARFARE PROGRAM OFC
ATTN: PMS 423

USCINCPAC STAFF
ATTN: WSE-PAC LTCOL R ROLLER

DEPARTMENT OF THE AIR FORCE

AERONAUTICAL SYSTEMS DIVISION
ATTN: ASD/ENACE

AFIA/INIS
ATTN: AFIA/INKD

AIR FORCE CTR FOR STUDIES & ANALYSIS
ATTN: AFCSA/SAMI

AIR FORCE SPACE COMMAND
ATTN: LKA

AIR UNIVERSITY LIBRARY
ATTN: AUL-LSE

DEPUTY CHIEF OF STAFF/XOX
ATTN: AFXOXFM

HEADQUARTERS U S AIR FORCES IN EUROPE/LG
ATTN: XPXF

SPACE DIVISION/IN
ATTN: IND

SPACE DIVISION/YA
ATTN: YAR

USAF/LEEEU
ATTN: LEEE

WEAPONS LABORATORY
ATTN: NTAA
ATTN: WL/SUL

DEPARTMENT OF ENERGY

LAWRENCE LIVERMORE NATIONAL LAB
ATTN: H CABAYAN

LOS ALAMOS NATIONAL LABORATORY
ATTN: REPORT LIBRARY

SANDIA NATIONAL LABORATORIES
ATTN: ORG 9300 J E POWELL
ATTN: TECH LIB

OTHER GOVERNMENT

CENTRAL INTELLIGENCE AGENCY
ATTN: OSWR/NED
ATTN: OSWR/STD/MTB

DEPARTMENT OF COMMERCE
ATTN: D PEACH
ATTN: G REEVE
ATTN: W UTLAUT

FEDERAL EMERGENCY MANAGEMENT AGENCY
ATTN: SL-EM
ATTN: R GATES EMP PRORAM

DEPARTMENT OF DEFENSE CONTRACTORS

AGBABIAN ASSOCIATES
ATTN: LIBRARY

ALLIED-SIGNAL, INC
ATTN: DOCUMENT CONTROL

BDM INTERNATIONAL INC
ATTN: E DORCHAK

BDM INTERNATIONAL INC
ATTN: B TORRES
ATTN: R-33, B PLUMMER

BOEING CO
ATTN: D EGELKROUT
ATTN: D CHAPMAN

BOEING CO
ATTN: C SUTTER

BOOZ-ALLEN & HAMILTON, INC
ATTN: TECHNICAL LIBRARY

BOOZ-ALLEN & HAMILTON, INC
ATTN: L ALBRIGHT

BOOZ-ALLEN & HAMILTON, INC
ATTN: T ZWOLINSKI

COMPUTER SCIENCES CORP
ATTN: A SCHIFF

E-SYSTEMS, INC
ATTN: MAIL STOP 3

EG&G SPECIAL PROJECTS INC
ATTN: J GILES

ELECTRO-MAGNETIC APPLICATIONS, INC
ATTN: D MEREWETHER

GENERAL ELECTRIC CO
ATTN: DAREN NERAD

GENERAL ELECTRIC CO
ATTN: P HEILAND

GENERAL RESEARCH CORP
ATTN: W NAUMANN

GRUMMAN AEROSPACE CORP
ATTN: H SMITH, TECH INFO CNTR

GTE GOVERNMENT SYSTEMS CORPORATION
ATTN: TECH LIBRARY

HERCULES DEFENSE ELECTRONICS SYSTEMS, INC
ATTN: R LAZARCHIK

HONEYWELL, INC
ATTN: SR&C LIBRARY

IIT RESEARCH INSTITUTE
ATTN: I MINDEL

INSTITUTE FOR DEFENSE ANALYSES
ATTN: CLASSIFIED LIBRARY
ATTN: TECH INFO SERVICES

JAYCOR
ATTN: E WENAAS

JAYCOR
ATTN: E WENAAS
ATTN: M SCHULTZ, JR

JAYCOR
ATTN: M BELL

KAMAN SCIENCES CORP
ATTN: LIBRARY/B KINSLOW

KAMAN SCIENCES CORP
ATTN: DASIAC
ATTN: E CONRAD

KAMAN SCIENCES CORPORATION
ATTN: TECHNICAL LIBRARY
ATTN: W MACKLIN

KAMAN SCIENCES CORPORATION
ATTN: DASIAC
ATTN: R RUTHERFORD

KEARFOTT GUIDANCE AND NAVIGATION CORP
ATTN: J D BRINKMAN

LITTON SYSTEMS, INC
ATTN: J SKAGGS

LOCKHEED MISSILES & SPACE CO, INC
ATTN: TECH INFO CTR D

LTV AEROSPACE & DEFENSE COMPANY
2 CYS ATTN: LIBRARY EM-08

METATECH CORPORATION
ATTN: W RADASKY

MISSION RESEARCH CORP
ATTN: C LONGMIRE
ATTN: EMP GROUP
ATTN: TECH INFO CENTER
ATTN: W CREVIER

MISSION RESEARCH CORP
ATTN: J LUBELL
ATTN: J R CURRY
ATTN: W BEREUTER

MISSION RESEARCH CORP, SAN DIEGO
ATTN: V VAN LINT

MITRE CORPORATION
ATTN: M FITZGERALD

PACIFIC-SIERRA RESEARCH CORP
ATTN: H BRODE
2 CYS ATTN: J BAHNS

PHOTOMETRICS, INC
ATTN: I L KOFSKY

R & D ASSOCIATES
ATTN: C MO
ATTN: DOCUMENT CONTROL
ATTN: G K SCHLEGEL

R & D ASSOCIATES
ATTN: J P CASTILLO
ATTN: W S KEHRER

RAND CORP
ATTN: ENGR & APPLIED SCI DEPT

RAYTHEON CO
ATTN: H FLESCHER

RCA CORPORATION
ATTN: G BRUCKER

RESEARCH TRIANGLE INSTITUTE
ATTN: M SIMONS

ROCKWELL INTERNATIONAL CORP
ATTN: B-1 DIV TIC (BAOB)

ROCKWELL INTERNATIONAL CORP
ATTN: J C ERB, OA13

ROCKWELL INTERNATIONAL CORP
ATTN: G SMITH

S-CUBED
ATTN: A WILSON
ATTN: J KNIGHTEN

SCIENCE & ENGRG ASSOCIATES, INC
ATTN: C THOMPSON
ATTN: R M SMITH

SCIENCE & ENGRG ASSOCIATES, INC
ATTN: V JONES

SCIENCE APPLICATIONS INTL CORP
ATTN: W ADAMS
ATTN: W CHADSEY
ATTN: W LAYSON

SCIENCE APPLICATIONS INTL CORP
ATTN: P J DOWLING

SRI INTERNATIONAL
ATTN: D ARNS
ATTN: E VANCE
ATTN: W GRAF

TEXAS INSTRUMENTS, INC
ATTN: NORTH BLDG LIBRARY

TRW INC
ATTN: LIBRARIAN

TRW INC
ATTN: A R CARLSON
ATTN: C E WULLER
ATTN: J PENAR

UNISYS CORPORATION-DEFENSE SYSTEMS
ATTN: TECHNICAL LIBRARY